Order Number 8914765

NMR studies of the alpha-mating factor from the yeast *Saccharomyces cerevisiae* in solution and in the presence of lipid vesicles

Jelicks, Linda Ann, Ph.D.

City University of New York, 1988

U·M·I
300 N. Zeeb Rd.
Ann Arbor, MI 48106

NMR STUDIES OF THE ALPHA-MATING FACTOR FROM THE YEAST *SACCHAROMYCES CEREVISIAE* IN SOLUTION AND IN THE PRESENCE OF LIPID VESICLES

by

LINDA ANN JELICKS

A dissertation submitted to the Graduate Faculty in Biochemistry in partial fulfillment of the requirements for the degree of Doctor of Philosophy, The City University of New York.

1988

This manuscript has been read and accepted for the Graduate Faculty in Biochemistry in satisfaction of the dissertation requirement for the degree of Doctor of Philosophy.

March 8, 1988
Date

Michelle S Bridle
Chair of Examining Committee

June 14, 1988
Date

Honor Scrutz
Executive Officer

Fred Naider
Robert Bittman
Philip Cohen
Andrew Boyd
Ruth E. Stark
Supervisory Committee

The City University of New York

Abstract

NMR STUDIES OF THE ALPHA-MATING FACTOR FROM THE YEAST *SACCHAROMYCES CEREVISIAE* IN SOLUTION AND IN THE PRESENCE OF LIPID VESICLES

by

Linda Ann Jelicks

Advisor: Professor Michelle S. Broido

The alpha-mating factor is a tridecapeptide pheromone ($^{+}NH_3$-Trp^{1}-His^{2}-Trp^{3}-Leu^{4}-Gln^{5}-Leu^{6}-Lys^{7}-Pro^{8}-Gly^{9}-Gln^{10}-Pro^{11}-Met^{12}-Tyr^{13}-COOH), secreted by the $\underline{\alpha}$-cells of the yeast *Saccharomyces cerevisiae*, which interacts with a membrane - bound receptor on *a*-cells and elicits hormone - like responses necessary for mating of the two different haploid cell types ($\underline{\alpha}$ and *a*). A number of biochemical and biophysical techniques have been used to study the structure and activity of this peptide. The NMR techniques utilized here provide a direct method for determining alpha-factor conformations in solution and in the lipid - bound state which are then correlated with biological activity.

Acquisition of two dimensional nuclear Overhauser effect (NOESY) spectra of the peptide in organic solvent (DMSO) and rotating frame nuclear Overhauser effect (ROESY) spectra in aqueous solution suggest the presence of a Type II beta-turn spanning residues 7-10 but no other preferred conformations. NOESY spectra acquired in the presence of lipid vesicles indicate that this turn is stabilized by the

interaction with lipid. Furthermore, the lipid induces a compact folded structure at the N-terminus of the peptide. In addition to these two-dimensional studies, results obtained for binding to several different lipids indicate that the peptide - lipid interaction is both electrostatic and hydrophobic in nature.

Effects of the peptide on the phospholipid vesicles were studied by ^{31}P and ^{2}H NMR and by quasielastic light scattering. The peptide induces an increase in vesicle size, appears to interact preferentially with the liquid crystalline state lipid relative to the gel state lipid, and imparts rigidity into this fluid lipid state. These effects are similar to those described in the literature for a number of membrane - active peptides.

Both the solution and lipid - bound conformations of the alpha-factor indicated by the 2D NOE studies are different from those proposed by other investigators who do not detect the beta-turn.

This thesis is dedicated to my mother, Roberta A. Jelicks and to the memory of my father, John P. Jelicks, Jr.

Acknowledgements

I would like to thank Professor Michelle S. Broido, my advisor, for being a friend, teacher, and role model. Words cannot fully express my gratitude for all the help she has given me. It has truly been a pleasure to work in her lab during my graduate studies.

I would also like to thank my fellow Kbears: Sam, Don, Chen, Paula and my best friend Sean (tbmtl). I'd also like to thank our honorary Kbear, Dr. Michael Blumenstein, who has managed to give me the large amount of NMR time needed to complete this project and who has given me lots of peptide - NMR advice.

Professor Fred Naider has been an inspiration since I first met him as my undergraduate Organic Chemistry teacher. I thank him for the many alpha-factor discussions we have had, for a seemingly never ending supply of alpha-factor and analogue peptides, and for giving me the opportunity to synthesize the alpha-factor in his lab.

Thanks also go to Professor Naider's research group: Murthi, for synthesizing alpha-factor and all of the dodecapeptide analogues I studied, Jose and Michael, for synthesizing alpha-factor and extended alpha-factors, and Ariel and Jaya for helping me synthesize the alpha-factor.

I'd like to thank Professor Robert Bittman for providing initial lipid samples and for teaching me how to prepare the sonicated lipid vesicles.

I'd like to thank Professor Ruth Stark for teaching me

about QLS and providing the instrument at CSI and also for many thoughtful NMR discussions.

Dr. R. Andrew Byrd has been invaluable to our group in keeping us updated on quirks of the JEOL 400 MHz NMR spectrometer and provided initial solid state ^{31}P NMR results on the alpha-factor - lipid interaction.

I'd also like to thank the biologist on my committee, Professor Peter Lipke, who did some of the original research on the effects of alpha-factor on a-cell morphology, and who has maintained an interest in all aspects of the alpha-factor project.

This list comprises only a small group of the many people who have been instrumental in helping me attain my goals. I apologize that I cannot mention them all and I wish to express my sincere thanks.

TABLE OF CONTENTS

List of Abbreviations

Å	Angstrom
Ala	alanine
Asp	aspartic acid
B, B_i	magnetic field, component of magnetic field in i direction
Boc	tertbutoxycarbonyl
C_{18}	octadecyl silica gel, HPLC column
CD	circular dichroism
Cha	beta-cyclohexyl-L-alanine
C_n	weight concentration of nth species (QLS)
CPMG	Carr-Purcell-Meiboom-Gill T_2 experiment
Cys	cysteine
D	diffusion coefficient (QLS)
DCC	dicyclohexylcarbodiimide
DMF	dimethylformamide
DMS	dimethylsulfide
DMSO-d_6	dimethyl sulfoxide-d_6
DNA	deoxyribonucleic acid
DOPC	dioleoylphosphatidylcholine
DOPE	dioleoylphosphatidylethanolamine
DPPA	dipalmitoylphosphatidic acid
DPPC	dipalmitoylphosphatidylcholine
DPPE	dipalmitoylphosphatidylethanolamine
DSPC	distearoylphosphatidylcholine
D_2O	deuterium oxide
E	energy

EDTA	ethylenedinitrilo-tetraacetic acid
FID	free induction decay
f_p, f_{pl}	mole fraction of free peptide (p) and bound peptide (pl)
FT	Fourier transform
f_1, f_2	frequency dimensions in 2D NMR experiments
Gln	glutamine
Glu	glutamic acid
Gly	glycine
G_n	fraction of light scattered by the nth species
$\hbar$	Planck's constant divided by 2π
^1H	spin 1/2 isotope of hydrogen
^2H	spin 1 isotope of hydrogen
HF	hydrogen fluoride
His	histidine
HOD	water, residual ^1H in D_2O
HPLC	high performance liquid chromatography
Hz	Hertz
I_i	component of nuclear spin in i direction
Ile	isoleucine
J	spin-spin coupling constant
k_b	Boltzmann constant
K_i	equilibrium constant for process i
k_i	rate constant for process i
KHz	kilohertz
Leu	leucine
Lys	lysine

L_F, L_B	concentration of free lipid and bound lipid
M_i	magnetization at time i
Met	methionine
mg	milligram
MHz	megahertz
ml	milliliter
mM	millimolar
M_n	molecular weight of the nth species
ms	millisecond
n	number of scans (or number of 1D experiments collected in 2D NMR experiments)
NMR	nuclear magnetic resonance
NOE	nuclear Overhauser effect
ns	nanosecond
OMPa	p-methoxyphenylacetic acid
OPa	phenacyl ester
P_F, P_B	concentration of free peptide (F) and bound peptide (B)
P_o	initial peptide concentration
PA	phosphatidic acid
PC	phosphatidylcholine
PE	phosphatidylethanolamine
Phe	phenylalanine
PI	phosphatidylinositol
ppm	parts per million
Pro	proline
PS	phosphatidylserine

^{31}P	spin 1/2 isotope of phosphorus
p	spin angular momentum
q	magnitude of scattering vector
QLS	quasielastic light scattering
$R(T)/R(0)$	autocorrelation function of scattered light (QLS)
rf	radiofrequency
R_h	hydrodynamic radius
r_{ij}	internuclear separation of i and j
s	second
T	absolute temperature
T_1	spin-lattice relaxation time
T_2	spin-spin relaxation time
T_2^*	apparent spin-spin relaxation time, calculated from $1/\pi\nu$, where ν is the full linewidth at half height
t_1, t_2	time dimensions in 2D NMR experiments
T_c	lipid phase transition temperature
TFA	trifluoroacetic acid
TMS	tetramethylsilane
TRNOE	transferred NOE
Trp	tryptophan
TSP	3-trimethylsilylpropionate, sodium salt
Tyr	tyrosine
V	variance (QLS)
W_i	rate of transition i (transition probability)
X,Y,Z	axes in fixed frame
X',Y',Z'	axes in rotating frame

$\|\alpha\rangle$, $\|\beta\rangle$	quantum mechanical wave functions of two state system
γ_N	gyromagnetic ratio of nuclear species N
η	nuclear Overhauser enhancement factor, solvent viscosity
θ	notation for angles
μ_N	magnetic dipole of nuclear species N
μ_s	microsecond
ρ_{noe}	direct relaxation rate (fixed frame)
ρ_{roe}	direct relaxation rate (rotating frame)
σ	shielding constant
σ_{noe}	cross relaxation rate (fixed frame)
σ_{roe}	cross relaxation rate (rotating frame)
σ_F	cross relaxation rate of free species
σ_B	cross relaxation rate of bound species
τ_c	correlation time
τ_m	mixing time
ω_i	angular frequency i
ν_i	$\omega_i/2$
Γ	decay constant (QLS)
Σ	sum
1D, 2D	one dimensional, two dimensional

List of Tables

List of Figures

CHAPTER I

Introduction

Hormones, pheromones, and neurotransmitters which interact with receptor molecules bound to the membranes of the target cells are often small, linear peptides. Consequently, linear peptides have elicited much study by biochemists. Peptide-receptor studies themselves are very difficult to undertake because of problems associated with identifying, isolating, and tagging receptor proteins, and with observing the peptide - receptor interaction experimentally. Because of such problems much early research effort was spent on determining peptide conformation in solution. More recently, researchers have begun to investigate the interaction of peptide messengers with the phospholipid molecules with which they must come in contact during the process of binding with the membrane-bound receptor.

In the past several years a controversy has arisen concerning the extent to which small linear peptides adopt ordered conformations in solution. Although there are many reports in the literature on the conformation of cyclic peptides in solution (1-8), most studies on linear peptide indicate that these peptides are essentially unordered in solution (7,9-14). Recently, however, it has been suggested that biologically active linear peptides can exhibit preferred conformations in solution (15-17). A survey of the current literature reveals that lipid

molecules themselves can induce order into small peptides (18-25). Further, it is conjectured that the ordered conformation in the presence of the hydrophobic environment of the lipid molecules may more closely resemble the biologically active conformation of the peptide than the conformation present in aqueous solution (22, 26, 27).

Nuclear Magnetic Resonance (NMR) has been shown to be an excellent tool for the study of the conformation of biological molecules in solution (27-33). In particular, the nuclear Overhauser effect (NOE) has been used to study through space connectivities to determine the conformations of peptides and proteins (27, 30 - 33). However, linear peptides, lacking the stability imparted by disulfide bonds, have often been considered too flexible to exhibit a preferred conformation observable on the NMR timescale. Further complicating the NMR determination of the structure of these peptides is the fact that the rotational correlation time (which characterizes the time required for random molecular reorientation) is often such that the NOE vanishes at the spectrometer frequencies used in high resolution studies (34, 35).

Alpha-factor, a small linear peptide secreted by the $\underline{\alpha}$ -mating type cells of Saccharomyces cerevisiae, is an excellent model system for conformational studies in solution and in the presence of lipid. The peptide diffuses through the culture medium and then interacts with a receptor on the membrane of the opposite, $\underline{a}$- mating type

yeast cells (36). The activity of alpha-factor has been studied extensively and there are complementary physical chemical and biological studies in the literature (20, 37 - 48).

Spectroscopic (NMR and Quasielastic Light Scattering (QLS)) studies of the alpha-factor peptide in solution and upon interaction with phospholipid aggregrates are the focus of this dissertation. Details of the biochemisty and biological actions of alpha-factor are discussed below. Basic principles of the NMR and QLS experiments are found in Chapter II, materials and methods in Chapter III, experimental results in Chapter IV, and discussion of the implications of the results is found in Chapter V.

Background

Saccharomyces have coexisted with and have been utilized by man for many centuries. In nature they are found in soil and on fruits and plants, especially those with a high sugar content. Yeasts have been exploited by man in the production of alcoholic beverages (brewer's yeast) and in baking (baker's yeast). Because Saccharomyces has been manipulated genetically, studied extensively both biologically and biochemically, and because it shares many characteristics with mammalian cells these yeasts are excellent models for the study of peptide messenger - cell membrane interactions (49).

Yeasts are classified as eukaryotic cells since they

have double membrane bound nuclei, mitochondria, and endoplasmic reticula studded with ribosomes. Morphologically they resemble plant cells having cell walls composed of polysaccharides. Much of the biochemistry of yeast is similar to that of animal cells and many of the metabolic pathways found in S. cerevisiae are present in animal cells but are absent in bacteria and other fungi (49). Examples of some molecules present in yeast but absent in bacteria and fungi include Elongation Factor 2, spermine, and the 18S rRNA which contains the modified base, N^4-acetylcytidine (found in rat and chicken liver) (50). The yeasts also have many features not shared with either plants or animals (51). Like other fungi, they can synthesize lysine from alpha-ketoglutarate via the alpha-aminoadipate pathway while bacteria and plants utilize aspartate and the diaminopimelate pathway (52,53).

The life cycle of Saccharomyces cerevisiae alternates between haploid and diploid growth phases. Conjugation, or mating, of the two haploid cell types a and α is a developmental alternative to vegetative multiplication (see Figure 1) (36). The cell-cell interactions necessary for mating are initiated by peptide pheromones which trigger biochemical changes in the target cells. The a-cell secretes the a-factor, a hydrophobic peptide with the amino acid sequence: NH_2-Tyr^1-Ile^2-Ile^3-Lys^4-Gly^5-(Val, Ile)^6-Phe^7-Trp^8-Asp^9-Pro^{10}-Ala^{11}-Cys^{12}-(S-R)-COOH (R is believed to be a farnesyl group), which interacts with the target

FIGURE 1

The life cycle of the yeast Saccharomyces cerevisiae showing the alternation between the haploid and diploid growth phases. Alpha-factor and a-factor are involved in the sexual agglutination and mating of the haploid cell types a and α.

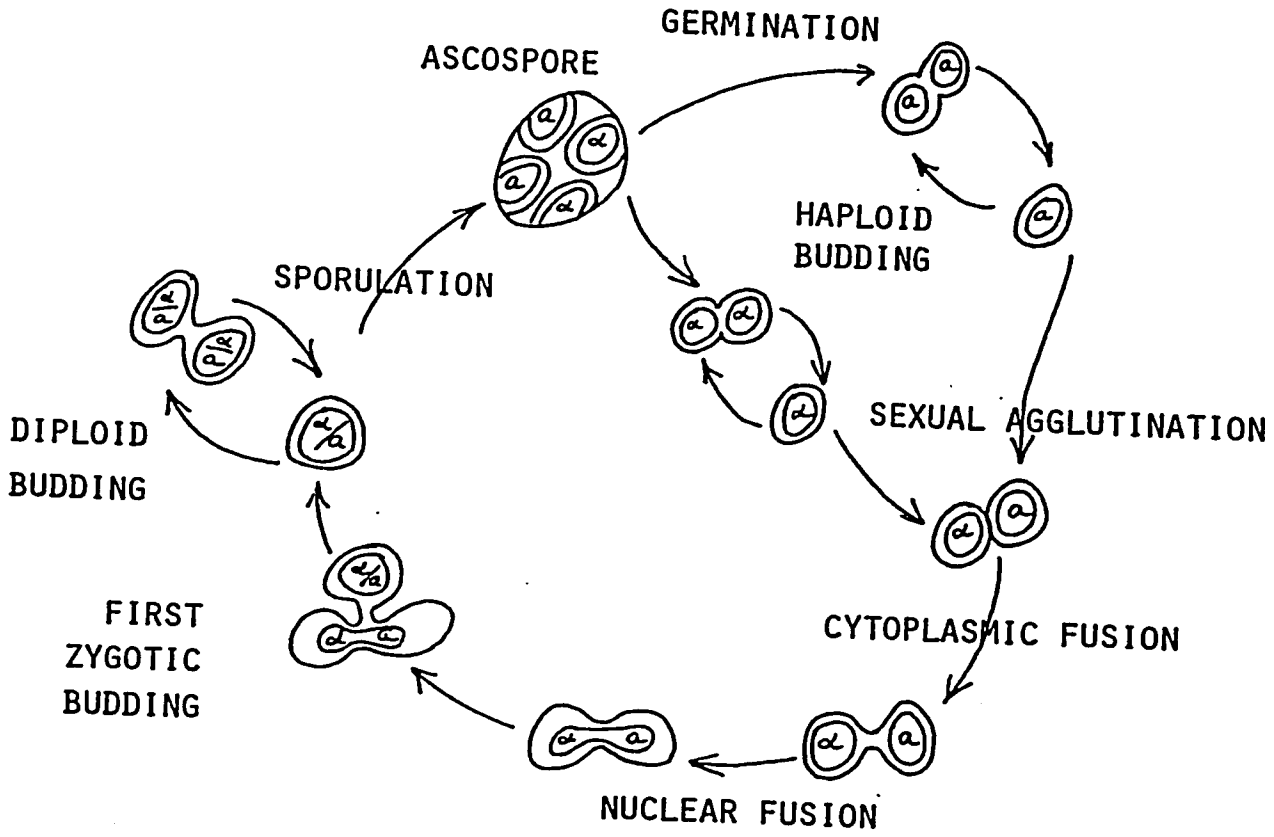
GERMINATION
ASCOSPORE
HAPLOID
BUDDING
SPORULATION
SEXUAL AGGLUTINATION
DIPLOID
BUDDING
CYTOPLASMIC FUSION
FIRST
ZYGOTIC
BUDDING
NUCLEAR FUSION

α-cells (54, 55). α-cells secrete the alpha-factor, NH_2-Trp^1-His^2-Trp^3-Leu^4-Gln^5-Leu^6-Lys^7-Pro^8-Gly^9-Gln^{10}-Pro^{11}-Met^{12}-Tyr^{13}-COOH, which interacts with a-cells. Both pheromones elicit hormone-like responses including: 1) an induction of sexual agglutinability leading to cell surface alterations which increase the strength and selectivity of cell-cell contact and change the cell morphology; 2) an arrest of cell growth in the G1 phase of the cell cycle and inhibition of DNA synthesis which serve to synchronize the cell division cycle of the mating partners; and 3) initiation of new cell wall and membrane synthesis which is more suitable for cell fusion than for budding (36).

Tridecapeptide alpha-factor and a dodecapeptide, des-Trp^1-alpha-factor (lacking the N-terminal Trp residue) have been isolated from spent culture medium of α-cells (49). The tridecapeptide and dodecapeptide have also been synthesized and both exhibit high biological activity. Shenbagamurthi et al. have found that the activity of the dodecapeptide is 6% that of the tridecapeptide while Masui et al. report the same activity for the two peptides (37, 38).

Previous studies by Naider et al. indicate that the biological activities of alpha-factor analogues are sensitive to the stereochemistry of the amino acid residue substituted for Gly^9 in the natural sequence (39, 41, 42). Results demonstrate that while D-Ala and D-Leu are well tolerated at position 9, L-Ala and L-Leu substitutions

result in pheromones which are at least two orders of magnitude less active than the native peptide. The CD (circular dichroism) patterns of alpha-factor and analogue peptides are different for active Gly^9 and D-X^9 peptides relative to those of inactive L-X^9 peptides (where X is either Ala or Leu) (39, 41). A Pro-Gly sequence is often present in beta-turns, conformational features commonly found in peptides (illustrated below with short interproton distances indicated), and such a sequence raises the possibility of a beta-turn spanning residues 7 -10 of the alpha-factor (56, 57). Theoretical considerations suggest that a Type II beta-turn can tolerate D-amino acids at the i+2 position of the turn but L-amino acids are only infrequently found at that position (58).

BETA-TURNS

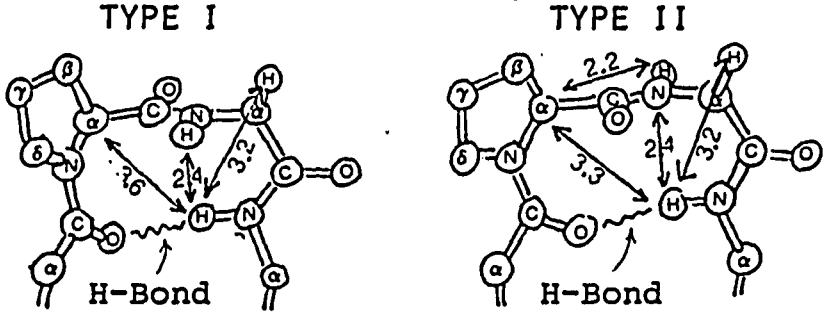

Higashijima, Masui, and coworkers have been investigating alpha-factor conformation and the correlation of biological activity to structural features (20, 38, 43-46, 48). There is, however, a great difference between the Naider group and theirs in the categorization of a pheromone as active or inactive. There are also internal inconsistencies in the activity categorization used by the Masui group. We consider any peptide that is more than two

orders of magnitude less active than the natural tridecapeptide to be inactive. In contrast, Masui and coworkers have termed as active a segment of alpha-factor (residues 1-10) exhibiting only one millionth the activity of the tridecapeptide while in a later study they have called inactive the Gly^3-alpha-factor which is one hundred thousand times less active than alpha-factor (38, 43, 46). These inconsistencies make it difficult to understand the conclusions of Masui et al. in correlating NMR spectral parameters with biological activity.

Masui et al. have proposed structures for alpha-factor both in solution and in the presence of phospholipid vesicles (43 -45, 48). Two different solution structures were proposed: one with three beta-turns spanning residues His^2- Gln^5, Lys^7- Gln^{10}, and Gln^{10} -Tyr^{13} and another with a folded alpha-helical structure at the N-terminus (residues 1- 6) and two beta-turns spanning residues Lys^7- Gln^{10} and Gln^{10}- Tyr^{13} (43, 44). The structure with three beta-turns was proposed on the basis of the amide proton chemical shifts, temperature coefficients, pH dependences, and amide - alpha proton spin - spin coupling constants of "active" versus "inactive" peptides (43). In the more recent solution study the alpha-helical, two beta-turn structure was proposed based on the previously obtained data and additional ^{13}C NMR, CD, the pH dependence of fluorescence intensity, and Gd(III) induced broadening studies (44). While chemical shifts can be useful in

determining the presence of conformations other than random coil they cannot provide explicit structural details. The reported temperature coefficients are inconclusive as none of them are in the range expected for intramolecular hydrogen bonding, and all of the coupling constants reported are in the range expected for rapid conformational averaging (59, 60). Gd (III) induced broadening of amide resonances shows greater effects on Gln^{10}, Lys^{7}, and Leu^{6} (Leu^{4} according to our assignments) than on Met^{12} and Gly^{9}. This observation suggests that there may be some folding of the C-terminal domain, but the details of the folding cannot be identified by such data. While ^{13}C NMR studies indicate that both the Lys^{7}- Pro^{8} and Gln^{10}- Pro^{11} peptide bonds are trans, they yield no other information about conformation. CD spectra and fluorescence data demonstrate differences between active and inactive peptides but do not confirm any of the proposed structural features. All of these methods can provide insight into existence of differences between active and inactive peptides but none of them can provide the detailed atom - atom distances necessary to identify specific three dimensional structures.

In more recent lipid studies, Masui et al. have utilized transferred nuclear Overhauser effects (TRNOE) to probe the membrane-bound conformation of alpha-factor and they have proposed an active lipid - bound conformation for the peptide which is different from either of their

proposed solution conformations. This structure is a compact helix at the N-terminus (residues 1 - 5) and an extended structure for residues 7 - 9 (45, 48). Further, while TRNOE studies can provide atom - atom distances, their studies were performed in D_2O and therefore no NOEs involving exchangeable protons were observed (vide infra). Exchangeable protons play important roles in maintaining some of the proposed structural features and their observation is key to determining such structure.

Masui et al. have correlated solution structures of a variety of truncated analogues with biological activity. The analogues have been classified into three groups based on amide proton spectral patterns (44). Two of these groups include both active and inactive analogues while the third consists only of inactive peptides. Based on this classification they conclude that <u>all</u> active peptides have a folded conformation at the N-terminus of the pheromone. <u>Some</u> of the inactive peptides lack this conformation, whereas, based on a simple comparison of the NMR spectral patterns other inactive peptides seem to adopt an N-terminal conformation similar to that of the tridecapeptide. It therefore appears to us that this conformation is either not related to or sufficient for biological activity. The lipid - bound conformations of the alpha-factor and analogue peptides were also related to activity (45, 48). Although these proposed solution and lipid - bound structures have been independently correlated

with biological activity there has apparently been no attempt to unify these correlations and the resulting structural pictures.

As discussed in subsequent pages, NMR in general, and NOEs in particular, can be very useful in probing detailed conformational features of alpha-factor peptides. NOEs between amide protons and alpha or side chain protons in peptides and proteins have been examined in detail and are known to be characteristic of specific structural features (27, 30-33). We have performed a variety of NMR experiments on alpha-factor peptides in solution and in lipid, including NOE experiments in both D_2O and H_2O. The structures proposed by Masui et al. are discussed in light of our results in Chapter V.

CHAPTER II

Fundamental Spectroscopic Principles

NMR: Basic Principles

Nuclei that possess magnetic dipole moments and spin angular momenta interact with a static magnetic field, $B_o = B_o z$, such that the static field exerts a torque which forces the magnetic moments into alignment with the field. The nuclei precess around the static field with an angular frequency, ω_o. According to the Larmor theorem:

$$\nu_o = \omega_o/2\pi = \gamma B_o/2\pi.$$

γ, the gyromagnetic ratio, is unique for different nuclear species and relates the spin angular momentum p to the magnetic dipole moment μ by $\mu = \gamma p = \gamma \hbar I$. I is the nuclear spin and is the quantization of angular momentum in units of $\hbar$ ($\hbar$= Planck's constant/2 π) (61).

In general, 2I +1 nuclear spin orientations are allowed by quantum mechanics. For spin 1/2 nuclei (^1H, ^{13}C, ^{31}P, etc.) two spin orientations are allowed: $/\alpha>$, parallel to the static field and $/\beta>$, anti-parallel to the field. In a magnetic field the energy difference between these two states is ω_o (in radians per second), where $\omega_o = \gamma B_o$. For nuclei with positive gyromagnetic ratio the state parallel to the field is of lower energy. At thermal equilibrium there is a very small excess population in the lower energy spin state depending on the absolute temperature and the magnetic field stength, i.e., governed by the Boltzmann distribution. At room temperature the

excess population in the lower energy state is ~ 10^{-5} providing a net magnetization in the +Z direction as illustrated below.

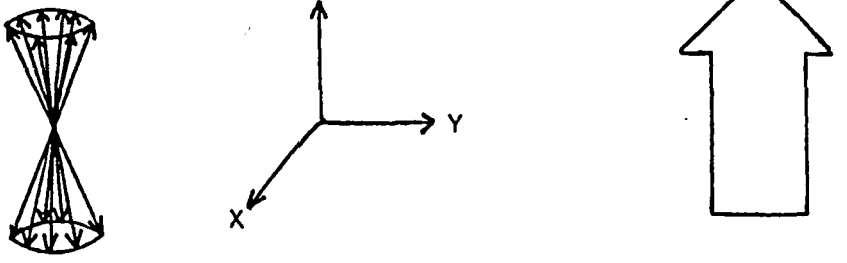

This net magnetization can be tipped from alignment with the static field by application of a rotating magnetic field, B_1, perpendicular to the static field. The magnetization will precess around the resultant field, $B_o z + B_1 x$ at a non-equilibrium angle. The resulting non-equilibrium spin distribution creates a component of magnetization in the transverse plane, and it is this transverse magnetization which is detected in an NMR experiment (62).

Visualizing NMR is simplified by use of a rotating frame of reference (X′,Y′,Z′), where Z and Z′ axes are superimposed but X′ and Y′ rotate with respect to X and Y of the fixed frame (shown below).

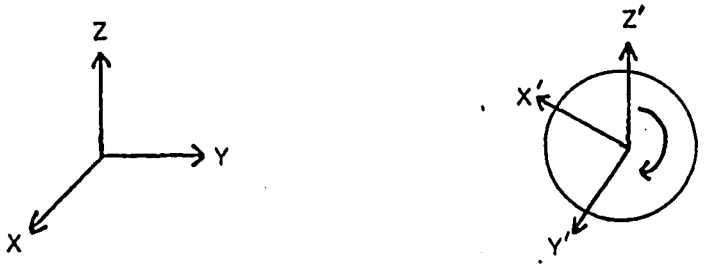

If the frame rotation frequency, ω, is less than the Larmor frequency, ω_o, the magnetization, when viewed in the rotating frame, will precess around Z′ at a reduced

frequency ($\omega_o - \omega$) and the effective field will be reduced, $B_{eff} = (B_o - \omega/\gamma)z'$. The resulting field upon application of B_1 will be $(B_o - \omega/\gamma)z' + B_1x'$. However, if the frame rotation is at the Larmor frequency, magnetization precessing in the X-Y plane will appear stationary in X'-Y', effectively negating the static field B_o. Thus, in the rotating frame the Larmor theorem states that the net magnetization will rotate about B_1 at the angular speed of $\omega_1 = \gamma B_1$ (63).

In practice, the sample signal frequency, ω_o, is detected relative to a reference frequency called the carrier or transmitter frequency. When the carrier frequency is at $\omega = \omega_o$ a rotating frame is created and the sample signal (sample resonance) is detected at $\omega_o - \omega$, that is, there is a frequency offset and the sample signal is "off-resonance". When the carrier frequency is set at ω_o, the sample signal is said to be "on resonance". A sample will actually consist of many different spins, each possessing a characteristic precession frequency. The detected signal will be a superposition of the individual frequencies. Figure 2 illustrates the different signals expected for each of the above situations (63).

In FT NMR B_1 fields are applied as short bursts or pulses of radiofrequency (rf) power. These are square pulses made by rapid on-off switching of the rf transmitter. This rapid switching generates frequency components which provide relatively even excitation over a

FIGURE 2

Time and frequency domain signals expected with different carrier position settings.
A. "on resonance"
B. "off resonance"
C. superposition of different frequencies detected in the time domain signal

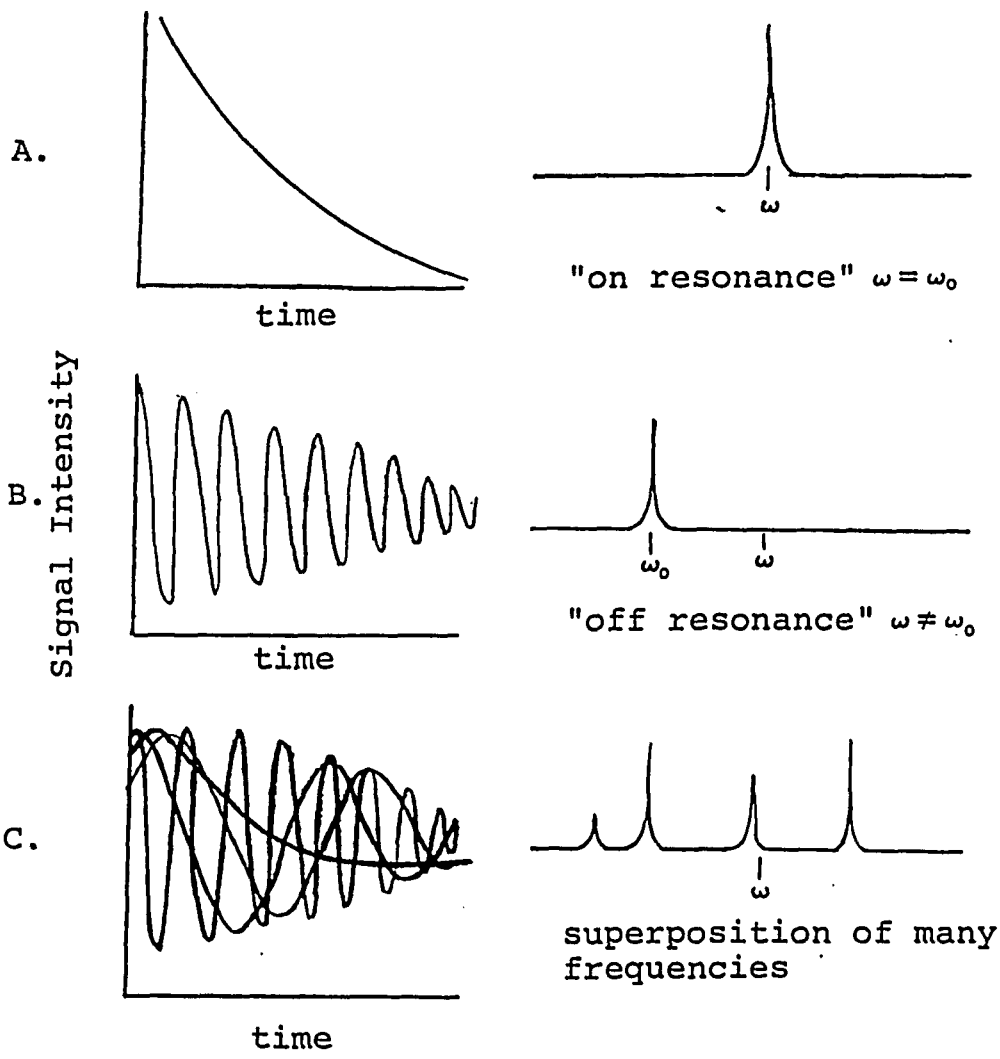
A.
time
ω
"on resonance" ω = ω₀
B.
Signal Intensity
time
ω₀
ω
"off resonance" ω ≠ ω₀
C.
time
ω
superposition of many frequencies

wide frequency range (exciting all resonances of the spectrum). By changing the strength (power) and/or duration (pulse width) of B_1 the net magnetization can be rotated from its equilibrium position as illustrated below (61).

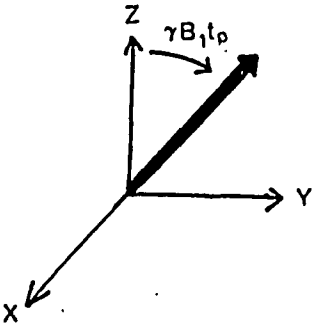

In a routine one pulse Fourier Transform (FT) NMR experiment, the pulse width is typically adjusted to give a tip angle of 90°. This rotates the magnetization completely into the X-Y plane and hence provides maximum signal for detection. After B_1 is turned off, the magnetization, while appearing stationary in the rotating frame, precesses in the laboratory frame at the Larmor frequency as shown below (62).

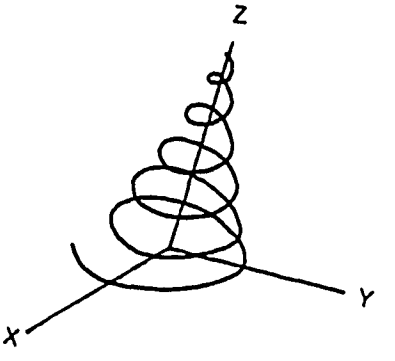

The precessing magnetization relaxes back to its equilibrium value and position, alignment along z and thermal spin populations. The rate of the return to equilibrium depends on the relaxation processes, T_1 (the spin-lattice or longitudinal relaxation) and T_2 (spin-spin

or transverse relaxation) (discussed in more detail below). As the magnetization precesses around B_o and returns to its equilibrium orientation, it induces a decaying voltage in the transverse-oriented detection coil. This induced signal, a free induction decay (FID), is a time domain function. Fourier analysis allows transformation of the time domain data into the frequency domain NMR spectrum (61).

If all nuclei (of the same isotope) in a molecule experienced only the external applied field they would precess at the same frequency, the NMR spectrum would consist of a single resonance line, and very little chemical information would be obtainable. Fortunately, the actual field experienced by each nucleus depends on the local electronic environment of the nucleus as well as the external field. In general, B_o induces electronic fields which oppose and thereby reduce the field experienced by the nuclei. Taking into account the local field, σB_o, the Larmor frequency becomes $\omega_o = B_o(1-\sigma)$. σ, the "screening" or "shielding" constant, expresses the reduction in effective field and is dependent upon chemical structure. Thus, different nuclei in a molecule will experience different local fields; it is this difference which is manifested as chemical shift, δ. (σ is actually a tensor, but for rapidly tumbling molecules and those with symmetric charge distributions the isotropic value $\sigma = 1/3\ (\sigma_{xx} + \sigma_{yy} + \sigma_{zz})$ is observed. Anisotropy arises in slowly tumbling

molecules with asymmetric charge distributions (64).)

The chemical shift is usually reported in parts per million (ppm), a dimensionless unit which is independent of the frequency and field strength and expresses the difference in σ for a particular nucleus relative to that of a standard. A common standard used in proton NMR is tetrametylsilane (TMS). δ for TMS is set at 0.0 ppm and the sample resonance position is reported relative to that. A nucleus that is less shielded (smaller σ) than TMS is assigned a larger δ (see Figure 3). The range of chemical shifts varies greatly for different nuclear species, ~10 ppm for protons and up to ~600 ppm for ^{31}P (65).

The effects of interactions between nuclear spins are more subtle than those with local electronic fields. Scalar or J-coupling is a through bond spin-spin interaction whereby the spin state , $/\alpha>$ or $/\beta>$, of nucleus A is communicated to nucleus B via the bonding electrons. As illustrated in Figure 3 the protons of a methyl group which is scalar coupled to a methine proton see both the $/\alpha>$and $/\beta>$ spin states of the methine proton. Since the probability of the methine proton being in either state is essentially equal, the methyl protons appear as two lines of equal intensity (a doublet). The methine proton sees all possible combinations of the spin states of the methyl protons and appears as four lines with intensities determined by the relative populations in each (a quartet). Because splitting between magnetically equivalent protons

FIGURE 3

The effects of chemical shift and scalar coupling.

A. An example of an NMR spectrum with the δ(ppm) scale and TMS set at 0.0 ppm.

B. The spin states of a methine proton and of methyl protons.

C. Splitting of NMR signals of the methine and methyl protons resulting from scalar coupling-the methine proton sees eight methyl spin state combinations of which two sets of three are degenerate, the methyl protons see the two possible methine spin states. The scalar coupling results in a four line signal (a quartet) for the methine proton and a two line signal (a doublet) for the methyl protons. The lines are separated by J, the scalar coupling constant. The relative intensities of the lines are determined by the populations in each spin state.

D. Scalar coupling is a through bond interaction-the spin state of one proton is communicated to another through the bonding electrons.

A.

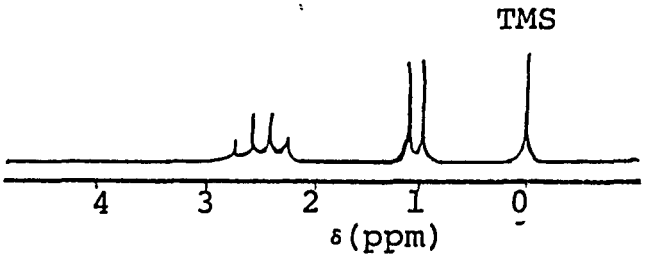

B.

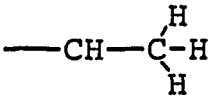

β		βββ	
	αββ	βαβ	ββα
	αβα	ααβ	βαα
α		ααα	

C.

D.

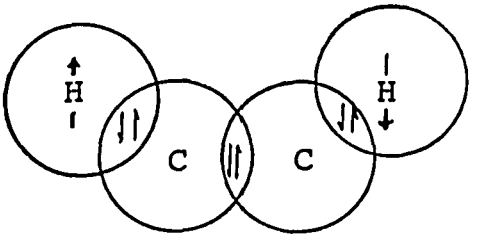

is not observed the three methyl protons do not affect each other. The lines of each multiplet (doublet or quartet) are separated by J, the scalar coupling constant, expressed in Hz. Scalar coupling constants are sensitive to torsion angles and their determinations are useful in deducing structure (66).

The effects of scalar coupling on components of magnetization are best illustrated by a vector diagram (drawn below). As described above, a spin, i, which is scalar coupled to another spin, j, will see both the $|\alpha\rangle$ and $|\beta\rangle$ spin states of j. When the net magnetization is rotated into the transverse plane by a 90° pulse along X two components of magnetization are present for the spin i, one rotating at $\omega_i+J/2$, component B in the diagram, and one rotating at $\omega_i-J/2$, component A in the diagram. The 180° pulse applied along Y rotates the magnetization components clockwise about Y and at the same time inverts the spin state of j, transferring A magnetization to B and B magnetization to A. Component A is now coupled to spin j in the $|\beta\rangle$ state and precesses at $\omega_i+J/2$ (the precession frequency of B) and vice versa.

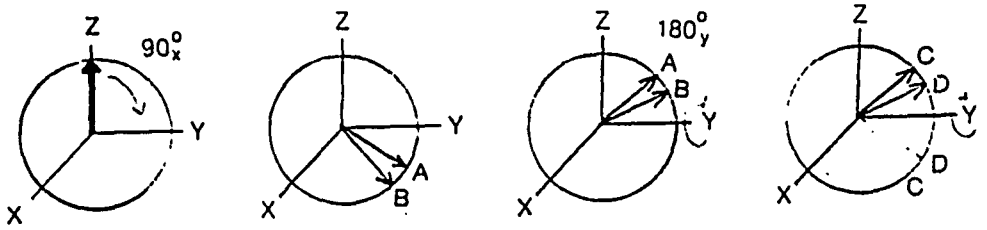

Scalar coupling results in modulation of phase by J. If C and D are the magnetization components of two uncoupled

spins the 180° pulse simply rotates the magnetization about Y. Without the scalar coupling network the inversion of spin state is not communicated, there is no phase coherence to the magnetization transfer (67).

Coherent transfer of magnetization is most efficient when coupled spins evolve only under the influence of scalar coupling and not under the effects of B_o (68). This can be achieved by application of a "spinlocking" field (69). The concept of a "spinlocking" field is illustrated below:

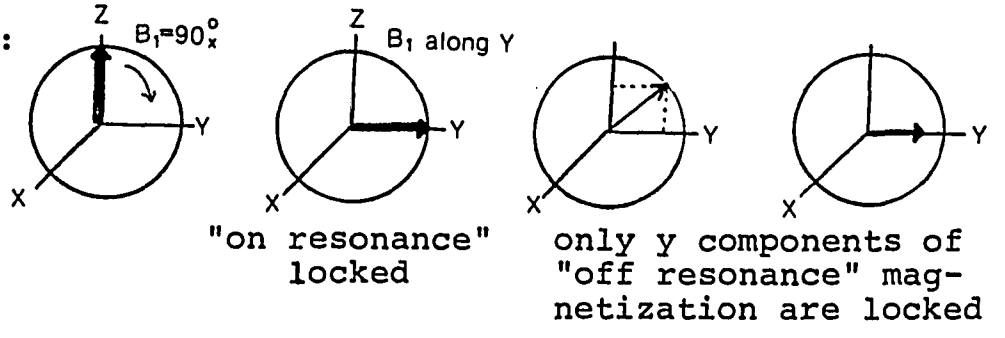

"on resonance" locked

only y components of "off resonance" magnetization are locked

a 90° B_1 pulse is applied along X rotating the magnetization into the transverse plane. The phase of B_1 is immediately changed so that it is along Y where it is maintained with the same magnitude. The components of magnetization parallel to B_1 are locked along Y. When the carrier is set directly between the resonance frequencies of two coupled nuclei, the nuclei have identical frequencies (with opposite sign) in the rotating frame, a condition known as Hartmann-Hahn match (70). Since the X components of magnetization (perpendicular to B_1) quickly dephase due to spatial inhomogeneity of the local B_1 field, Hartmann-Hahn transfer between nuclei far from resonance is less efficient. Hartmann-Hahn transfer is the basis for

Homonuclear Hartmann-Hahn Spectroscopy (HOHAHA) which detects the oscillatory exchange (1/J) of spin-locked magnetization between scalar coupled spins, thus allowing identification of the scalar coupling networks of spins (aiding in resonance assignments) (71).

In addition to scalar interactions, nuclear spins can be involved in dipole-dipole interactions. A magnetic dipole generates a local field, $B_{dd}= \mu (3\cos\theta -1)r^{-3}$, where μ is the dipole generating the field, θ is the angle between the dipole and the point where the field is measured, and r is the distance to that point.

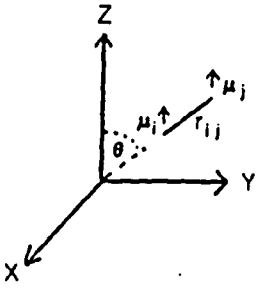

The classical energy of interaction between two magnetic dipoles is given by:

$$E= \mu_1 \cdot \mu_2/r^3 - 3(\mu_1 \cdot r)\ (\mu_2 \cdot r)/r^5.$$

Although the local fields generated by nuclear dipoles are large, chemical shift differences due to dipole-dipole splitting are not observed in most solution state spectra. The interaction does, however, provide an important relaxation mechanism. Interacting dipoles need not be on the same molecule and therefore the distance r may vary randomly. θ varies randomly with molecular motion regardless of whether the dipoles are on the same molecule. These random fluctuations cause individual spins to

experience time-dependent fields, perturbing the populations in each spin state and affecting both transverse and longitudinal magnetization (64, 72).

The transitions possible between two spin 1/2 particles (A and B) which are dipolar but not scalar coupled are illustrated below. Each spin can be in either the /α> or /β> spin state and therefore four combinations are possible: αα, βα, αβ, and ββ.

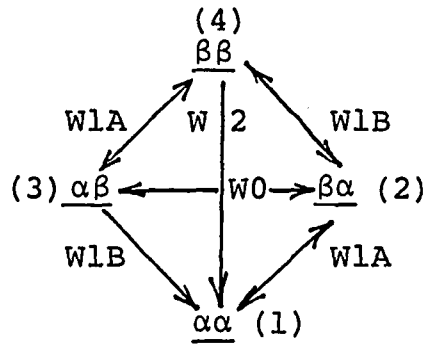

W1A represents A spin transitions connecting (1) to (2) and (3) to (4). W1B represents B spin transitions connecting (1) to (3) and (2) to (4). These are single quantum transitions involving the change in spin state of only one nucleus. W0 is an energy conserving flip-flop transition (connecting (3) to (2)), a zero quantum transition that involves no net change as both spins flip yet remain in opposite orientation (αβ to βα, βα to αβ). W2, a double quantum transition connecting (1) to (4), involves the simultaneous flipping of identical spins (αα to ββ, ββ to αα). These incoherent processes arise from population perturbations and not by phase coherences described above for scalar coupled nuclei (72).

If a radiofrequency pulse is applied at the A spin resonance position with enough power to saturate the A

spins, the populations connected by W1A rapidly equalize (3 = 4 and 1 = 2) and no NMR signal is observed for A. When saturation is applied for a longer time new population distributions arise through W0 (decreases the population of B spins by equilibrating (2) and (3)) and W2 (increases B population by equilibrating (1) and (4)) transitions. The net change in the population of B is the result of competition between W0 and W2 and gives rise to a change in intensity of the B signal. This change is the nuclear Overhauser enhancement factor (η) and thus the intensity of the B spin resonance is 1 + η (the NOE), where 1 = the intensity of the B spin in the absence of irradiation (73).

The nuclear Overhauser enhancement, η, is the ratio of σ_{noe}, the cross relaxation rate, to ρ_{noe}, the direct relaxation rate, and depends on the transition probabilities W1, W0, and W2 (σ_{noe}= W2-W0, ρ_{noe}= 2W1 +W0+ W2). Assuming isotropic motions, σ_{noe}, ρ_{noe}, and therefore the NOE depend on the motional correlation time, τ_c, the frequency, ω_o, and the internuclear distance, r as shown in Equations 1 and 2 :

(1) $$\sigma_{noe}=\left(\frac{\gamma^4\hbar^2}{10r^6}\right)\left(\frac{6\tau_c}{1+4\omega_o^2\tau_c^2}-\tau_c\right)$$

(2 $$\rho_{noe}=\left(\frac{\gamma^4\hbar^2}{10r^6}\right)\left(\tau_c+\frac{3\tau_c}{1+\omega_o^2\tau_c^2}+\frac{6\tau_c}{1+4\omega_o^2\tau_c^2}\right)$$

When $\tau_c^2 < 5/4\ \omega_o^2$, the "extreme narrowing" condition, η is positive and when $\tau_c^2 > 5/4\ \omega_o^2$, η is negative. When $\tau_c^2 >> \omega_o$, W0 transitions dominate and spins diffuse internally

rather than releasing energy to the lattice. The extreme narrowing condition is usually observed for small molecules in solutions of low viscosity where motions are fast and the W0 transition has very low probability. For molecules with longer correlation times and slower motions the energy conserving W0 transition becomes more probable (72, 74).

As shown in Figure 4, $\eta = 0$ when $\omega_o \tau_c = 1.12$. As a consequence of this, no or very small enhancement is detected for molecules with correlation times of 0.1 -1.0 nsec observed at high spectrometer frequencies. However, NOEs measured under spinlocked conditions, i.e. NOEs in the rotating frame, are still manifest. (75) In the rotating frame there are no subtractive terms in the cross relaxation rate and thus such NOEs are always positive and increase with τ_c (Compare Equations 3 and 1) (35, 75).

(3) $$\sigma_{roe} = \left(\frac{\gamma^4 \hbar^2}{20 r^6}\right) \left(4\tau_c + \frac{6\tau_c}{1 + \omega_o^2 \tau_c^2}\right)$$

(4) $$\rho_{roe} = \left(\frac{\gamma^4 \hbar^2}{20 r^6}\right) \left(5\tau_c + \frac{9\tau_c}{1 + \omega_o^2 \tau_c^2} + \frac{6\tau_c}{1 + 4\omega_o^2 \tau_c^2}\right)$$

Population perturbations can give rise to incoherent magnetization transfer between nuclei undergoing chemical exchange (real chemical motion involving bond breaking, ring flipping, etc.) as well as between those that are dipolar coupled (73). In both cases the perturbation of one population will necessarily affect another population. Both types of NOE experiments (laboratory and rotating

FIGURE 4

Plot of the nuclear Overhauser enhancement factor (η) versus the correlation time (τ_C). At $\omega_O \tau_C = 1.12$ $\eta = 0$ and no NOE is detected.

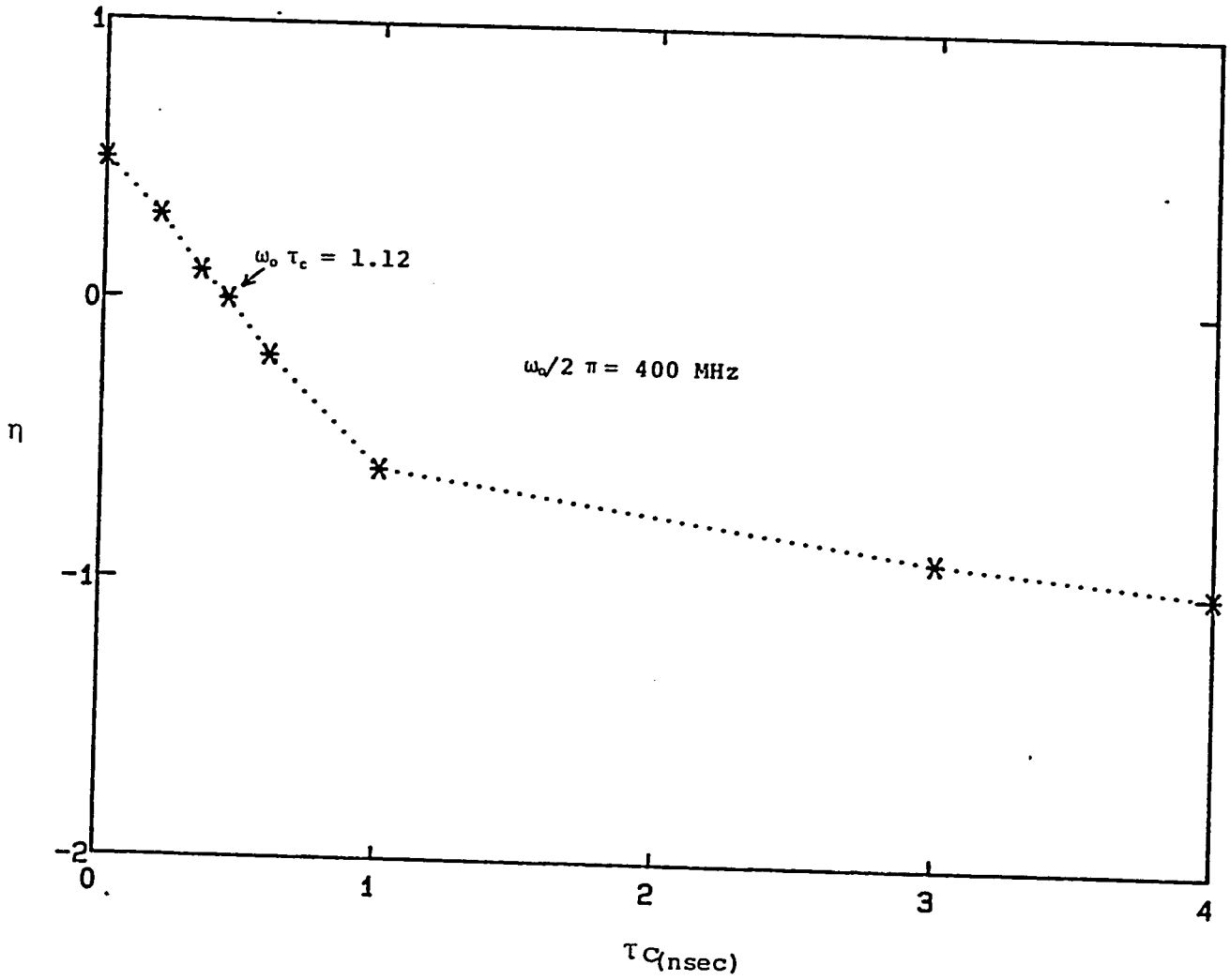
1
0
-1
-2
η
$\omega_o \tau_c = 1.12$
$\omega_o/2\pi = 400$ MHz
0
1
2
3
4
τ_c(nsec)

frame) involve perturbed populations and therefore detect chemical exchange as well as NOE interactions (72, 76).

If a nucleus exchanges between two sites with a rate that is slow on the NMR timescale two different resonances are observed. Perturbation of the population at one site is communicated through chemical exchange to the other site. This behavior is exploited by the transferred NOE (TRNOE) experiment (77). The scheme for the TRNOE is shown below. The TRNOE relies on both chemical exchange and the dipole-dipole interaction to communicate cross-relaxation interactions (NOEs) between two nuclei in a bound state (P_B and L_B) to nuclei in the free state (P_F and L_F). To properly analyze and interpret TRNOEs the NOEs present in the free state must be known.

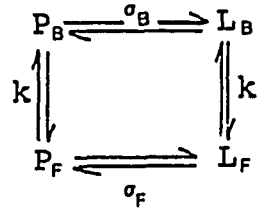

When chemical exchange is fast on the NMR timescale only one resonance is observed and its chemical shift is weighted by the fraction of the population at each site. This behavior can be used to determine binding constants for complex formation by observing the normal NMR spectrum obtained with varying amounts of ligand or receptor.

Consider a 1:1 complex formed between peptide (P) and lipid (L), i.e., the equilibrium:

$$P + L \underset{}{\overset{K_{pl}}{\rightleftharpoons}} PL$$

A nucleus will experience two sites:

$$P \underset{K_p}{\overset{K_{pl}}{\rightleftharpoons}} PL$$

If [L] is very high compared to [P] then k_{pl} is a pseudo first order rate constant for association and k_p is a pseudo first order rate constant for dissociation.

As stated above the observed chemical shift will be a weighted average:

$$\delta_{obs} = f_p \delta_p + f_{pl} \delta_{pl}$$

where δ_{obs} is the chemical shift of the peptide resonance observed at a specific lipid concentration, δ_p is the chemical shift of the free peptide resonance, δ_{pl} is the chemical shift of the fully bound peptide resonance, f_p is the mole fraction of the free peptide, and f_{pl} is the mole fraction of the bound peptide.

This can be rewritten as :

$$f_{pl} = (\delta_{obs} - \delta_p)/(\delta_{pl} - \delta_p)$$

For the peptide-lipid interaction:

$$P + L \underset{}{\overset{K_{pl}}{\rightleftharpoons}} PL$$

$$K_{pl} = [PL]/ [P] [L]$$

and $f_{pl} = [PL]/ [P]_{total}$

$[P]_{total} = [PL] + [P]$ and $[PL] = K_{pl} [P] [L]$.

Substitution gives:

$$f_{pl} = K_{pl} [L]/ 1 + K_{pl} [L]$$

from which the binding constant, K_{pl} can be calculated (78).

NMR: One Dimensional Experiments

The pulse sequence for a simple one pulse experiment

is shown schematically in Figure 5. During the preparation period the spins come to thermal equilibrium following which the 90° pulse tips the magnetization down to the X-Y plane. After the pulse the spins precess with their characteristic frequencies and the FID is detected along the Y axis as a function of t_2. The FID is then Fourier transformed to yield the NMR spectrum in the frequency domain. Because of the low sensitivity inherent in the NMR experiment signal averaging is often required to obtain meaningful intensity. Signal increases at a rate proportional to the number of acquisitions, n, while noise, which is random, is increased by $\sqrt{n}$. Thus, four times as many acquisitions are required to increase the signal to noise ratio, S/N, by two (see Figure 6) (63).

One variation of the simple one pulse experiment utilizes selective irradiation of solvent resonances, useful when an intense solvent signal (e.g. water) will overpower both the spectrum and the electronics. By saturating the water signal much of the NMR signal is nulled and the digitizer is able to provide sufficient resolution of the smaller resonances. Figure 7 is an example of the spectra obtained with and without saturation of the water resonance (63).

Modern NMR experiments also utilize rf phase cycling, ie. systematic change of the pulse and receiver phases. This helps to eliminate artifacts arising from pulse imperfections and field inhomogeneity. Phase cycling also

FIGURE 5

Pulse sequence for a simple 1D NMR experiment. Magnetization is tipped down to the transverse plane by the 90^{o} pulse. The signal is detected during t_2 and is Fourier transformed to yield the NMR spectrum.

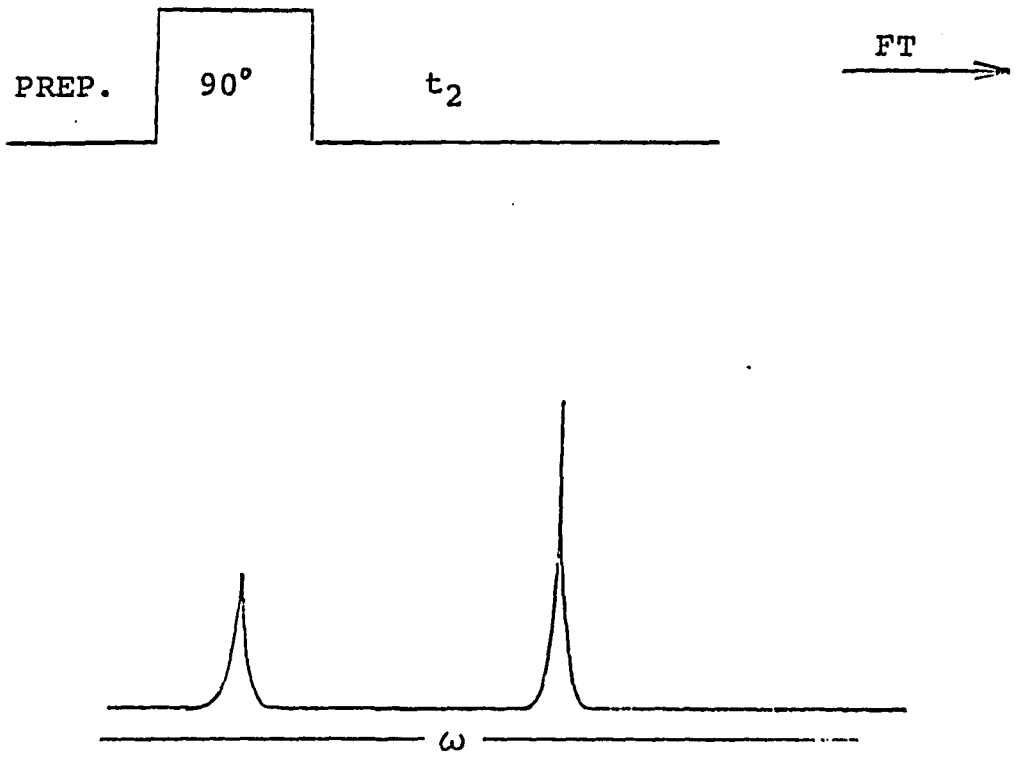
PREP.
90°
t_2
FT
ω

FIGURE 6

Results of signal averaging on the signal to noise ratio.
1% ethylbenzene in deuterated chloroform at 23°C.
A. 1 scan
B. 4 scans
C. 16 scans
D. 64 scans

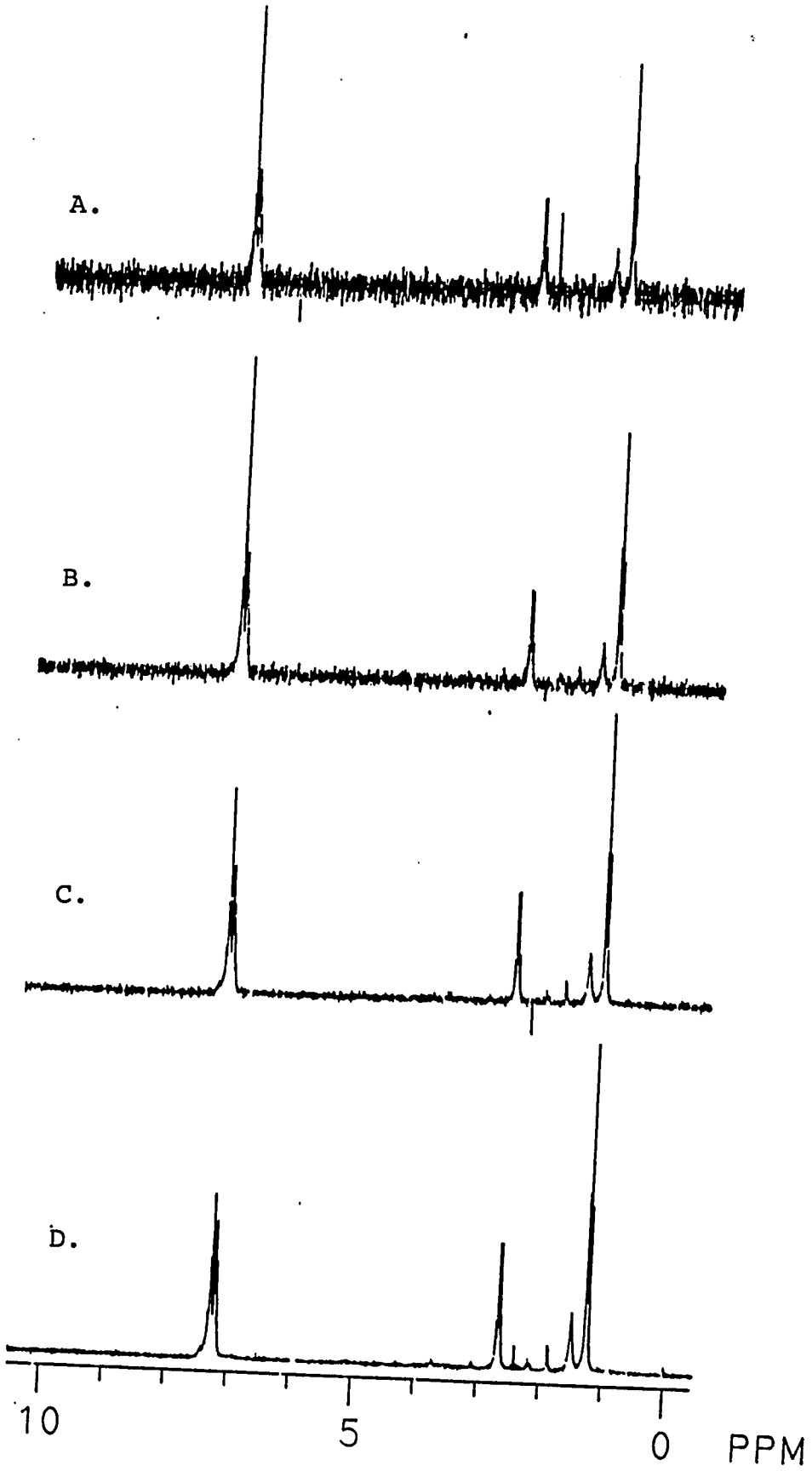
A.
B.
C.
D.
10
5
0
PPM

FIGURE 7

Comparison of spectra obtained with and without saturation of the solvent resonance.
2mM DNA octamer in D_2O at 5^oC.
A. 16 scans with saturation of the residual HOD peak (at approximately 5 ppm)
B. 16 scans without saturation of the HOD peak.

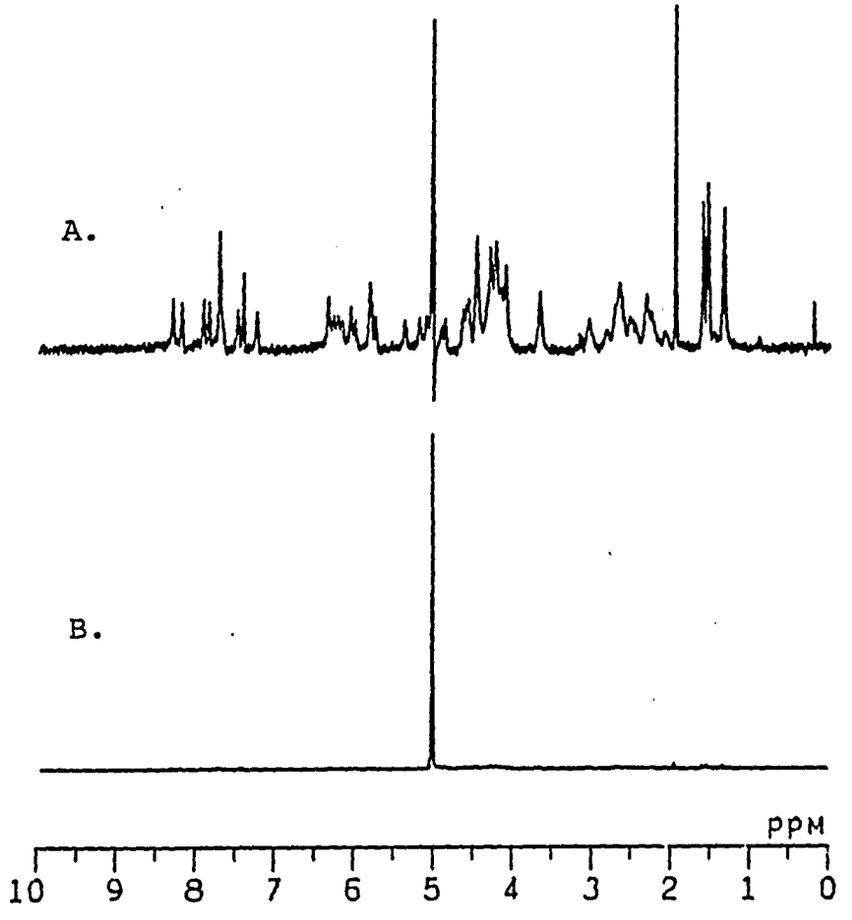
A.
B.
ppm
10
9
8
7
6
5
4
3
2
1
0

suppresses spurious (non-NMR) signals (computer clock, radio) and is used to suppress undesired NMR signals excited by certain pulse sequences (73).

Several frequently used one dimensional NMR experiments are those used to measure relaxation times. Relaxation times can yield information on molecular motion, order, diffusion, and structure. T_1, the spin-lattice or longitudinal relaxation time, describes the rate of recovery of the Z component of the magnetization towards its equilibrium value and involves transfer of energy from the spin system to the lattice. T_2, the spin-spin or transverse relaxation time which describes the loss of phase coherence of a spin system is an entropic effect and involves energy transfer only within the spin system. Both T_1 and T_2 depend on high frequency (rapid) motions, however T_2 is also very sensitive to low frequency (slow) motions (63).

Relaxation processes that contribute to T_1 and T_2 include those arising from dipolar interactions (discussed above), spin rotation, chemical shift anistropy, scalar interactions, and quadrupolar interactions. Chemical shift anisotropy (CSA) is particularly important as a relaxation mechanism for nuclei with asymmetric charge distributions and large chemical shift ranges (^{31}P, for example). For nuclei in axially symmetric sites σ becomes $1/3(\sigma_{\parallel} + 2\sigma_{\perp})$. Quadrupolar relaxation arises from interaction of the nuclear spin ($I > 1/2$) with fluctuating electric field

gradients generated by molecular motion. This mechanism dominates for quadrupolar nuclei (^{2}H, ^{14}N, etc.) with non-spherical electrical charge distributions. Spin rotation and scalar relaxation are not important mechanisms for ^{1}H, ^{2}H, and ^{31}P (79).

T_1 relaxation times are often measured with the inversion-recovery pulse sequence shown in Figure 8. The 180° pulse inverts the magnetization which relaxes back toward its equilibrium value during tau. A 90° pulse at the end of tau rotates the magnetization back to the transverse plane where the FID is detected. If tau is very long (5-20 times T_1) the spins will have fully relaxed and the maximum magnetization will be detected; if tau is very short the spins will have only begun to relax and the magnetization will still be inverted upon application of the detection pulse. T_1 can be determined from intensities as a function of tau (80).

T_2 relaxation times are often reported as T_2^*. These values are calculated from the full linewidth of the resonance at half-height from the relationship $T_2^*=1/\pi\nu$. However because the linewidth is sensitive to field (and sample) inhomogeneity as well as relaxation processes T_2 and T_2^* can differ. Actual T_2 relaxation times are measured in a manner similar to T_1 using the spin-echo pulse sequence shown in Figure 9. The 90° pulse rotates magnetization to the transverse plane where it precesses during tau. Spins lose phase coherence and relax by any of

FIGURE 8

T_1 relaxation time measurement.
A. Inversion-recovery pulse sequence for measurement of T_1 relaxation times.
B. Example of a stack plot of the spectra obtained with varying τ values.
C. Plot of peak height versus τ used to determine T_1.

(The stack plot presented in the figure is taken from reference 79)

A.

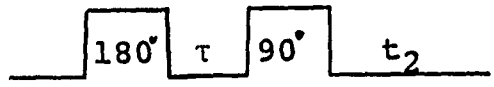
180°
τ
90°
t_2

B.

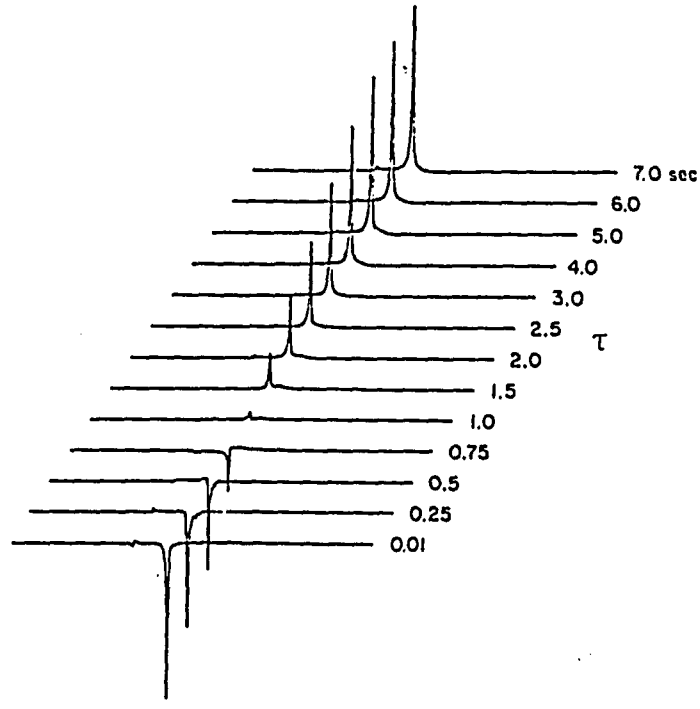
7.0 sec
6.0
5.0
4.0
3.0
2.5
2.0
1.5
1.0
0.75
0.5
0.25
0.01
τ

C.

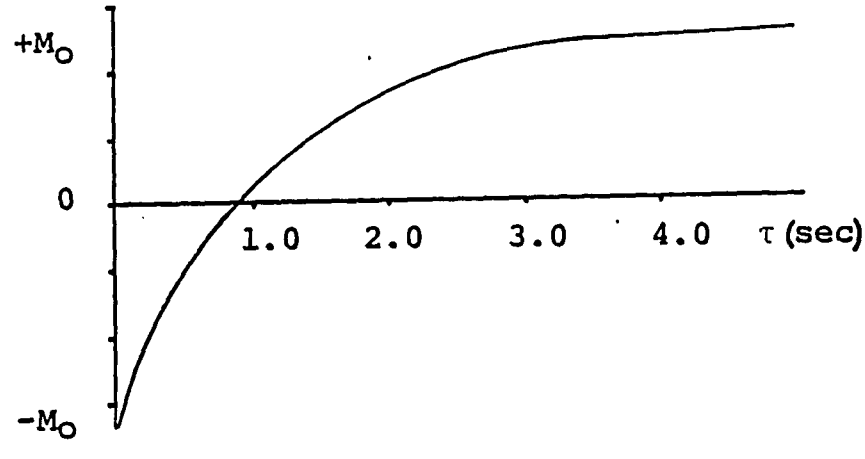
+M_o
0
-M_o
1.0
2.0
3.0
4.0
τ (sec)

FIGURE 9

T_2 relaxation time measurement.
A. Spin-echo pulse sequence.
B. Behavior of magnetization:
   a. the magnetization is at equilibrium, with net magnetization along +z.
   b. the 90° pulse tips the magnetization to the transverse plane.
   c. during τ spins have dephased.
   d. the 180° pulse flips the magnetization around the y axis.
   e. after another τ the spins have rephased and an echo (with reduced intensity relative to the intensity present at b) is detected during t_2.
C. Plot of peak height versus τ from which T_2 is determined.

A.

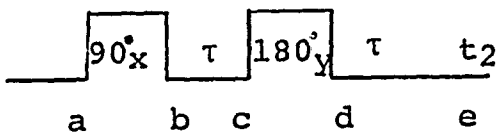

B.

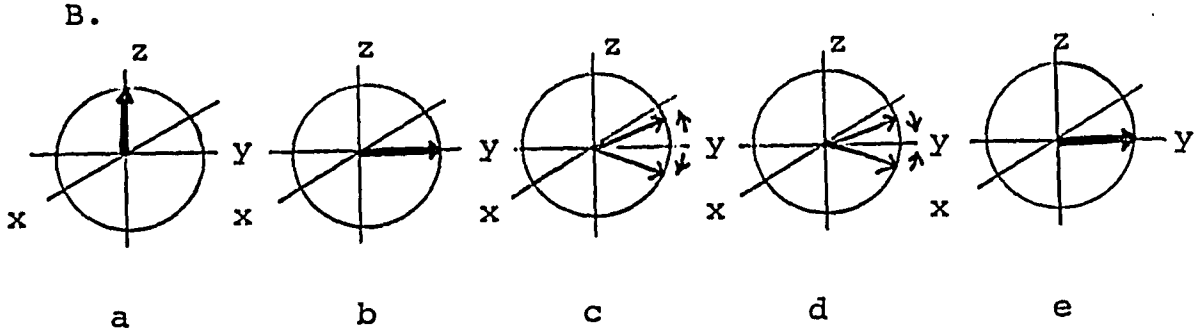

C.

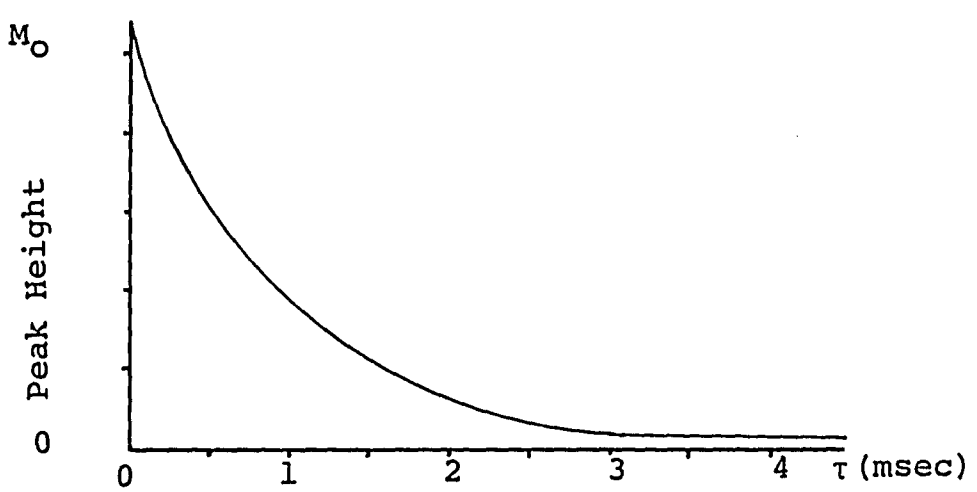

the mechanisms described above. The 180° pulse along the Y axis flips the spins such that they will rephase after another tau period. This leads to an echo, acquired during t_2, which has reduced intensity due to T_2 relaxation ocurring during tau. The behavior of the magnetization is shown schematically in Figure 9 (61).

The spin echo method was originally proposed by Hahn (with both pulses along X) to overcome field inhomogeneity which contributes to the linewidth. The procedure is repeated with varying tau values. A modification of the basic Hahn spin-echo experiment described by Carr and Purcell involves the application of a series of 180° pulses collected after successive delays of 2 tau (tau being shorter than in the Hahn spin-echo experiment). The Carr-Purcell method saves time since a train of echoes is acquired with a single experiment. Further, the reduction in echo amplitude caused by the diffusion of nuclei in an inhomgeneous field during tau is avoided by use of the short tau. A further modification by Meiboom and Gill involves application of 180° pulses along Y instead of X which serves to reduce effects caused by imperfect pulse widths. The CPMG experiment can be performed like the Hahn spin-echo by simply varying tau which is effective when T_2 is short enough that effects of field inhomogeneity will not be observed. For longer T_2s and/or conditions where field inhomogeneity is expected the experiment can be performed by applying successive 180° pulses. T_2 is

determined from a plot of the peak amplitude as a function of tau (Figure 9) (61, 80).

NMR: Two Dimensional Experiments

A General Description

In the one dimensional NMR experiments described above the FID is obtained as a function of one time variable, the detection period, t_2. In two dimensional NMR a second time variable is introduced and is incremented so that the acquired FIDs are a function of two time periods: an evolution time, t_1, and the detection period, t_2 (73).

There are four basic intervals in the two dimensional NMR experiment: preparation, evolution, mixing, and detection:

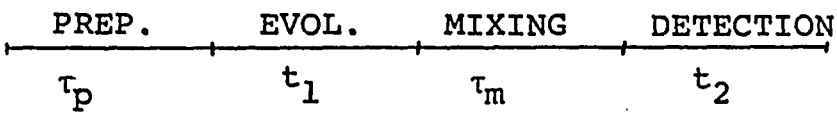

During the preparation period equilibrium is established and a pulse (or pulses) of duration τ_p creates a non-equilibrium state which is then allowed to evolve during the evolution period, t_1. Spectral information is enhanced during the mixing period by either a mixing pulse as in the COSY experiment or by a mixing time and pulse(s) as in the NOESY experiment (both discussed in more detail below). As in the one-dimensional experiment the signal is detected during t_2 (81).

Two dimensional data are acquired as a collection of one-dimensional FIDs differing only in the length of the t_1

period (see Figure 10). Typically, 512 real and 512 imaginary points are recorded in the t_2 domain for each of the 512 t_1 values; t_1 values are incremented by a fixed amount in consecutive spectra. The individual spectra are Fourier transformed in the t_2 dimension and the data set is then transposed. A second Fourier transform is performed in the t_1 dimension to yield the final two dimensional spectrum. The time domain data (t_2 and t_1) can be multiplied by a variety of different mathematical functions to enhance spectral resolution (82).

The final spectrum, a square 512 point by 512 point data matrix, can be presented as a stack plot (similar to those shown for T_1 data) or as a contour plot. A contour plot is made by slicing through the 2D data set as if the peaks were mountains and then presenting different elevations or thresholds. The resolution in each single spectrum in the two dimensional data set is much less than that of a normal one dimensional NMR spectrum, usually acquired with 16-32 K data points. However because there are <u>two</u> dimensions in the 2D spectrum resonances are usually well resolved (82).

There are three classes of response which appear in a two dimensional spectrum: axial peaks, diagonal peaks, and cross peaks. The axial peaks arise from longitudinal magnetization which remains after t_1 and they appear with their normal f_2 frequencies at $f_1 = 0$. These yield little useful information and phase cycling of the pulses and

FIGURE 10

Scheme of 2D data acquisition:
"n" number of 1D experiments are acquired as a function of the two time variables-t_1 and t_2.
These are Fourier transformed in the t_2 dimension.
The data is then transposed and Fourier transformed in the t_1 dimension.
The final spectrum can be presented as a Stack Plot or a Contour Plot.

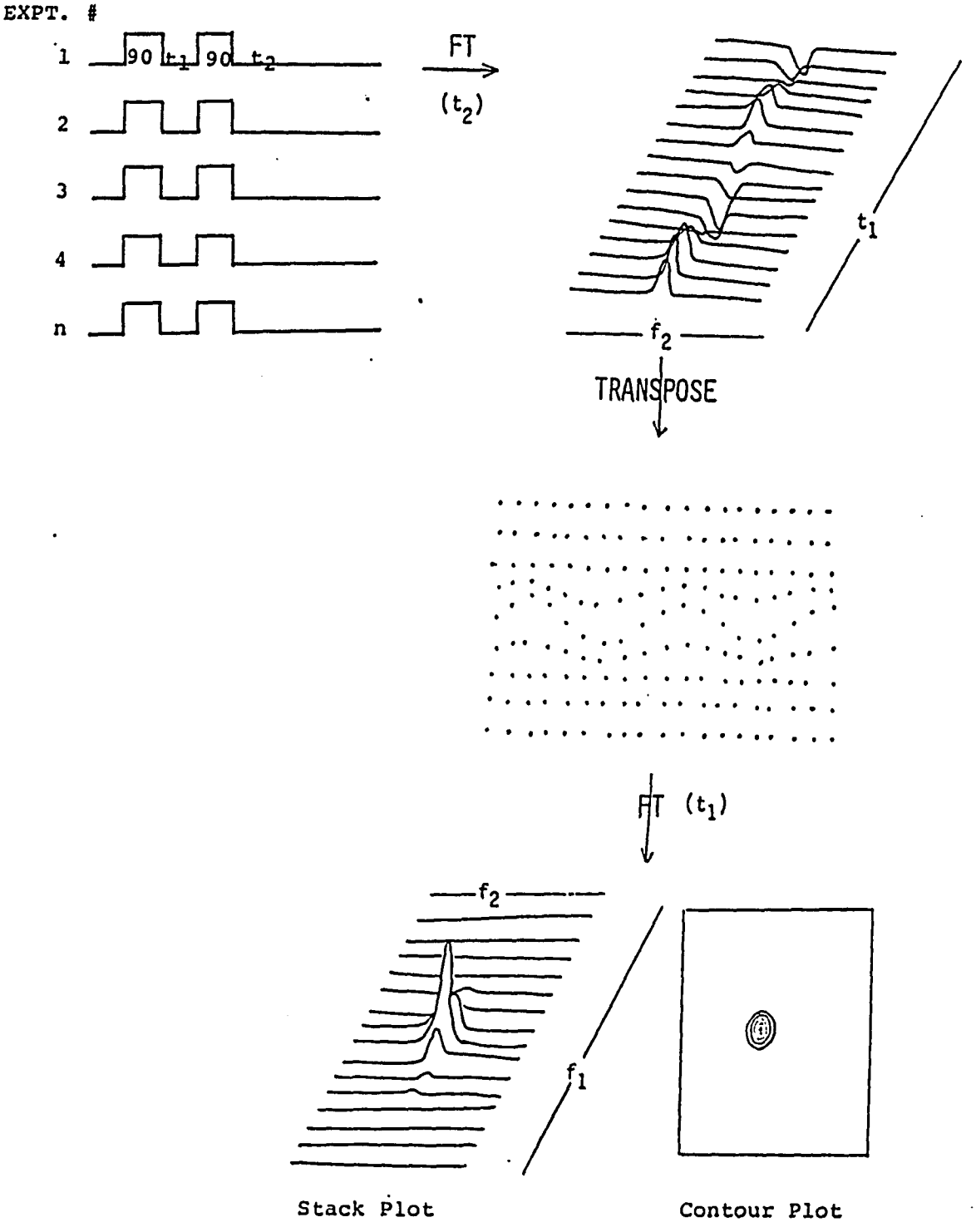
EXPT. #
1
90 t_1 90 t_2
2
3
4
n
FT
(t_2)
t_1
f_2
TRANSPOSE
FT (t_1)
f_2
f_1
Stack Plot
Contour Plot

receiver is usually employed to suppress them. Diagonal peaks appear at $f_2=f_1$, and are due to transverse magnetization which is associated with the same resonance during t_2 and t_1. These peaks are representative of the one dimensional spectrum. Cross peaks indicate magnetization which is associated with one frequency during t_2 and another during t_1. The information content of the cross peaks is determined by the pulse sequence (i.e., scalar coupling in the COSY experiment, dipolar coupling in the NOESY experiment) (81).

Correlated Spectroscopy

The well known COSY (Correlated Spectroscopy) experiment was first proposed by Jeener at the Ampere International Summer School, Baske, Polje, Yugoslavia in 1971, yet instrumental requirements prohibited its implementation for several years. Today this experiment is one of the most commonly performed 2D NMR experiments because of its power in assigning the resonances of even very complicated spectra. The COSY spectrum traces spin system connectivities via the spin-spin coupling network. The pulse sequence shown in Figure 11 consists of two 90 degree pulses separated by t_1. The first pulse tips the net magnetization from the z axis into the transverse plane where the spins precess with their characteristic frequencies during t_1. The second pulse serves as a mixing pulse and generates new coherences which depend on homonuclear spin coupling. This mixing of spin states

FIGURE 11

COSY, NOESY, and ROESY pulse sequences.
A. COSY
B. NOESY
C. ROESY

A.

COSY

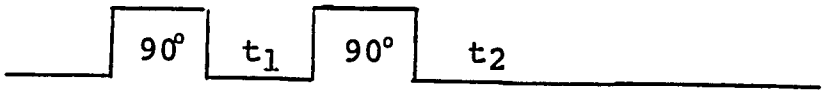

B.

NOESY

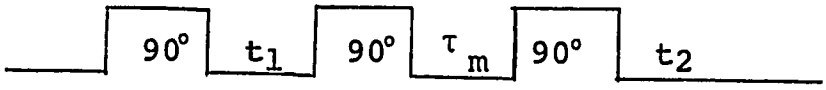

C.

ROESY

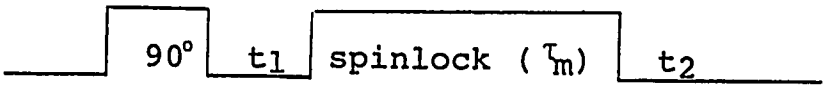

transfers transverse magnetization between multiplets. The COSY spectrum has cross peaks connecting multiplets which are scalar coupled and diagonal peaks representing the one-dimensional spectrum (67).

Nuclear Overhauser Effect Spectroscopy

Nuclear Overhauser Effect Spectroscopy (NOESY) takes advantage of the nuclear Overhauser effect, providing distance information about dipolar coupled spins. The NOESY pulse sequence is shown in Figure 11. The first two pulses are like those of the COSY experiment. However, during the mixing time, τ_m, incoherent magnetization transfer occurs between dipolar coupled spins. Longer mixing times allow dipolar interactions between protons that are further apart in space. Phase cycling must be employed to suppress contributions from the coherent processes generated by the "COSY" pulses. The resulting spectrum contains cross peaks between spins which are dipolar coupled and are of positive intensity relative to the diagonal (again representative of the one dimensional spectrum). The signs of cross peaks in the 2D spectrum are opposite to the effect observed in the one dimensional experiment, that is, positive η is manifested as a negative crosspeak in the 2D spectrum while negative η gives rise to a positive crosspeak. This results because the one dimensional experiment involves a transfer of negative magnetization, saturation, while the 2D experiment involves an exchange of positive magnetization. As in the one

dimensional experiment interactions between nuclei undergoing chemical exchange can also be observed (74).

Rotating Frame Nuclear Overhauser Effect Spectroscopy

Rotating Frame Nuclear Overhauser Effect Spectroscopy (ROESY) described by Bothner-By (75) and Bax and Davis (35) measures the rotating frame NOEs under spin locked conditions. As discussed earlier, rotating frame NOES are always positive (although they can be very small) while laboratory frame NOEs go through a null at $\omega_o\tau_c$=1.12. It is under these conditions that the ROESY experiment is advantageous over the NOESY experiment.

The ROESY pulse sequence is shown in Figure 11. A 90° pulse tips the magnetization down to the transverse plane where the spins evolve during t_1 as described before. However, the application of a strong rf field during τ_m spin locks magnetization components along the field (along the y axis) where dipolar exchange occurs. The FID is acquired during t_2 and FT yields the final spectrum which contains positive cross peaks indicating NOEs between dipolar coupled spins. Unlike the NOESY spectrum, the diagonal peaks (representative of the one dimensional spectrum) and cross peaks between spins undergoing chemical exchange or Hartmann-Hahn transfer are negative relative to the NOE crosspeaks (76). Because this experiment employs a spin locking field it is also possible to detect coherence transfer between spins due to Hartmann-Hahn transfer and scalar interactions (COSY type transfer) (35). Cosy type

cross peaks integrate to zero because they appear as dispersive signals while Hartmann-Hahn type cross peaks are of the same phase as the diagonal (negative relative to NOEs). Because Hartmann-Hahn peaks are of opposite intensity, contributions due to this type of transfer will decrease the observed NOE intensity. Measurements with different carrier positions allow the determination of contributions from a Hartmann-Hahn match. Figure 12 shows an example of a ROESY spectrum plotted with negative and positive contours.

Quasi-Elastic Light Scattering

Quasi-elastic Light Scattering (QLS) is used to determine the mean hydrodynamic radius, R_h, of micelles and vesicles. (83) The intensity of the light scattered by a sample placed in a beam (of light) will fluctuate in a time-dependent fashion as a result of the Brownian motions of the particles in the sample. (84) The light scattered 90° from the incident beam is detected by a photon counting system. Analysis of the autocorrelation function of the scattered light (Equation 5) yields an average diffusion coefficient (Equation 6) from which a mean hydrodynamic radius is extracted (Equation 7) (85):

(5) $R(\tau)/R(0) = (\Sigma_{n=1}^{\infty} G_n e^{-\Gamma_n \tau})^2$

Γ is the constant for the decay in intensity of the scattered light and is proportional to 1/D, with D being the diffusion coefficient for a monodisperse system. $e^{-\Gamma_n \tau}$ is the autocorrelation function of each species (in a

FIGURE 12

Positive and negative contours of a schematic ROESY spectrum.
A. Positive contours, NOE crosspeaks, are presented.
B. Negative contours, diagonal peaks, crosspeaks between chemically exchanging protons or due to Hartmann-Hahn interactions.
The dotted lines are presented to show connectivities between diagonal and crosspeaks and to indicate the position of some of the diagonal peaks in the spectrum with positive contours

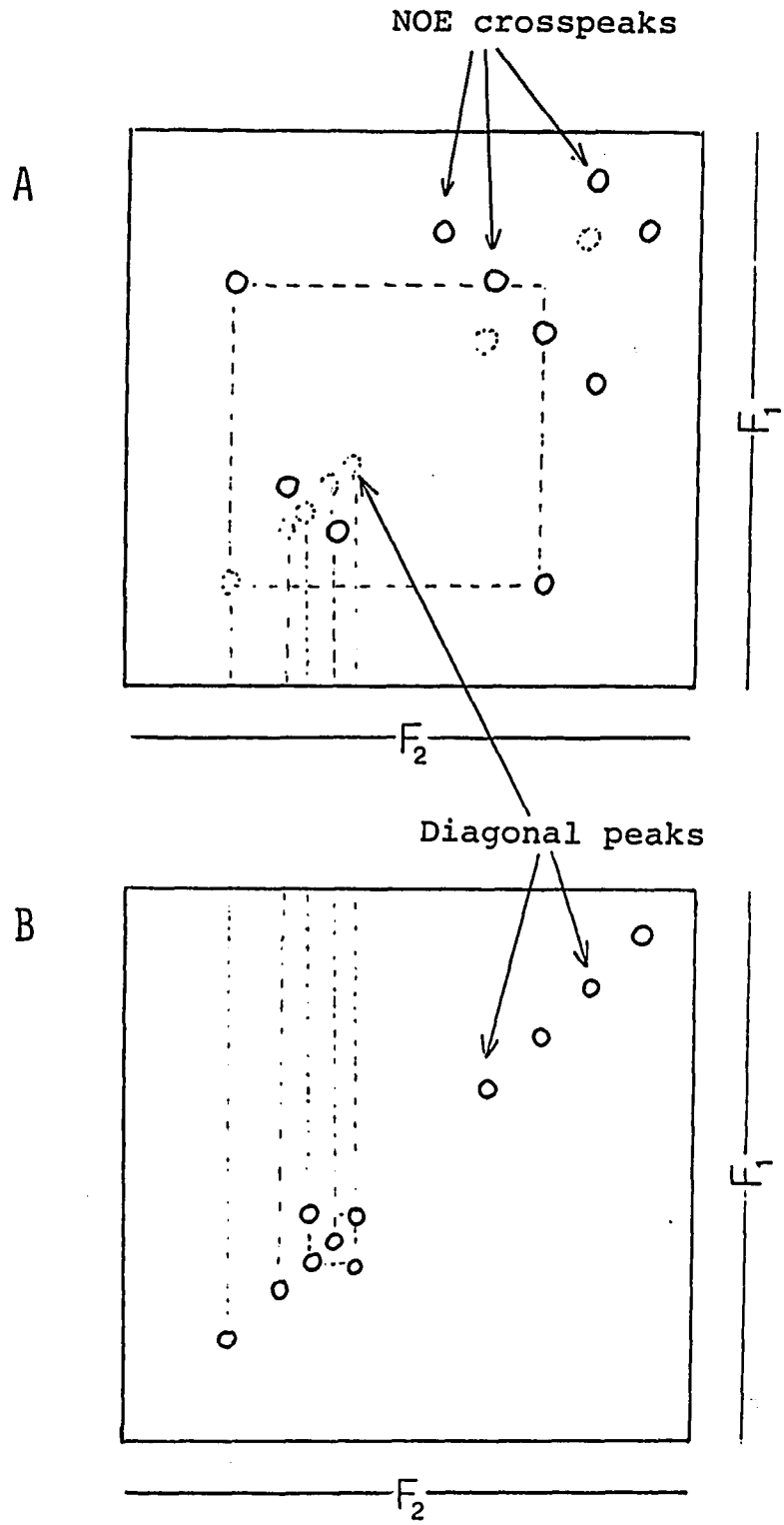
NOE crosspeaks
A
F_1
F_2
Diagonal peaks
B
F_1
F_2

polydisperse system) and is weighted by G_n, the fraction of the light scattered by each species where:

$$G_n=C_nM_n/(\Sigma C_nM_n)$$

(C_n and M_n are the weight concentration and the molecular weight of the nth species respectively).

For a monodisperse system Γ is simply proportional to 1/D and the mean translational diffusion coefficient, D, is calculated from the average decay constant:

(6) $D=\bar{\Gamma}/q^2\Gamma$

(where $\bar{\Gamma}=\Sigma G_n\Gamma$ and q is the magnitude of the scattering vector).

The mean hydrodynamic radius is calculated from the Stokes-Einstein relation (assuming a spherical particle):

(7) $R_h = k_bT/(6\ \pi\eta D)$

(where k_b is the Boltzmann constant, T is the absolute temperature, and η is the solvent viscosity). The polydispersity of a system is characterized by the variance, which is the standard deviation of the mean decay constant:

$V = 100\ x\ (\bar{\Gamma}^2-\Gamma^2)^{1/2}/\Gamma$ (85).

CHAPTER III

Materials and Methods

The Samples

Solution Phase Samples

Studies in Dimethyl Sulfoxide (DMSO-d_6)

The peptides listed below were placed in Wilmad 528-PP (5 mm) NMR tubes and each was dissolved in 0.5 ml of DMSO-d_6 (Cambridge Isotope Laboratories (CIL), Woburn, Massachussetts).

Sample	Weight (mg)
alpha-factor tridecapeptide	2.0
des-Trp^1,Cha^3-alpha-factor	4.0
" [α-^{2}H]Met^{12}	4.0
" [α-^{2}H]Tyr^{13}	4.0
" [α-^{2}H]Gln^{10}	2.0
" D-Leu^9	2.0
" L-Leu^9	2.0
" D-Ala^9	2.0
" L-Ala^9	2.0
His-Cha-Leu-Gln-Leu-Lys-Pro	5.0
Gly-Gln-Pro-Met-Tyr	5.0
[α-^{2}H]Gln^{10}-Ala-alpha-factor	2.0
[α-^{2}H]Gln^{10}-Glu-Ala-alpha-factor	2.0

Studies in Aqueous Solution

Each of the peptides listed below was placed in a Wilmad 528-PP (5 mm) NMR tube and was dissolved in either D_2O

(CIL) or in H_2O/D_2O (9/1), the pH adjusted to ~4.6. No corrections were made for deuterium isotope effects on pH.

Sample	Weight(mg)
alpha-factor	2.0
[α-^{2}H]Leu^6-alpha-factor	2.0
[α-^{2}H]Leu^{4,6}- "	2.0
[α-^{2}H]Gln^{10}- "	2.0
[α-^{2}H]Met^{12}- "	2.0

Lipid-Peptide Studies

Initial Studies

Lipid sample:

1) lysomyristoylphosphatidylcholine (2mM)
   (provided by Prof. Robert Bittman, Queens College, CUNY)
2) eggphosphatidylcholine:phosphatidylglycerol(16mM, 3:1) (provided by Prof. Bittman)

Alpha-factor concentration : 2mM for studies with lysomyristoylphosphatidylcholine, 4mM for studies with egg phosphatidylcholine:phosphatidylglycerol.

Major Studies

Lipid Samples:

L-α-dipalmitoylphosphatidylcholine (DPPC) (Sigma Chemical Corporation, St. Louis, Missouri) T_c~41°C MW=734.0

L-α-dipalmitoylphosphatidylcholine, chain deuterated (DPPC-d_{62}) (CIL)

L-α-dioleoylphosphatidylcholine (DOPC) (Sigma) T_c ~-22°C MW=786.1

L-α-dioleoyl-[9,10-^{2}H]-phosphatidylcholine (DOPC) (a gift of CIL)

L-α-distearoylphosphatidylcholine (DSPC) (Sigma) T_c (~58°C, ~54°C)* MW=790.2

L-α-dipalmitoylphosphatidylethanolamine (DPPE) (Sigma) T_c ~60°C MW=692.0

L-α-dioleoylphosphatidylethanolamine (DOPE) (Sigma) T_c ~0°C MW=744.0

L-α-dipalmitoylphosphatidic acid, sodium salt (DPPA) (Sigma) T_c ~67°C MW=670.9

Plant phosphatidylinositol, Soybean (PI) (Avanti Polar Lipids, Birmingham, Alabama) T_c ~50° MW=885.1

Brain phosphatidylserine, Bovine (PS) (Avanti) T_c ~5°C MW=832.0

The T_c values listed above are those reported in the literature for pure lipid samples. T_c is the temperature at which the hydrocarbon chains of the lipid undergo a transition from the gel to liquid crystalline state.

The above lipids (except for lysomyristoylphophatidylcholine, which formed micelles upon vortexing) were prepared as vesicles (vide infra) in D_2O (CIL) or H_2O/D_2O (9:1) at a pH of ~7.0 and with a lipid concentration of 16mM unless otherwise noted in the text. The mixed vesicles were prepared with the following weight percentages of the various phospholipid components: 35% PI, 28% PE, 28% PC, 7.5% PS, and 1.5% PA. These percentages are similar to

*Both 58°C and 54°C were reported for the T_c of DSPC.

those found in the yeast plasma membrane (86). Samples for the ^{1}H NMR studies of the peptide-lipid interaction were 4mM alpha-factor (unless otherwise noted). Those for ^{2}H and ^{31}P NMR studies were 1mM alpha-factor (50 μM EDTA was added to prevent paramagnetic broadening of the spectral lines). Samples for QLS measurements were prepared from the NMR samples and were diluted: 10 μl in 1 ml of distilled water. Although this is a 1/100 dilution we believe the QLS measurments represent the vesicle sizes and dispersity present in the more concentrated NMR samples. NMR samples were placed in either Wilmad 528-PP 5mm or 513-PP 10mm NMR tubes for ^{1}H or ^{31}P and ^{2}H studies respectively. Peptide was added to the vesicle preparation as a concentrated solution at pH ~7.0. Sample pH recordings do not take the deuterium isotope into consideration.

Peptide Synthesis

All dodecapeptide and tridecapeptide alpha-factor samples used in the solution studies in DMSO were synthesized by Dr. Ponniah Shenbagamurthi (College of Staten Island, CUNY) as previously described (40, 42). The heptapeptide and pentapeptide fragments were also synthesized by Dr. Shenbagamurthi (17). Tetradecapeptide and pentadecapeptide alpha-factor samples were synthesized by Michael Tallon (College of Staten Island) (87). Tridecapeptide samples for the aqueous solution studies were synthesized by Jose Pardinas (College of Staten

Island).

Tridecapeptide samples for the lipid-peptide studies were synthesized by the solid phase techniques described by Merrifield (88) using a Vega Model 250 Peptide Synthesizer.

The spacer group, t-butoxycarbonyl-O-(2-Bromo-CBZ)-L-tyrosine p-methoxy phenylacetic acid phenacyl ester (Boc(BrZ)Tyr-OMPA-OPa), was synthesized as described by Tam et al. (89). This was reduced to Boc(BrZ)Tyr-OMPA-OH with zinc dust/acetic acid and was coupled to aminomethylated polystyrene resin (synthesized by Dr. Jaya Srinivasin College of Staten Island) using dicyclohexylcarbodiimide (DCC) as the coupling agent. Both the reduced spacer and DCC were present in two fold excess. The reaction vessel was shaken for 16 hours. The resin was dried in a dessicator. The Kaiser test revealed no free amino groups (90).

The BOC-Tyr-resin was then used in solid phase synthesis of alpha-factor similar to that described by Tallon et al. (87). Deprotection (removal of the BOC groups) was achieved by acidolysis with 40% trifluoroacetic acid (TFA, Aldrich))/2% dimethyl sulfide (DMS, Aldrich) in methylene chloride (CH_2Cl_2, Fisher). This produced a polymer-bound TFA salt. Excess TFA was removed by repeated washings with CH_2Cl_2 and 8% N,N- diisopropylethylamine (Aldrich) in CH_2Cl_2. The free amino group of the growing resin-bound peptide was then condensed with the next BOC-amino acid using DCC/CH_2Cl_2. 1-Hydroxybenzotriazole and

DCC in dimethylformamide (DMF, J. T. Baker Chemical Company) replaced the DCC/CH_2Cl_2 as the coupling reagents for the two glutamine residues. All residues were double coupled regardless of results of the Kaiser test. After each double coupling the resin was washed with CH_2Cl_2 and isopropyl alcohol.

BOC-amino acids with potentially reactive side chain functional groups were added as derivatives with TFA-resistant groups (alpha-BOC-epsilon-(2-chloro-CBZ)-L-lysine, BOC-tryptophan (CHO), BOC-N-imidazole-tosyl-L-histidine). All BOC-amino acids were from Bachem Inc., Torrance, CA, except for Boc-Trp(CHO), which was from Peptides International, Louisville, KY.

After coupling of the final BOC-amino acid the resin-bound peptide was deprotected and the peptide was cleaved from the resin by high (concentration) HF (anhydrous hydrogen fluoride, Matheson) cleavage in the presence of scavengers (p-cresol and p-thiocresol, 90:7.5:2.5 (v:v), Aldrich) and methionine. The temperature during the cleavage was maintained at approximately -20°C for the first 30 minutes and between -5° and -10°C for the final 30 minutes. Crude peptide was washed with ethyl acetate and ether to remove scavengers. Peptide was then extracted from the resin with 6% acetic acid, the solution was evaporated to low volume and was lyophilzed. Deformylation of Trp was achieved by treatment with 1 M piperidine in 60% aqueous DMF for 24 hours at 0°C. After evaporation and

lyophilization the peptide was purified using a Waters Associates System 500 preparative HPLC (high performance liquid chromatography) reverse phase C_{18} column and a methanol/water/TFA step gradient (with increasing methanol). Purity was checked by analytical HPLC (methanol/water/TFA) against a standard alpha-factor sample.

Vesicle Preparation

Synthetic and/or natural phospholipids (obtained from Sigma, CIL, or Avanti Polar Lipids) were dissolved in chloroform and stored as stock solutions. The required amount of phospholipid solution was transferred to a vial and the solvent removed by evaporation under a stream of nitrogen gas. Traces of chloroform were removed from the resulting lipid film by desiccating under vacuum overnight. Buffer solution (5mM sodium acetate) was warmed to a temperature 10 to 15° above the transition temperature (T_c) of each specific lipid. Five small glass beads were added to aid in dispersal of the lipid film which was vortexed for ~one minute. The sample was then transferred to a polycarbonate vial and vesicles were prepared by sonication with a Heat Systems W-380 Sonicator equipped with a cup horn using the procedure described by Barrow and Lentz (91). The water bath was maintained at a temperature 10-15° above the lipid phase transition temperature. Sonication was continued until the sample appeared optically clear. Most samples required less than one hour

to reach optical clarity. The DPPE samples required 3 - 4 hours. Samples were centrifuged for 10 -20 minutes at 13,000 rpm in a Micro Centaur microcentifuge to remove large and multilamellar vesicles and were stored at room temperature. All experiments were performed within one week of sample preparation. During this time samples remained optically clear and ^{1}H NMR spectra were unchanged. The vesicle sizes were determined by quasielastic light scattering measurements obtained with a Lexel Model 65 Argon - Ion Laser and Langley Ford Model 1096 Correlator located in the laboratory of Prof. Ruth Stark at the College of Staten Island.

NMR Spectroscopy

All NMR experiments were performed on the JEOL GX-400 spectrometer of the CUNY NMR Facility at Hunter College. The spectrometer operates at a ^{1}H resonance frequency of 400 MHz (161.8 MHz for ^{31}P and 61.4 MHz for ^{2}H).

One dimensional ^{1}H spectra in DMSO-d_6 or D_2O were acquired with the normal one pulse experiment described in Chapter II. One dimensional spectra in water were acquired with saturation of the water resonance during the 1.0 s relaxation delay. Chemical shifts are reported relative to TMS (tetramethylsilane) for DMSO and TSP (3-trimethylsilylpropionate, Na salt) for aqueous solutions (both TMS and TSP resonate at 0.0 ppm). Typically 16K points were acquired over a 4000 - 5000 Hz spectral width. Sixteen - 64 FIDs were signal averaged and were Fourier

transformed after exponential multiplication with 0.5 - 1.0 Hz line broadening.

^{31}P NMR spectra were acquired with broadband noise decoupling of protons. Typically 2K points were acquired over a spectral width of 1000 Hz. A 1 s relaxation delay was used between scans. The 90° pulse width was 20.5 μs. 1024 FIDs were signal averaged and 5 - 10 Hz line broadening was applied. Chemical shifts are reported relative to external 1% H_3PO_4 (in D_2O) at 0.0 ppm. Because T_2 was very short the effects of diffusion during a short tau were negligible and permitted the use of a modified Hahn spin-echo sequence varying tau (as described in Chapter II). Typically eight tau values were used with all other spectral parameters as above. T_2 experiments were repeated for the DPPC sample only since the supply of other lipids was limited and samples stored for a week or more became turbid (indicating aggregation).

^{2}H NMR spectra were acquired with 1K points over a spectral width of 500 Hz while the spectrometer was in an unlocked condition. A relaxation delay of 0.1 - 2.25 s was used depending on the sample and temperature (0.1 s for DOPC at 25°C, 2.25 s for DPPC at 50°C). 256 FIDs were acquired and Fourier transformed with 5 Hz line broadening. DPPC spectra at 25°C required 1024 - 2048 FIDs for sufficient S/N. The 90° pulse was 29.4 μs. T_2 measurements were performed using modified Hahn spin-echo (varying tau) and CPMG spin-echo sequences (collecting

successive echos) as described in Chapter II. T_1 values were determined by the inversion-recovery method. Typically 11 - 20 tau values were used for each T_1 or T_2 calculation. T_1 tau values included several infinity values with the rest ranging from 0.2 to 2.5 T_1 (T_1 was initially estimated by finding the tau value producing a null, tau_{null}= 0.69 T_1). Chemical shifts are reported relative to a natural abundance water sample run prior to each ^2H spectrum (water was calibrated to resonate at 4.78 ppm at 25°C, 4.60 ppm at 41°C, and 4.51 ppm at 50°C). As with ^{31}P relaxation studies, experiments were repeated only for the DPPC sample.

COSY spectra were recorded in the absolute value mode with the sequence outlined in Chapter II. Resolution enhancement was achieved by application of a sine-bell multiplication in both time dimensions. 512 t_1 values were recorded with 32 acquisitions per spectrum and post acquisition delays of 1.0 s. COSY spectra in water were obtained using a COSY pulse sequence modified to include a 1.0 s presaturation pulse subsequent to the relaxation delay.

ROESY and NOESY spectra were recorded in the pure absorption mode as described by States et al. (92). Gaussian or exponential multiplication was applied in the t_2 dimension and Gaussian multiplication was applied in the t_1 dimension. In DMSO and D_2O, 32 acquisitions per t_1 value were recorded with post acquisition delays of 2.5 s.

Experiments in DMSO and D_2O required approximately 13 hours for data acquisition. NOESY experiments in water were performed while saturating the water resonance during all but the acquisition period. In the ROESY experiment the water resonance was saturated only during the relaxation delay. Experiments in water required approximately 36 hours for data acquisition to achieve sufficient S/N.

The NOESY spectra were acquired using the pulse sequence described in Chapter II with mixing times of 100, 250, 400, or 600 ms. Several data sets were acquired with a modified pulse sequence which included a 180^{o} refocusing pulse inserted into the mixing period and shifted with t_1 in order to minimize contributions from J crosspeaks (93). The majority of the spectra were acquired without this refocusing pulse since no differences were observed between the spectra recorded with or without this pulse.

The ROESY spectra were acquired using the pulse sequence described in Chapter II with a 200 ms mixing time (spin lock). The spin locking field was adjusted to be approximately 3 KHz, a field strength which minimizes contributions from J-coupling and Hartmann-Hahn transfer (76). The spectra were also acquired with different carrier positions to confirm that the crosspeaks observed were not being affected by a Hartmann-Hahn match which could significantly reduce the NOE crosspeak intensity.

The two-dimensional data matrices were not symmetrized and spectra are often presented at contour levels higher

than those from which tabulated data was extracted. Specific temperatures and any deviations from the above procedures are described in the figure legends and the text.

The two-dimensional data sets acquired for the alpha-factor - lipid interaction were processed using the FTNMR software package by Dr. Dennis Hare. An 80^{o} shifted sine-squared bell multiplication was applied in both dimensions of the 2D data.

CHAPTER IV

Experimental Results

Solution Studies

The solution studies of alpha-factor reported herein have focused on the native tridecapeptide and five dodecapeptide analogues. The dodecapeptides are all analogues of the des-Trp^1-alpha-factor which have Cha (beta-cyclohexyl-L-alanine) substituted for the natural Trp^3. In addition to the dodecapeptide with the natural Gly at position 9 we have studied analogues with D-Ala, L-Ala, D-Leu, and L-Leu substitutions at position 9. We have also studied two elongated alpha-factor peptides, Ala-alpha-factor and Glu-Ala-alpha-factor. These synthetic peptides are similar to incompletely processed forms of alpha-factor isolated from yeast culture media (94).

Figure 13 shows the 25°C, one-dimensional 400 MHz spectra of alpha-factor and the des-Trp^1,Cha^3-dodecapeptide in DMSO. Figure 14 shows the 25°C, one-dimensional spectra of alpha-factor in 90% H_2O/10% D_2O, alpha-factor in DMSO, and various active and inactive dodecapeptide analogues in DMSO. In Figure 14 only the downfield resonances are shown since the side chain resonance positions are very similar in all of the peptides studied. Comparison of spectra of the inactive analogues (14 E and G) with those of all active peptides shows that there is much less chemical shift differentiation of amide resonances in inactive peptides than in active peptides (see in particular, the

FIGURE 13

400 MHz ^{1}H NMR spectra of the alpha-factor and the des-Trp^{1}, Cha^{3}-dodecapeptide in DMSO-d_6 at 25°C.
A. Alpha-factor
B. des-Trp^{1}, Cha^{3}-dodecapeptide

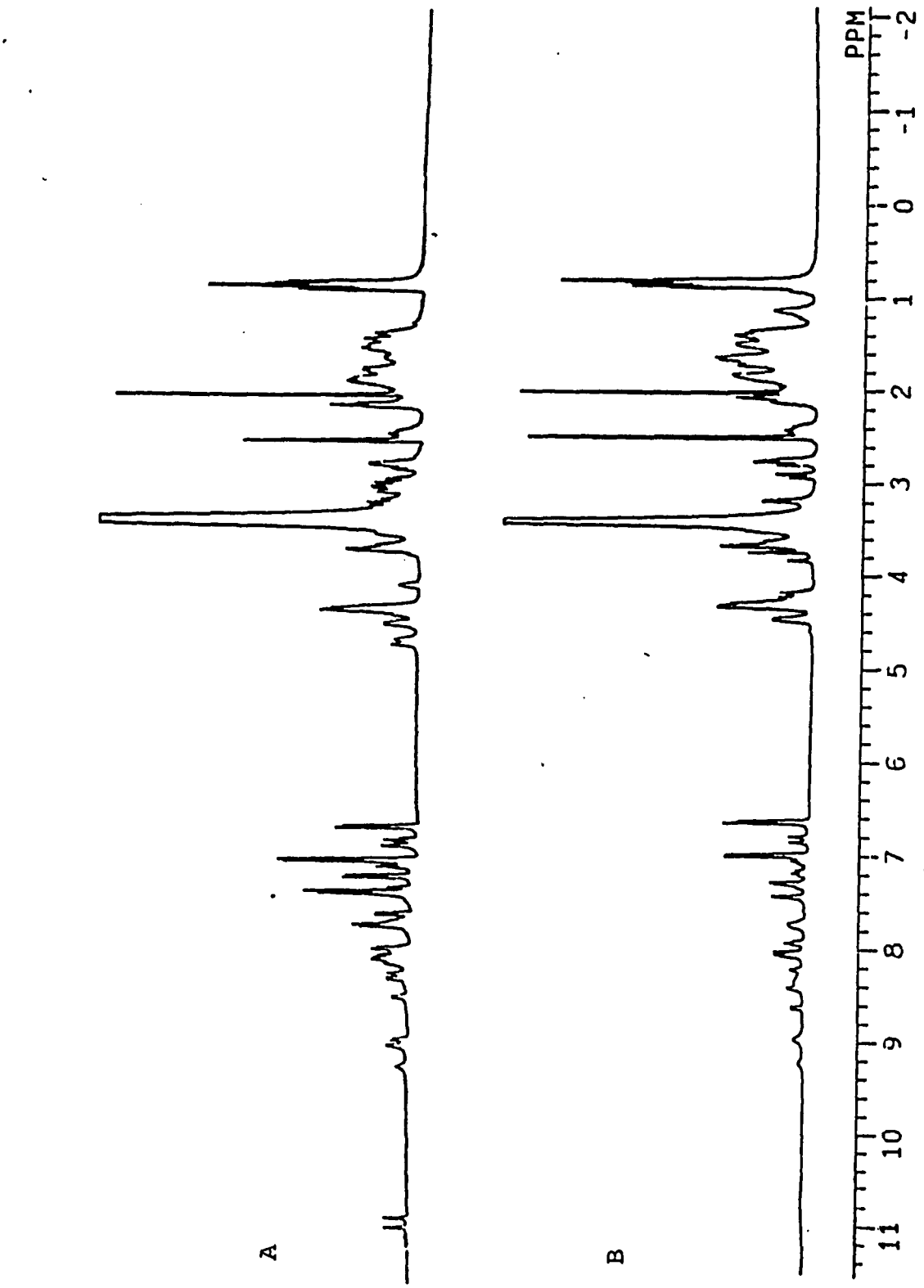
A
B
PPM
11
10
9
8
7
6
5
4
3
2
1
0
-1
-2

FIGURE 14

Downfield regions of the ^{1}H NMR spectra of several alpha-factor peptides.
A. alpha-factor (H_2O/D_2O, 9/1)
B. alpha-factor (DMSO)
C. des-Trp^{1}, Cha^{3}-dodecapeptide (DMSO)
D. des-Trp^{1}, Cha^{3},D-Ala^{9}-dodecapeptide (DMSO)
E. des-Trp^{1}, Cha^{3},L-Ala^{9}-dodecapeptide (DMSO)
F. des-Trp^{1}, Cha^{3},D-Leu^{9}-dodecapeptide (DMSO)
G. des-Trp^{1}, Cha^{3},L-Leu^{9}-dodecapeptide (DMSO)
All spectra are at 25°C.

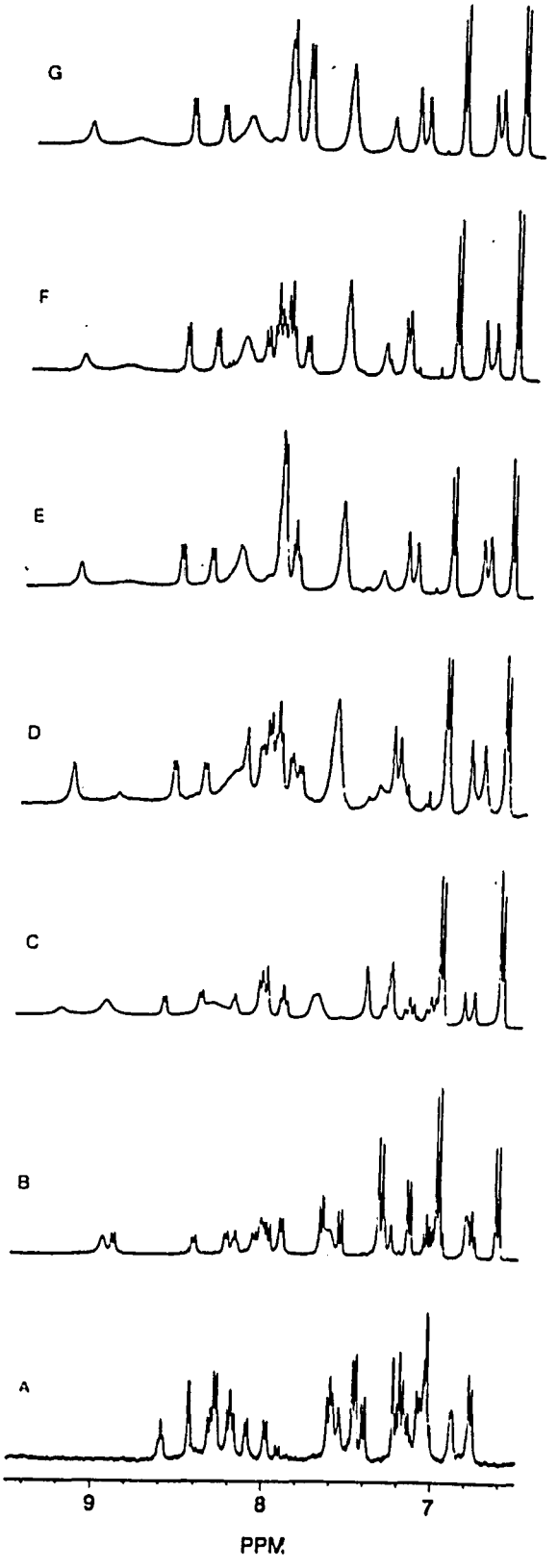
G
F
E
D
C
B
A
9
8
7
PPM

region 8.0 to 8.3 ppm).

The amide protons of the des-Trp^1,Cha^3-dodecapeptide in DMSO were previously assigned by monitoring the collapse of the amide doublets (arising from amide proton - alpha proton spin - spin coupling) following site - specific alpha - deuteration (40). In that study side chain amide and amino groups and aromatic ring protons were also assigned. These assignments were confirmed and the additional spin - spin connectivities of each amino acid residue were identified using COSY spectra. The COSY spectrum of the des-Trp^1,Cha^3-dodecapeptide in DMSO is shown in Figure 15. By using the characteristic crosspeak patterns expected for different amino acid side chains it was possible to trace the spin-couplings from the amide proton to the alpha proton to the side chain protons (an example of such a pathway, tracing the Lys^7 connectivities, is presented in Figure 15) (95, 96). As expected, amide proton connectivities appear in DMSO and in H_2O but not in D_2O. However, because the alpha proton connectivities to the side chain protons are characteristic of specific types of amino acids, the individual spin systems of the component amino acids of the peptide chain were identified and the amide proton resonances of the alpha-factor in H_2O were assigned. Although several of the alpha proton resonances (in a given peptide) overlap, the power of correlated spectroscopy allowed full assignment to be made. Where there was severe overlap of resonances, selective

FIGURE 15

COSY spectrum of the des-Trp^1, Cha^3-dodecapeptide in DMSO (at 25°C, 400 MHz, alpha-deuterated at Tyr^{13}). The complete assignment of the Lys^7 proton resonances is shown (dotted lines).
Insert I is an expansion of the boxed region which shows the alpha proton - beta proton crosspeaks.
Insert II is the same region of the COSY spectrum of the dodecapeptide which is alpha-deuterated at Met^{12} instead of Tyr^{13}. The arrows indicate the crosspeaks between the Tyr^{13} alpha and beta protons which confirmed the assignment of the Tyr^{13} alpha proton. Incomplete deuteration results in small residual intensity of the Tyr^{13} alpha - beta crosspeak in the des-Trp^1, Cha^3, (α-^2H)Tyr^{13}-dodecapeptide spectrum.

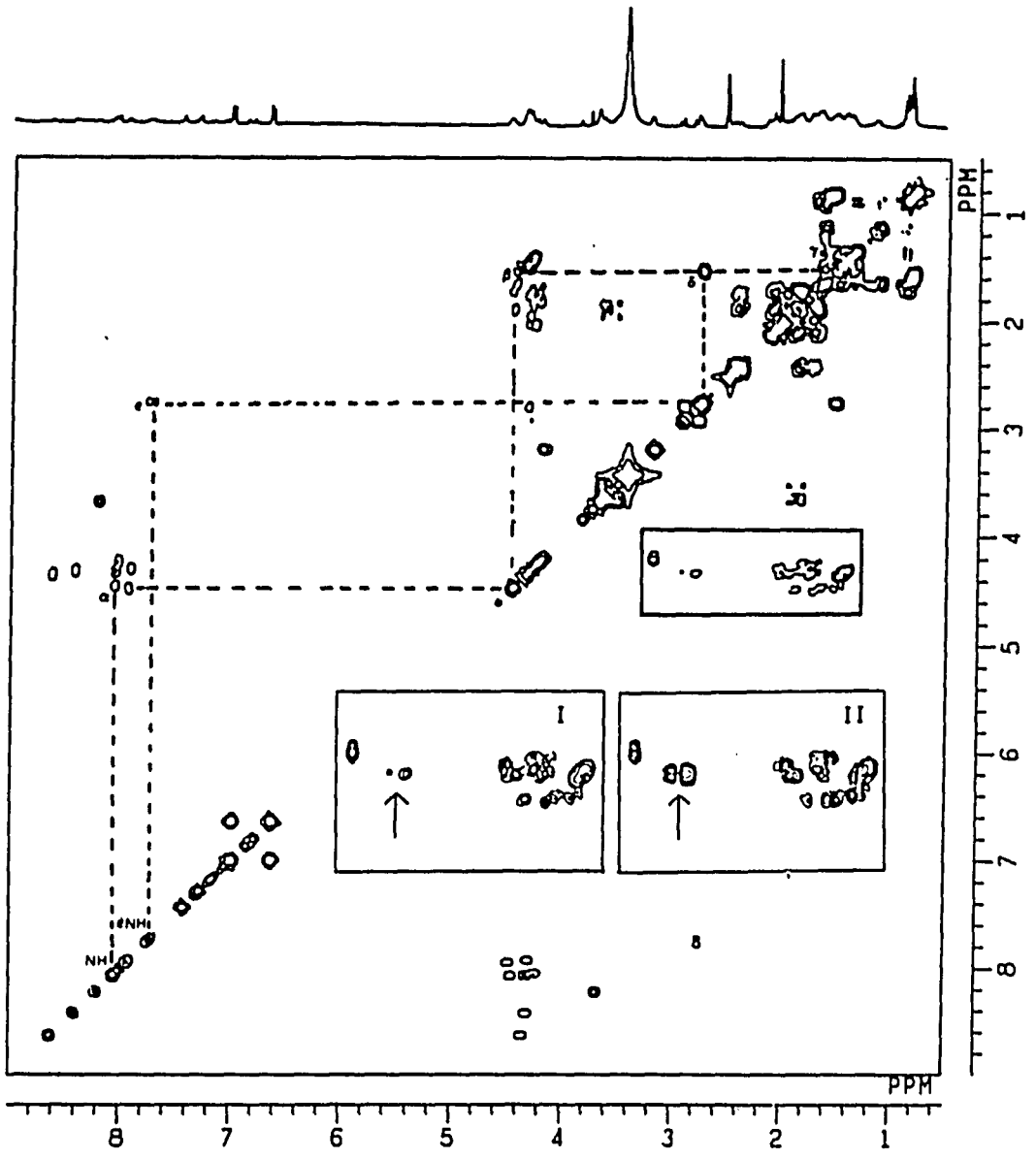
PPM
PPM
I
II
NH
NH
8
7
6
5
4
3
2
1

deuteration at a given alpha proton position provided confirmation of assignments, as illustrated in the inserts (I and II) of Figure 15. The alpha proton to beta proton crosspeaks for Tyr^{13} decrease in intensity in the [α-^2H]Tyr^{13} dodecapeptide analogue in comparison to the [α-^2H]Met^{12} analogue. This leads to the unequivocal assignment of the alpha proton of Tyr^{13}.

Sequential NOE connectivities between the alpha proton of one amino acid residue in a peptide chain and the amide proton of the next amino acid residue are frequently utilized to unambiguously assign all of the backbone resonances of peptides (59). Unfortunately, we observe very few of these sequential NOEs in the NOESY spectra obtained under the conditions of our experiments (see Table I) and therefore the assignment of the duplicated proline and glutamine residues was facilitated by the utilization of heptapeptide (His-Cha-Leu-Gln-Leu-Lys-Pro) and pentapeptide (Gly-Gln-Pro-Met-Tyr) fragments. COSY spectra of these fragments revealed that the alpha protons of the Pro^8/Pro^{11} and the alpha and amide protons of the Gln^5/Gln^{10} pairs resonate at different chemical shift positions in the tridecapeptide. The use of fragments to aid in assignments assumes superposition of the fragment spectrum with the molecule under investigation; this proved to be true for the peptides studied (data not shown).

Resonance assignments of the proton spectrum of tridecapeptide alpha-factor in aqueous solution and in DMSO

TABLE I (facing page)

NOEs Observed in Solution Studies of Alpha-factor Peptides

Possible Significance of the NOEs

[a] α_i-NH $_{i+1}$ used in combination with other NOEs to identify: 3_{10}helix, α-helix.

[b] α_i-NH $_{i+1}$ repetitive sequence used in combination with other NOEs to identify: 3_{10}helix, α-helix.

[c] α_i-NH $_{i+2}$ used in combination with other NOEs to identify: 3_{10}helix, α-helix.

[d] α_i-NH $_{i+1}$ used in combination with other NOEs to identify: 3_{10}helix, α-helix beta antiparallel or parallel sheets, a repetitive sequence is indicative of extended structure, also used to identify beta turns.

[e] α_i-α_i this intraresidue NOE is also observed by the Masui group in their vesicle studies.

[f] NH_i-NH $_{i+1}$ a repetive sequence is used to identify: 3_{10}helix, α-helix, beta antiparallel or parallel sheets, beta turns.

[g] α_i-α_{i+1} used to distinguish cis proline from trans proline in an X-Pro sequence.

Note that some of the NOEs listed here do not appear on the NOE spectra presented. We have examined all spectra at lower contours to compile this table.

* The extended alpha-factor molecules exhibit an additional NOE between the Ala αCH and the Trp^3NH. This α_i-NH_{i+3} NOE may be suggestive of an alpha-helix or 3_{10} helix. The distances expected for these structures are 3.4 Å and 3.3 Å respectively.

The designations of crosspeak intensity are based on observation at different mixing times:

VS = observed at 100 and 200 ms
S = observed at 200 and 250 ms
W = observed at 400 ms
VW = observed at 600 ms

TABLE I

Conformationally significant NOEs observed for the alpha-factor peptides studied. (VS=very strong, S=strong W=weak, VW=very weak intensity.)

NOE	PEPTIDES: tridecapeptide DMSO NOESY	tridecapeptide DMSO ROESY	tridecapeptide H_2O ROESY	des-Trp[1],Cha[3]-dodecapeptide analogues in DMSO (NOESY): Gly[9] active	D-Ala[9] active	D-Leu[9] active	L-Ala[9] inactive	L-Leu[9] inactive	extended alpha-factor analogues *: Ala-alpha-factor	Glu-Ala-alpha-factor
$Trp^{1,3}\beta$-$His^{2}NH$ [a]	S									
$Trp^{1}\alpha$-$Trp^{3}NH$ [b]	S	S								
$His^{2}\beta$-$Leu^{4}NH$ [c]	S									
$His^{2}\alpha$-$Cha^{3}NH$ [d]					S	S	S	S		
$His^{2}\beta$-$Cha^{3}NH$ [a]				S						
$Trp^{3}\beta$-$Leu^{4}NH$ [a]	S									
$Trp^{3}\alpha$-$Leu^{4}NH$ [d]		S	S						S	S
$Cha^{3}\alpha$-$Leu^{4}NH$ [d]				S	S	S	S	S		
$Leu^{4}\alpha$-$Leu^{6}NH$ [b]			S							
$Leu^{4,6}\alpha$-$Leu^{4,6}\beta$ [e]	S	S								
$Gln^{5}NH$-$Leu^{6}NH$ [f]	VW									
$Leu^{6}\alpha$-$Lys^{7}NH$ [d]					S					
$Lys^{7}\alpha$-$Pro^{8}\beta$ [g]	VS	VS	VS	VS	VS	VS	VS	VS	VS	VS
$Pro^{8}\alpha$-$X^{9}NH$ [d]	VS	VS	VS	VS	VS	VS			VS	VS
$Pro^{8}\alpha$-$Gln^{10}NH$ [b]	W									
$X^{9}\alpha$-$Gln^{10}NH$ [d]	S			S	S	S				
$X^{9}NH$-$Gln^{10}NH$ [f]	VW								S	S
$Gln^{10}\alpha$-$Pro^{11}\beta$	VS	VS	VS	VS	VS	VS	VS	VS	VS	VS

are reported in Table II. Assignments of the des-Trp^1,Cha^3-dodecapeptide in DMSO are found in Table III and the amide and alpha proton assignments of the other dodecapeptide analogues are found in Table IV. Assignments of the amide and alpha proton resonances of the extended tetradecapeptide and pentapeptide alpha-factor analogues in DMSO are reported in Table V.

Figure 16 is a series of plots, for all peptides under investigation, showing the difference between the experimentally determined amide proton resonance position and the value reported for the specific amino acid residue when found in a random coil structure (95, 96). Note that in all active peptides the amide resonance of residue 9 is downfield shifted from the random coil value while this resonance is upfield shifted in the inactive peptides (Figure 16 E and G).

The temperature coefficients of the amide protons of the alpha-factor in both water and in DMSO and of three of the dodecapeptide analogues were determined by monitoring the change in the amide proton resonance position while varying the temperature from 25° to 55°C in 5° increments. These values are reported in Table VI. None of the observed temperature coefficients are in the range expected when there is intramolecular hydrogen bonding (less than 2.0×10^{-3} ppm/K) (60).

Coupling constants ($^3J_{NH-\alpha CH}$) between the amide and alpha protons were determined for the alpha-factor in DMSO

TABLE II

^{1}H assignments for alpha-factor in DMSO (D) and in water (W)

Residue		NH	αCH	βCH	γCH	δCH	Other
Trp[1]	D	7.95	4.00	3.06			ring protons:
				2.94			7.72,7.49,7.30,
							6.95,6.71
							indole NH 10.83
	W		4.18	3.18			ring protons:
				3.13			7.85, 7.43
							7.18,7.13,7.03
							indole NH 10.04
His[2]	D	8.21	4.60	3.12			C_2H 8.95
							C_4H 7.42
	W		4.52	3.20			C_2H 8.44
				3.15			C_4H 7.02
Trp[3]	D	8.92	4.67	3.01			ring protons same
				2.96			as Trp[1]
							indole NH 10.91
	W	8.10	4.56	3.01			ring protons same
				2.95			as Trp[1]
							indole NH 10.14
Leu[4]	D	8.46	4.35	1.37	1.57	0.82	
	W	8.19	4.20	1.48	1.59[a]	0.85	
					1.40	0.78	
Gln[5]	D	8.08	4.25	1.83[a]	2.10		γNH_2 7.30
				1.70			6.80,6.70[a]
				1.68			
	W	8.20	4.22	1.99[a]	2.25		γNH_2 7.55[a]
				1.93			6.90

TABLE II (continued)

Leu[6]	D	7.90	4.27	1.37	1.46	0.82	
	W	8.28	4.08	1.32	1.59[a]	0.85	
					1.40	0.78	
Lys[7]	D	8.04	4.42	1.46	1.37	1.46	εCH_2 2.72
							εNH_3 7.72
	W	8.32	4.63	1.64	1.40	1.64	εCH_2 2.95
							εNH_3 7.68
Pro[8]	D		4.27	2.06	1.94[a]	3.66	
				2.04	1.89	3.49	
					1.86		
					1.84		
	W		4.29	2.25	2.03[a]	3.76	
				1.90	1.99 1.97	3.64	
Gly[9]	D	8.21	3.62				
	W	8.60	4.00				
			3.81				
Gln[10]	D	7.90	4.44	1.83[a]	2.10		γNH_2 7.30
				1.70			6.80,6.70[a]
				1.68			
	W	7.99	4.63	2.08	2.32		γNH_2 7.55[a]
							6.90
Pro[11]	D		4.32	2.06	1.94[a]	3.66	
				2.04	1.89	3.49	
					1.86		
					1.84		
	W		4.34	2.14	2.03[a]	3.76	
				1.74	1.99	3.64	
					1.97		
Met[12]	D	8.02	4.30	1.85	2.40		SCH_3 2.02
				1.72			
	W	8.29	4.35	1.90	2.46		SCH_3 2.01
				1.84	2.38		
Tyr[13]	D	7.98	4.30	2.88			$C_{2,6}H$ 6.98
				2.74			$C_{3,5}H$ 6.62
	W	7.62	4.38	3.06			$C_{2,6}H$ 7.03
				2.85			$C_{3,5}H$ 6.75

[a] these resonances were overlapping and could not be assigned to individual residues of the duplicated amino acids.

TABLE III

^1H assignments for the des-Trp^1,Cha^3-alpha-factor in DMSO

Residue	NH	αCH	βCH	γCH	δCH	Other
His^2	8.26	4.20	3.18			C_2H 8.95
						C_4H 7.42
Cha^3	8.61	4.34	1.49			ring protons:
						1.64,1.22,1.15,
						1.13,0.90,0.86
Leu^4	8.40	4.30	1.43	1.71[a]	0.88	
				1.55	0.83	
Gln^5	8.01	4.22	1.81	2.12		γNH_2 7.27
			1.71	2.11		6.79
Leu^6	7.92	4.24	1.43	1.71[a]	0.88	
				1.55	0.83	
Lys^7	8.06	4.45	1.52	1.37	1.52	ϵCH_2 2.75
			1.48			ϵNH_3 7.71
Pro^8		4.28	2.06	1.94[a]	3.66	
			2.04	1.89	3.49	
				1.85		
				1.80		
Gly^9	8.20	3.73				
		3.66				
Gln^{10}	7.94	4.46	1.81	2.12		γNH_2 7.27
			1.71	2.11		6.84
Pro^{11}		4.32	2.06	1.94[a]	3.66	
			2.04	1.89	3.49	
				1.85		
				1.80		
Met^{12}	8.04	4.32	1.86	2.39		SCH_3 2.00
			1.77	2.44		
Tyr^{13}	8.01	4.30	2.90			$C_{2,6}H$ 6.98
			2.77			$C_{3,5}H$ 6.63
						OH 9.22

[a] these resonances were overlapping and could not be assigned to the individual residues of the duplicated amino acids.

TABLE IV

Amide and alpha proton assignments for the active and inactive des-Trp^1,Cha^3,X^9-alpha-factor analogues in DMSO. X^9= D-Leu, D-Ala, L-Leu, or L-Ala.

	active peptides				inactive peptides			
Residue	D-Leu^9		D-Ala^9		L-Leu^9		L-Ala^9	
	NH	αCH	NH	αCH	NH	αCH	NH	αCH
His^2		4.16		4.12	8.23	4.27		4.15
Cha^3	8.56	4.36	8.56	4.35	8.57	4.33	8.56	4.35
Leu^4	8.38	4.30	8.39	4.30	8.39	4.28	8.39	4.29
Gln^5	7.97	4.24	7.97	4.21	7.98	4.21	7.98	4.22
Leu^6	7.85	4.29	7.83	4.29	7.87	4.29	7.89	4.29
Lys^7	8.04	4.49	8.06	4.45	8.01	4.44	7.96	4.44
Pro^8		4.23		4.26		4.30		4.30
x^9	8.09	4.27	8.16	4.21	7.87	4.18	7.96	4.16
Gln^{10}	7.92	4.43	7.88	4.42	7.88	4.44	7.91	4.46
Pro^{11}		4.30		4.34		4.30		4.30
Met^{12}	8.02	4.32	8.02	4.30	8.00	4.29	7.99	4.30
Tyr^{13}	7.94	4.33	7.95	4.30	7.96	4.28	7.97	4.30

TABLE V

Amide and alpha proton assignments for the tetradecapeptide analogue, Ala-alpha-factor, and the pentadecapeptide, Glu-Ala-alpha-factor.

Residue	tetradecapeptide		pentadecapeptide	
	NH	αCH	NH	αCH
Glu^{+2}				3.79
Ala^{+1}	8.39	3.75	8.29	4.33
Trp^{1}	8.29	4.58	8.11	4.52
His^{2}	8.10	4.58	8.06	4.58
Trp^{3}	8.49	4.58	8.17	4.58
Leu^{4}	8.20	4.31	8.51	4.33
Gln^{5}	8.03	4.27	8.06	4.24
Leu^{6}	7.85	4.27	7.88	4.29
Lys^{7}	8.01	4.45	8.06	4.45
Pro^{8}		4.30		4.24
Gly^{9}	8.18	3.66	8.18	3.69
Gln^{10}	7.89	4.46	7.89	4.48
Pro^{11}		4.34		4.31
Met^{12}	8.01	4.30	8.02	4.26
Tyr^{13}	7.98	4.32	7.97	4.27

FIGURE 16

Plots of differences in amide proton chemical shift relative to random coil values for alpha-factor peptides. Shift in resonance position from the random coil value is plotted versus amino acid residue. +1 refers to Ala in the Ala-alpha-factor and Glu-Ala-alpha-factor. 1 - 13 refer to the residue in the alpha-factor (1 refers to Trp^1, 2 refers to His^2, etc.). There are no random coil values reported for Cha therefore there is a break in the line at that position. Proline has no amide proton therefore the lines are broken at residues 8 and 11.

A. Glu-Ala-alpha-factor in DMSO
B Ala-alpha-factor in DMSO
C. alpha-factor in DMSO
D. des-Trp^1, Cha^3,D-Ala^9-dodecapeptide in DMSO
E. des-Trp^1, Cha^3,L-Ala^9-dodecapeptide in DMSO
F. des-Trp^1, Cha^3,D-Leu^9-dodecapeptide in DMSO
G. des-Trp^1, Cha^3,L-Leu^9-dodecapeptide in DMSO
H. alpha-factor in H_2O/D_2O, 9/1.

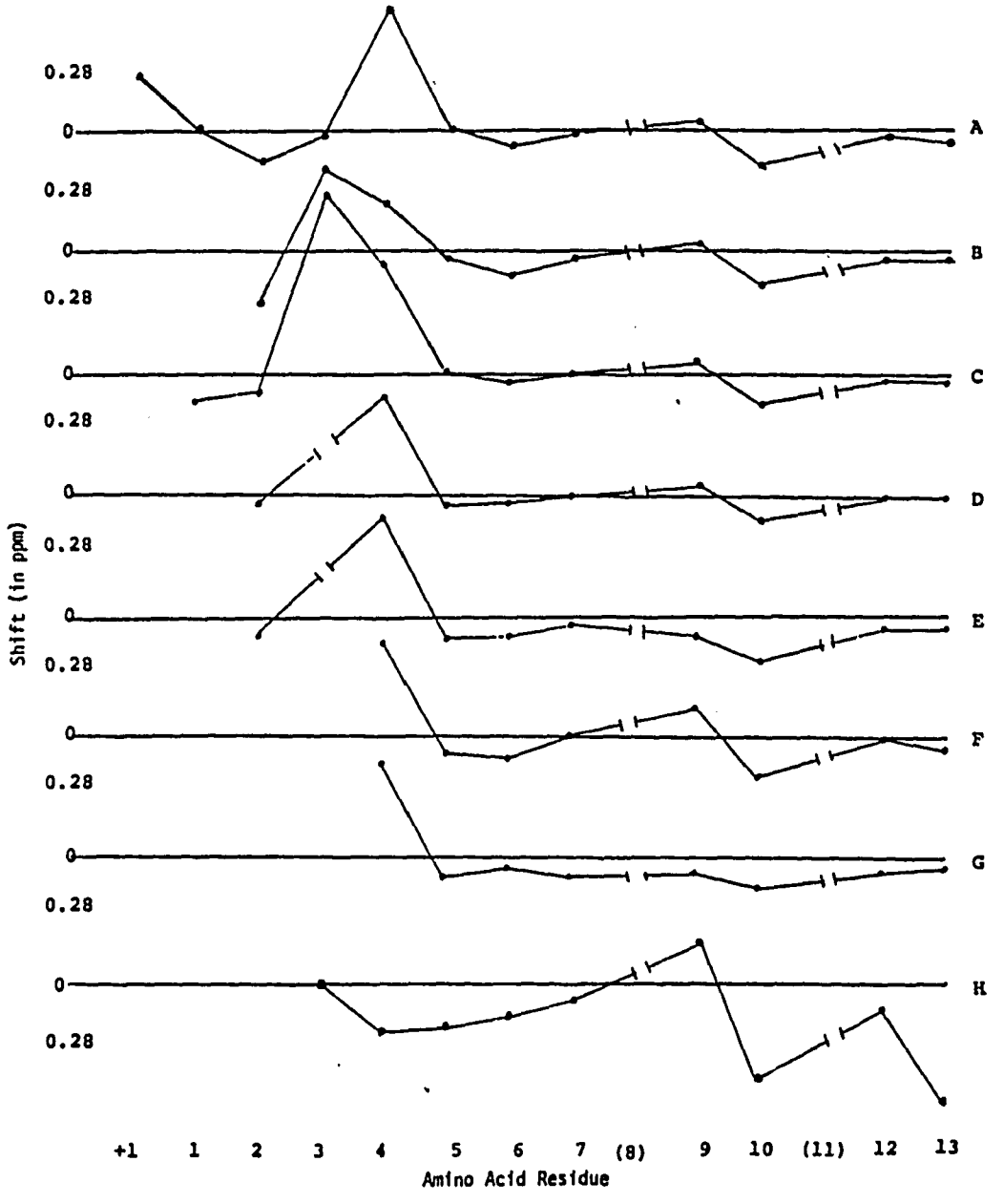
0.28
0
A
B
C
D
E
F
G
H
Shift (in ppm)
+1
1
2
3
4
5
6
7
(8)
9
10
(11)
12
13
Amino Acid Residue

TABLE VI

Amide proton temperature coefficients determined for alpha-factor and three analogue peptides. The values reported are $x10^3$ ppm/K.

NH	alpha-factor		des-Trp[1],Cha[3]-	des-Trp[1],Cha[3],L-Leu[9]-	des-Trp[1],Cha[3],D-Leu[9]-
	DMSO	water	alpha-factor	alpha-factor	alpha-factor
His[2]	3.3		4.0	a	4.8
Trp[3] (Cha[3])	4.0	7.6	3.0	3.3	3.5
Leu[4]	7.0	7.3	4.4	5.1	5.0
Gln[5]	4.5	7.3	4.8	4.5	5.5
Leu[6]	3.2	8.9	5.3	3.2	4.6
Lys[7]	a	8.0	a	a	5.6
Gly[9] (Leu[9])	4.4	8.9	5.3	4.4	4.7
Gln[10]	3.2	5.3	3.9	3.2	5.1
Met[12]	a	8.4	a	a	5.8
Tyr[13]	a	4.3	a	a	5.9

[a] the temperature coefficients could not be determined due to severe overlapping of the resonances.

and in water and are reported in Table VII. All observed coupling constants are in the range of 6- 8 Hz. These values are expected when there is rapid motional averaging or rigid helical conformation (59).

In order to further probe the solution behavior of the alpha-factor peptides NOESY spectra were acquired at various mixing times. The mixing times used were 100, 250, 400, and 600 ms and the results compiled from these spectra are reported in Table I.

The 400 MHz, 400 ms, 25°C NOESY spectrum of alpha-factor in DMSO is shown in Figure 17. Region I shows the amide proton - alpha proton NOE crosspeaks. The crosspeak connecting the Gly^9 amide proton and the Pro^8 alpha proton is indicated by the arrow. This connectivity is expected for a Type II beta-turn. The correlation of this NOE with activity and its structural relevance is discussed in Chapter V. Region II shows the connectivities between the Pro delta protons and the Lys^7 and Gln^{10} alpha protons. These NOEs are diagnostic of trans X - Pro bonds at these positions (32). Spectra were also acquired at 40°C and the same crosspeaks appear although they are of lower intensity.

Figure 18 is an expansion of part of the amide proton to alpha proton crosspeak region of the 400 ms, 25°C NOESY spectra of the active and inactive position 9 substituted dodecapeptide analogues in DMSO. This region is the same as that of the insert in Figure 17. The crosspeak between

TABLE VII

$^3J_{NH-\alpha CH}$ values for the alpha-factor in DMSO and in water.

Residue	J (Hz) in DMSO	J (Hz) in water
His^2	6.6	a
Trp^3	8.0	6.1
Leu^4	7.3	8.6
Gln^5	8.0	7.9
Leu^6	7.3	7.3
Lys^7	8.0	7.3
Gly^9	5.9	6.1
Gln^{10}	7.3	7.0
Met^{12}	7.3	7.3
Tyr^{13}	8.0	7.6

[a] in water the His^2 amide proton is not observed.

FIGURE 17

NOESY spectrum of alpha-factor in DMSO (400 MHz, 25°C, 400 ms.
Region I shows the amide proton - alpha proton NOE crosspeaks. The arrow indicates the crosspeak between the Pro^{8} alpha proton and the Gly^{9} amide proton.
Region II shows the connectivities between the Lys^{7} and Gln^{10} alpha protons and the Pro delta protons.

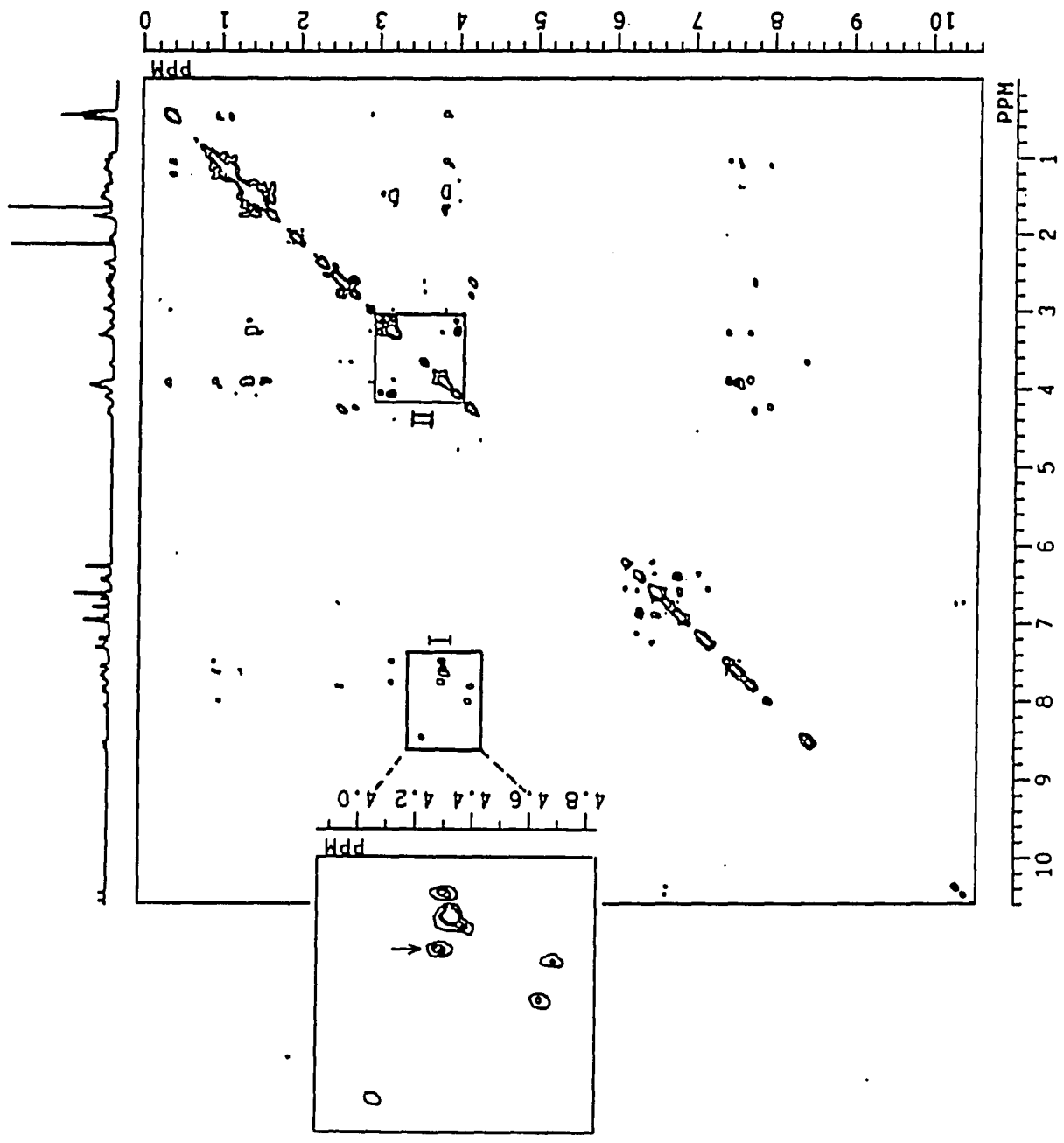
PPM
PPM
PPM
I
II
4.8 4.6 4.4 4.2 4.0

FIGURE 18

Expansions of the amide proton - alpha proton cross-peak region of active and inactive dodecapeptide NOESY spectra (400 MHz, 25°C, 400 ms, in DMSO).
L-Leu^9 refers to the inactive des-Trp^1, Cha^3,L-Leu^9-dodecapeptide
L-Ala^9 refers to the inactive des-Trp^1, Cha^3,L-Ala^9-dodecapeptide
D-Leu^9 refers to the active des-Trp^1, Cha^3,D-Leu^9-dodecapeptide
D-Ala^9 refers to the active des-Trp^1, Cha^3,D-Ala^9-dodecapeptide

The arrow indicates the crosspeak between the Pro^8 alpha proton and the X^9 amide proton (present in spectra of active analogues only).

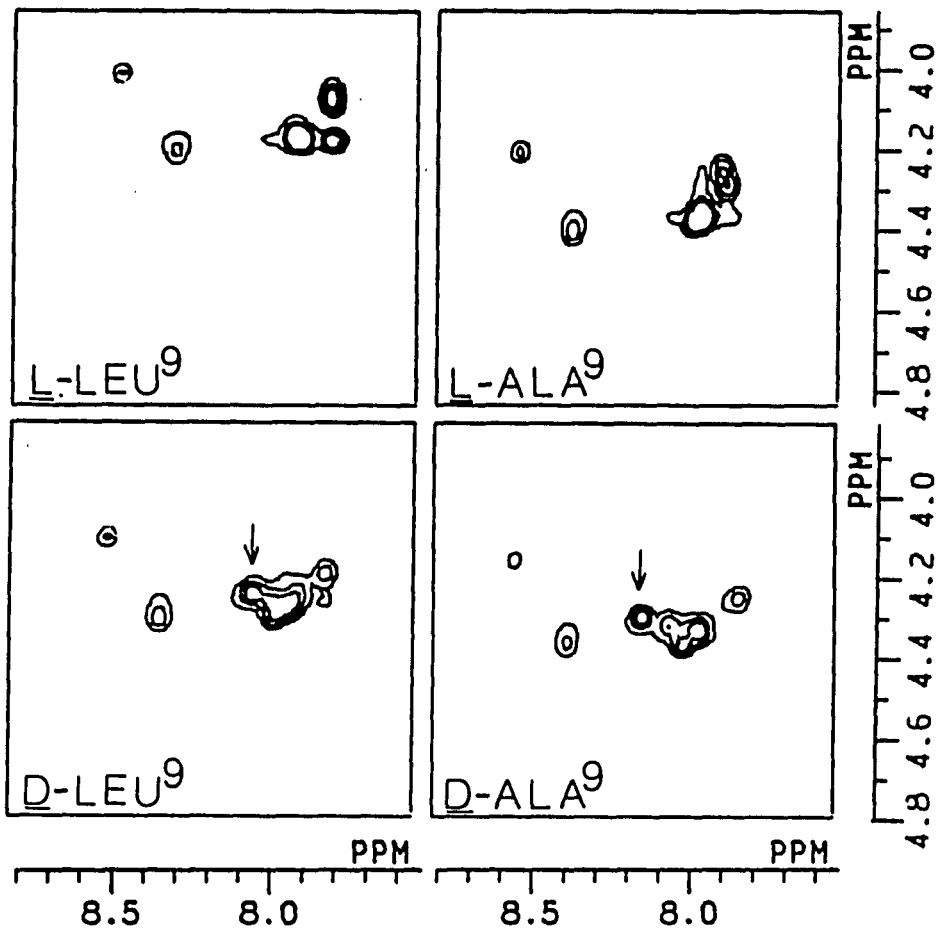
L-LEU9
L-ALA9
D-LEU9
D-ALA9
PPM
8.5
8.0
PPM
4.0
4.2
4.4
4.6
4.8

the X^9 amide proton and the Pro^8 alpha proton is indicated by the arrow. This crosspeak is present in spectra of the active analogues but is absent in spectra of the inactive analogues.

Figure 19 is the 400 MHz, 400 ms, 25°C NOESY spectrum of alpha-factor in D_2O. In contrast to the spectrum obtained in DMSO (Figure 17), this spectrum yields very little conformational information. If the peptide is extremely flexible and has no preferred conformation in aqueous solution we would expect to see NOEs only between scalar coupled protons which are necessarily close in space. Surprisingly, very few such NOEs are seen. It should be recalled that the NOE becomes zero at $\omega_o\tau_c = 1.12$ (discussed in Chapter II) and it is thus probable that the absence of NOEs is caused by the magnitude of τ_c, rather than by lack of structure.

Figure 20 shows the 400 MHz, 200 ms, 25°C ROESY spectrum of the alpha-factor in D_2O acquired to determine whether the absence of crosspeaks in the NOESY spectra was indeed due to a lack of structural features or caused by the correlation time dependence of the experiment. Expansions I and II are for comparison with the boxed region and show the difference between the NOESY spectra obtained in D_2O and in DMSO and the ROESY spectrum in D_2O. III is an expansion of the amide proton to alpha proton crosspeak region of the 200 ms, 25°C ROESY spectrum of alpha-factor in 90% H_2O/10% D_2O. The arrow indicates the

FIGURE 19

NOESY spectrum of alpha-factor in D_2O (400MHz, 25°C, 400 ms)

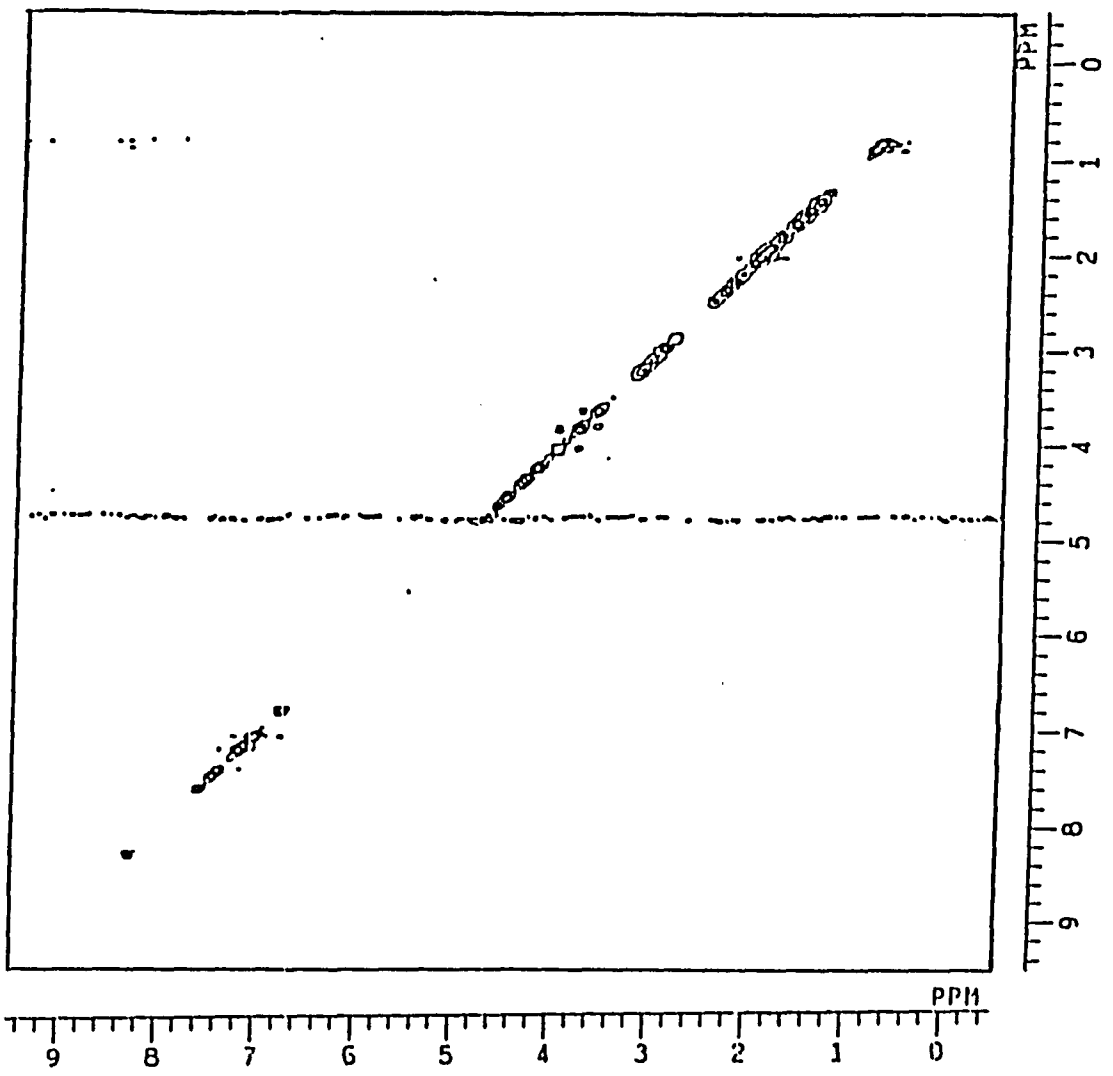
PPM
0
1
2
3
4
5
6
7
8
9
PPM
9
8
7
6
5
4
3
2
1
0

.01

FIGURE 20

ROESY spectrum of alpha-factor in D_2O (400 MHz, 25°C, 200 ms).
Expansion I is for comparison with the boxed region showing the difference between the NOESY (Figure 19, shown in I) and ROESY in D_2O.
Expansion II is the same region of the NOESY spectrum in DMSO (Figure 17).
Expansion III is the amide proton - alpha-proton cross-peak region of the ROESY spectrum in H_2O/D_2O, 9/1. The arrow indicates the crosspeak between the Pro^8 alpha proton and the Gly^9 amide proton.
The arrows on the boxed region and Expansion II indicate the crosspeaks between the Lys^7 and Gln^{10} alpha protons and the Pro delta protons.

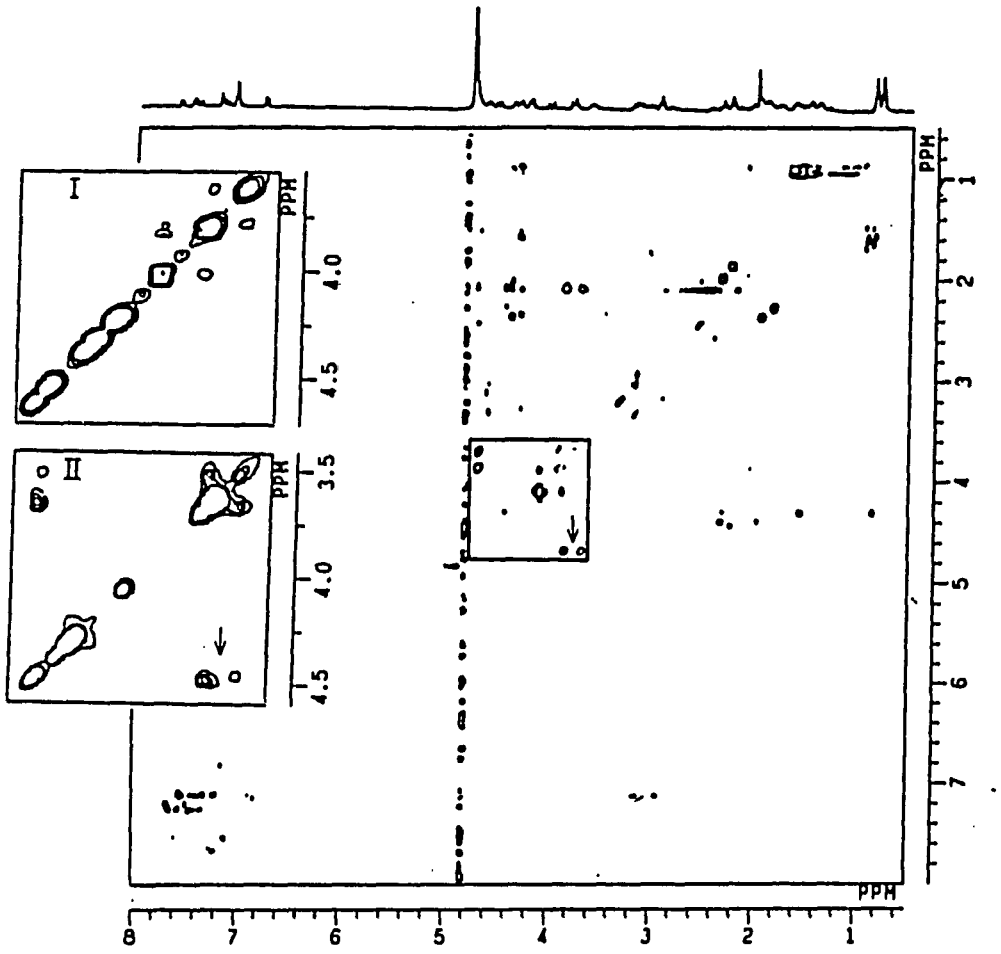
I
II
PPM
4.0
4.5
3.5
8
7
6
5
4
3
2
1

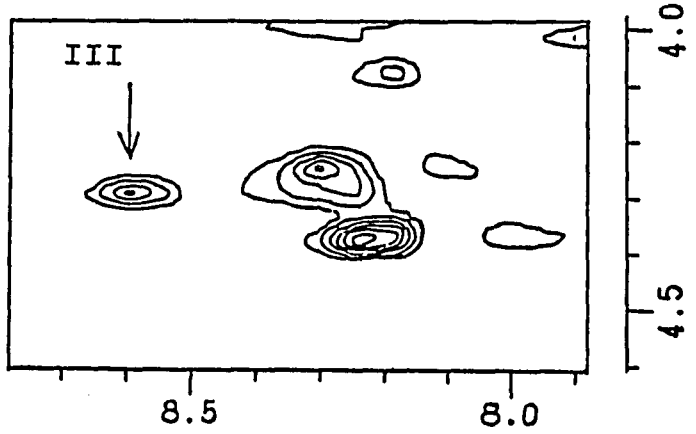
III
4.0
4.5
8.5
8.0

crosspeak between the Gly^9 amide proton and the Pro^8 alpha proton. These figures clearly show that the lack of NOESY crosspeaks is due to τ_c.

Figure 21 shows a comparison of the upfield regions of the 400 ms 25°C NOESY spectrum and the 200 ms ROESY spectrum of the alpha-factor in DMSO. Many of the same crosspeaks appear in both spectra. Figure 22 presents the same region of the 400 ms NOESY spectrum and the 200 ms ROESY spectrum of the alpha-factor in D_2O and clearly shows the advantage of the ROESY experiment in this study. Figure 23 presents the diagonal, chemical exchange, and Hartmann-Hahn crosspeaks (negative contours) of the ROESY spectrum in D_2O. Comparison of Figure 23 with the NOESY spectrum of alpha-factor in D_2O (Figure 19) shows that the only crosspeaks appearing in the NOESY spectrum are actually those due to scalar coupling or chemical exchange and not NOE interactions. The conformational importance of all tabulated NOEs is detailed in Chapter V.

Lipid Studies

Although solution studies provide information about the conformations accessible to the native peptide and as to intrinsic structural differentiation between analogues, the conformation of linear peptides in solution may not neccessarily reflect the active tertiary structure assumed at the receptor. The tridecapeptide studies were extended to determine any changes in conformation induced by the

FIGURE 21

Comparison of the alpha-factor NOESY and ROESY spectra in DMSO.
A. Upfield region of the 400 ms NOESY spectrum at 25°C.
B. Upfield region of the 200 ms ROESY spectrum at 25°C.

A.

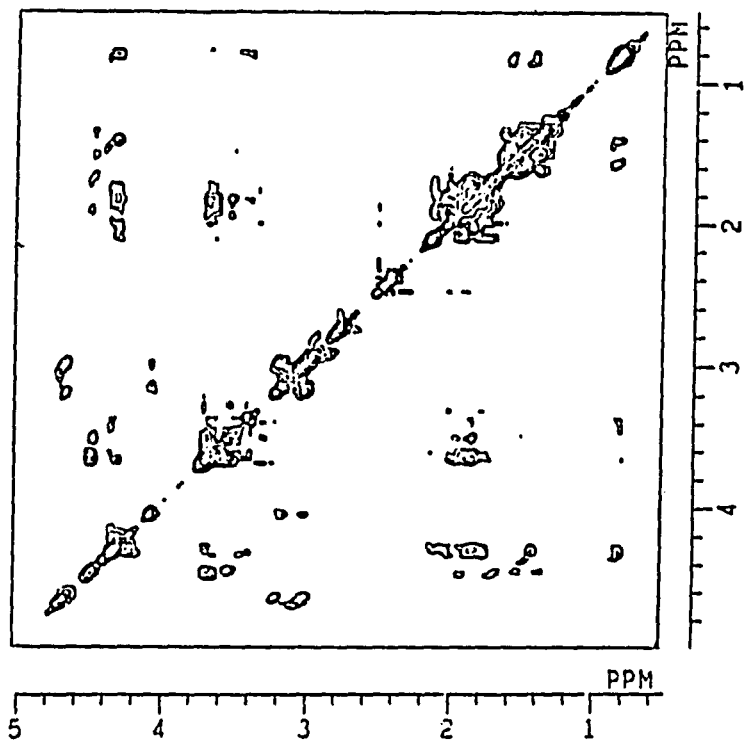

B.

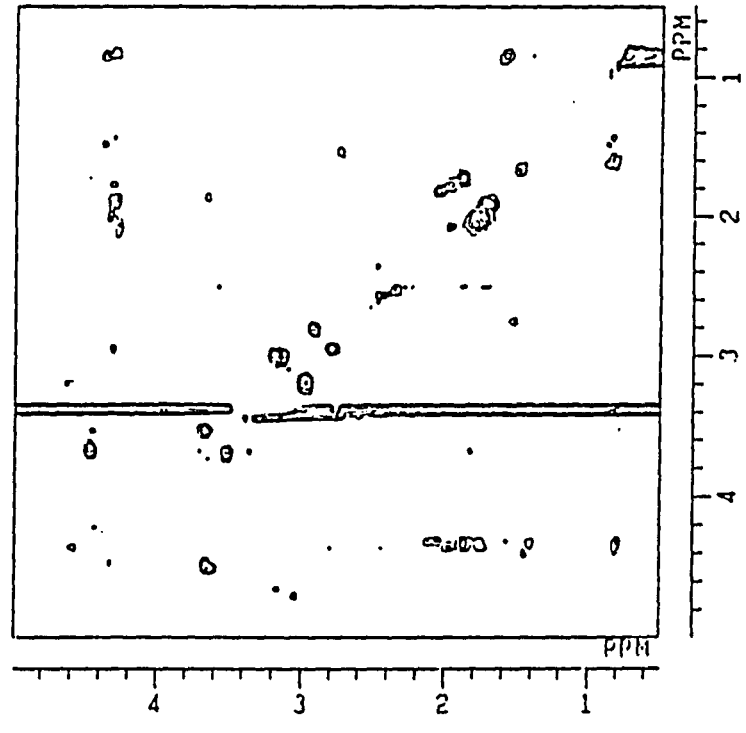

FIGURE 22

Comparison of the NOESY and ROESY spectra of alpha-factor in D_2O.
A. Upfield region of the 400 ms NOESY spectrum at 25°C.
B. Upfield region of the 200 ms ROESY spectrum at 25°C.

A.

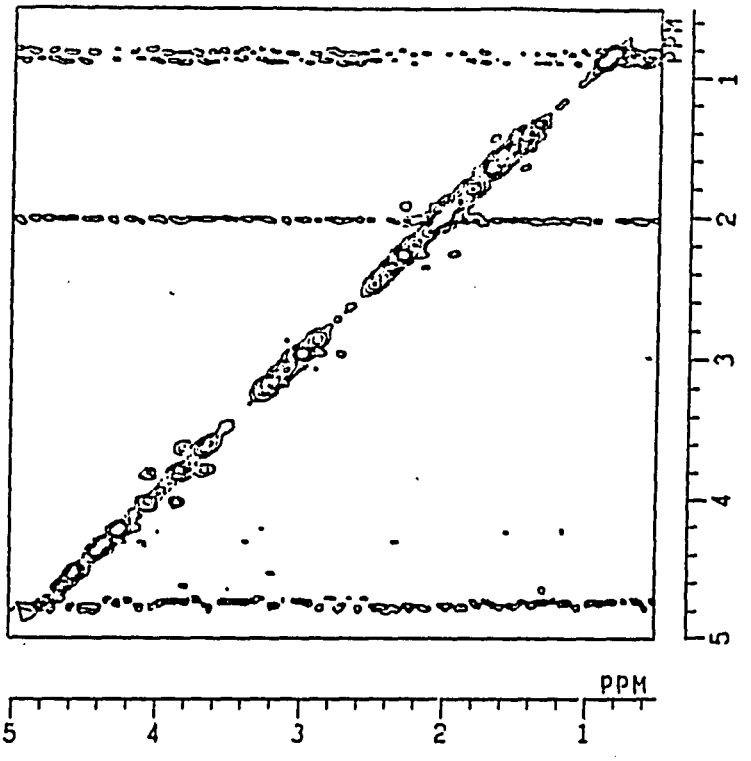

B.

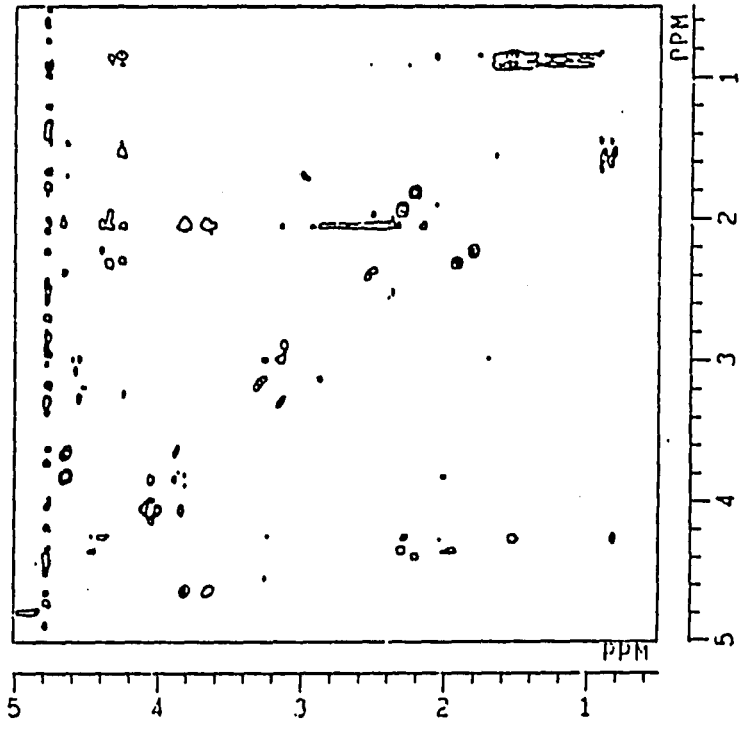

FIGURE 23

Negative contours of the ROESY spectrum of alpha-factor in D_2O (400 MHz, 25°C, 200 ms).
The diagonal and crosspeaks arising from chemical exchange or Hartmann-Hahn transfer are presented.

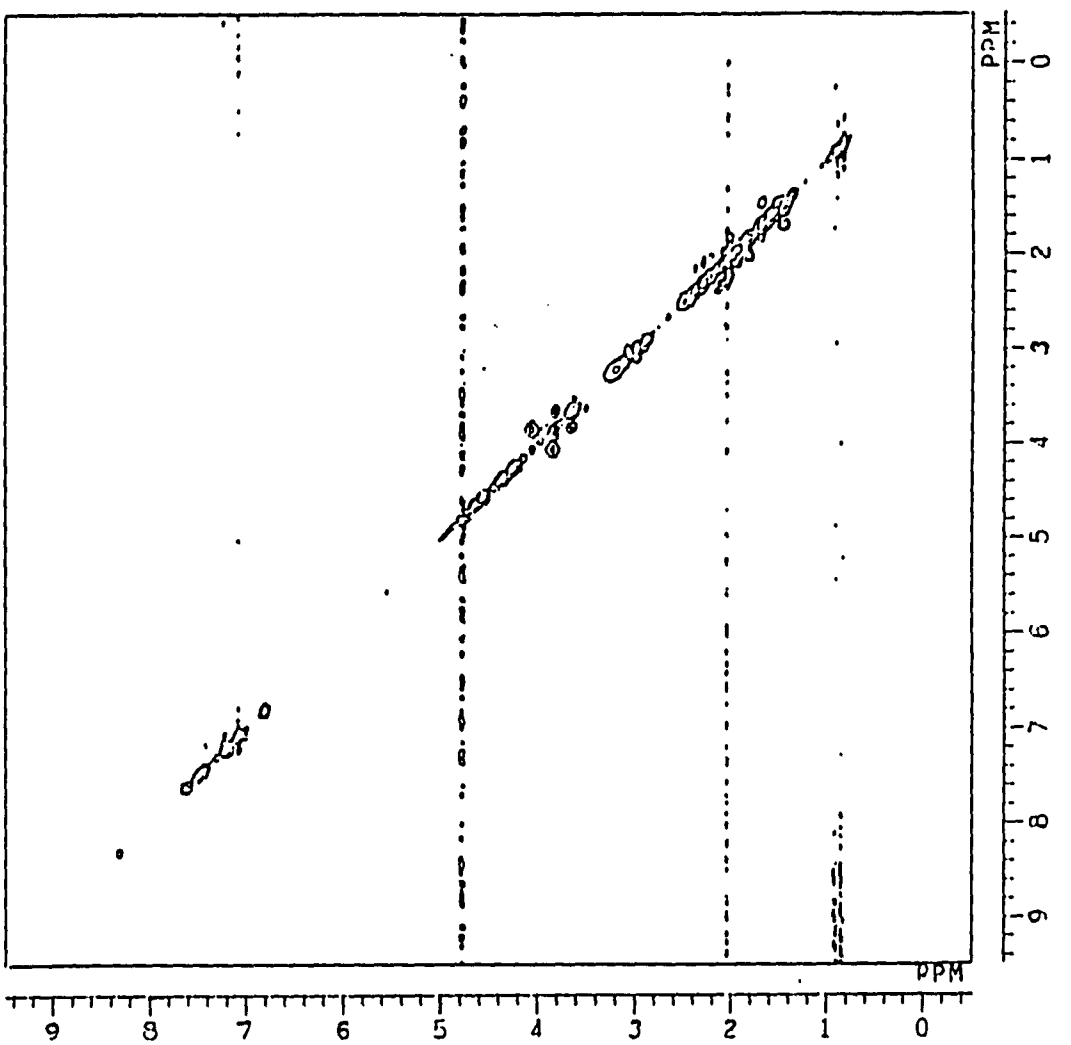
PPM
0
1
2
3
4
5
6
7
8
9
PPM
9
8
7
6
5
4
3
2
1
0

interaction of the peptide with various phospholipids representative of those it must encounter in the yeast plasma membrane (86).

Initial ^{1}H NMR studies of alpha-factor in the presence of lysomyristoylphosphatidylcholine micelles or mixed vesicles (egg phosphatidylcholine:egg phosphatidylglycerol, 3:1) showed broadening of all peptide resonances (not shown). In addition, a preliminary solid state ^{31}P NMR spectrum of alpha-factor and unsonicated DPPC (sample had been subjected to repeated freeze-thaw cycles), obtained by Dr. R. Andrew Byrd, consists of a single isotropic ^{31}P resonance (not shown) whereas a powder type spectrum is expected for unsonicated lipid dispersions (97). These initial results suggested a significant interaction between the peptide and lipid. ^{31}P, ^{2}H, and ^{1}H NMR, as well as QLS studies, were performed in order to further characterize this interaction.

Small unilamellar vesicles (prepared by sonication, as described in Chapter III) have a bilayer arrangement of phospholipid molecules like biological membranes and have been characterized by NMR and QLS (83, 91, 98, 99). Furthermore, ^{1}H resonances of peptides bound to vesicles are usually not broadened as extensively as they are when the peptide is bound to less mobile, multilamellar lipid dispersions. The appearances of the ^{1}H, ^{2}H, and ^{31}P resonances are consistent with the vesicle sizes determined by QLS and with the lipid state expected at each

temperature. Gel state lipid spectra are much broader than liquid crystalline state spectra and the lipid $(CH_2)_n$ resonance is often undetectable in the gel state ^1H spectra of large vesicles (99, 100).

QLS measurements were obtained for most vesicle preparations without alpha-factor and with alpha-factor added and are reported in Tables VIII and IX, respectively. Most vesicle preparations consisted of large vesicles ~850 - ~1150 Å in diameter although the unsaturated lipids, DOPC and DOPE, formed smaller vesicles (~500 Å). Upon addition of alpha-factor all vesicles, except those formed from a mixed lipid preparation (representative of the phospholipid composition of the yeast plasma membrane), increased in size. (DOPC vesicle size increased only by a very small amount.) The polydispersity, which is a measure of the uniformity of the vesicle size distribution, also increased upon addition of alpha-factor.

Figure 24 shows the ^{31}P NMR spectrum of dipalmitoylphosphatidylcholine (DPPC) with and without alpha-factor at 25°C, 41°C, and 50°C. At 25°C this lipid is in the gel state while at 50°C it is in the more fluid liquid crystalline state. Near 41°C the lipid undergoes the transition from the gel to the liquid crystalline state. Figures 25 and 26 show similar spectra (at temperatures in the gel state, near the transition temperature, T_c, and in the liquid crystalline state) obtained with distearoylphosphatidylcholine (DSPC) and

TABLE VIII

QLS data for the pure lipid samples at 23° C

Lipid Sample	Diameter(Å)	Polydispersity Index(V) (%)
DPPC	1056	21
	1055	20
	1028	21
	1028	22
	1167	39
	1162	38
	850**	33
	851**	32
DSPC	1078	12
	1078	11
DPPA	1100	76
brain PS	1089	57
	1165	63
Mixed PL	859	28
	862	29
DOPC	437	49
	495	59
	467	48
	473	49
DOPE	626	35
	590	24
DPPE*	18,000	70
	28,000	70

*Accurate measurements were not obtainable for the DPPE sample due to the large amount of scattering of light even by dilute samples.

Two measurements were made for each sample. Multiple values reported above represent measurements of different samples.

**This DPPC sample was sonicated for a longer period of time than the others.

TABLE IX QLS Data for Alpha-factor - Lipid Samples at 23°C

Lipid Sample	Diameter(Å)	Polydispersity index(V) (%)	Comment
DPPC + α-factor*	4624	38	
	5580	45	
	28,710	37	after 4 days
	29,460	39	after 4 days
	3793	32	16:0.2
	4403	36	16:0.4
	5813	42	16:0.6
	5907	47	16:0.8
	4624	38	
DSPC "	13,640	47	after 2 days
	13,640	47	after 2 days
DPPA "	3500	114	
brain PS "	no measurement		
Mixed PL "	644	41	
	662	42	
DOPC "	449	29	
	450	29	
	519	38	
	538	40	
	530	42	
	573	54	
DOPE "	3051	24	

Lipid:Peptide ratio was 16:1 unless otherwise noted under "Comment"
Accurate measurements were not obtained for DPPE + α-factor.
Conditions are the same as for pure lipid samples.

FIGURE 24

^{31}P NMR spectra of DPPC vesicles with (top spectrum) and without (bottom spectrum) alpha-factor added.
A. at 25°C
B. at 41°C
C. at 50°C
At 25°C pure DPPC is in the gel state, near 41°C it undergoes the transition to the liquid crystalline state, and at 50°C it is in the liquid crystalline state.
There is no evidence of chemical shift anisotropy.

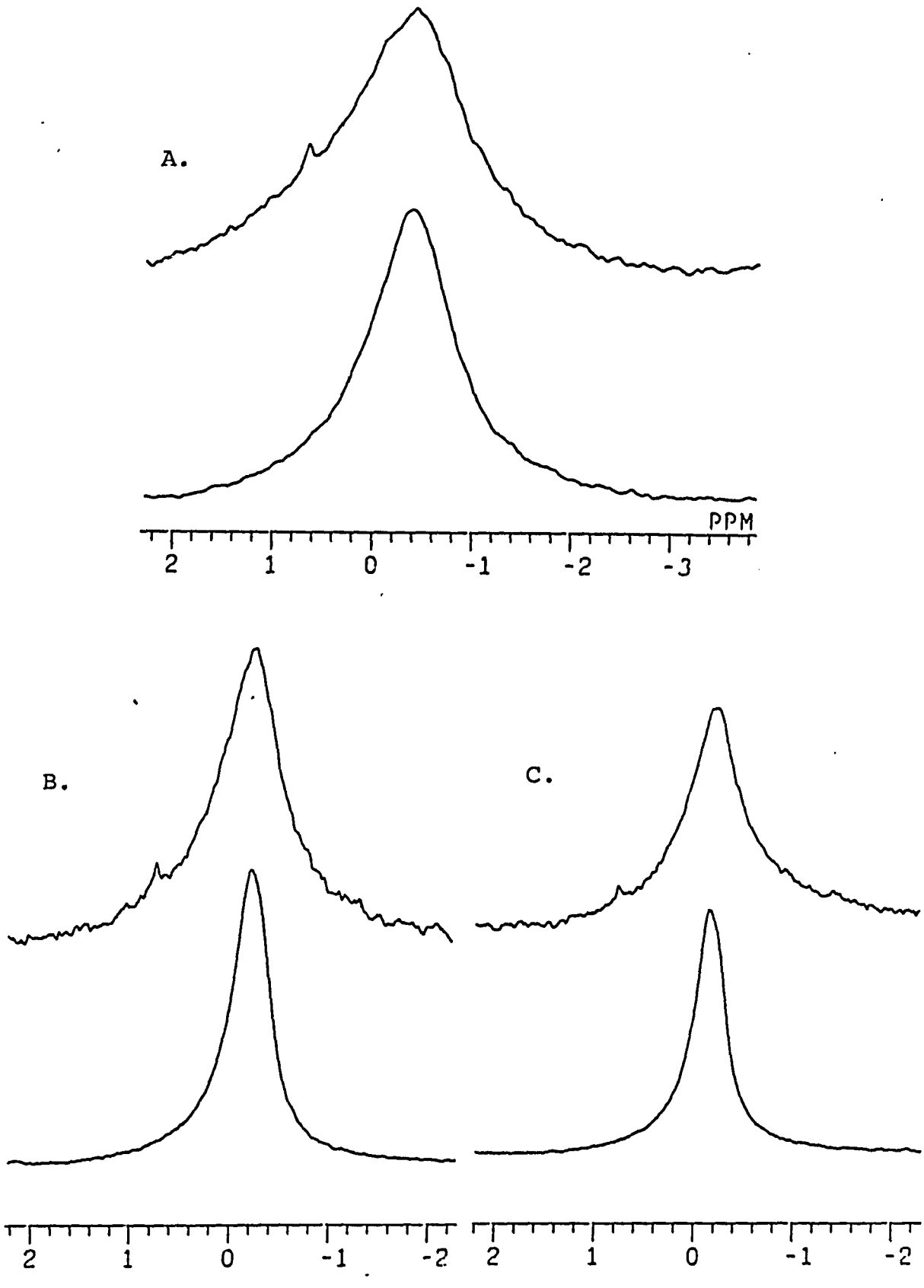
A.
PPM
2
1
0
-1
-2
-3
B.
2
1
0
-1
-2
C.
2
1
0
-1
-2

FIGURE 25

^{31}P NMR spectra of DSPC vesicles with (top spectrum) and without (bottom spectrum) alpha-factor added.
A. at 25°C
B. at 58°C
C. at 65°C

At 25°C pure DSPC is in the gel state, at 58°C* it undergoes the transition to the liquid crystalline state, and at 65°C it is in the liquid crystalline state.

As with DPPC, there is no evidence of chemical shift anisotropy.

*The transition temperature for DSPC has been reported as 54°C as well as 58°C.

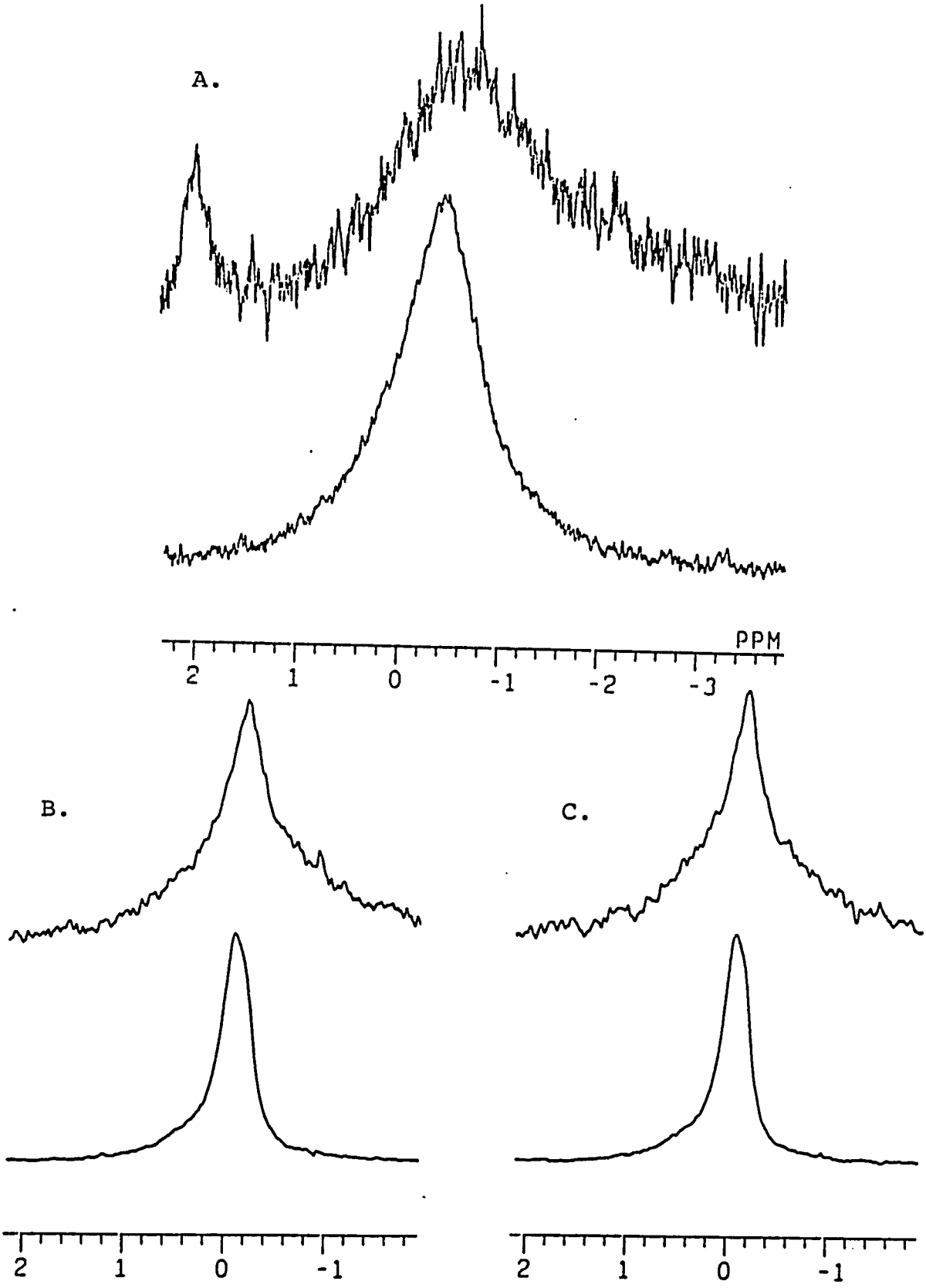
A.
PPM
2
1
0
-1
-2
-3
B.
2
1
0
-1
C.
2
1
0
-1

FIGURE 26

^{31}P NMR spectra of DPPA vesicles with (top spectrum) and without (bottom spectrum) alpha-factor added.
A. at 25°C
B. at 67°C
C. at 75°C
At 25°C pure DPPA is in the gel state, at 67°C it undergoes the transition to the liquid crystalline state, and at 75°C it is in the liquid crystalline state.
There is no evidence of chemical shift anisotropy.

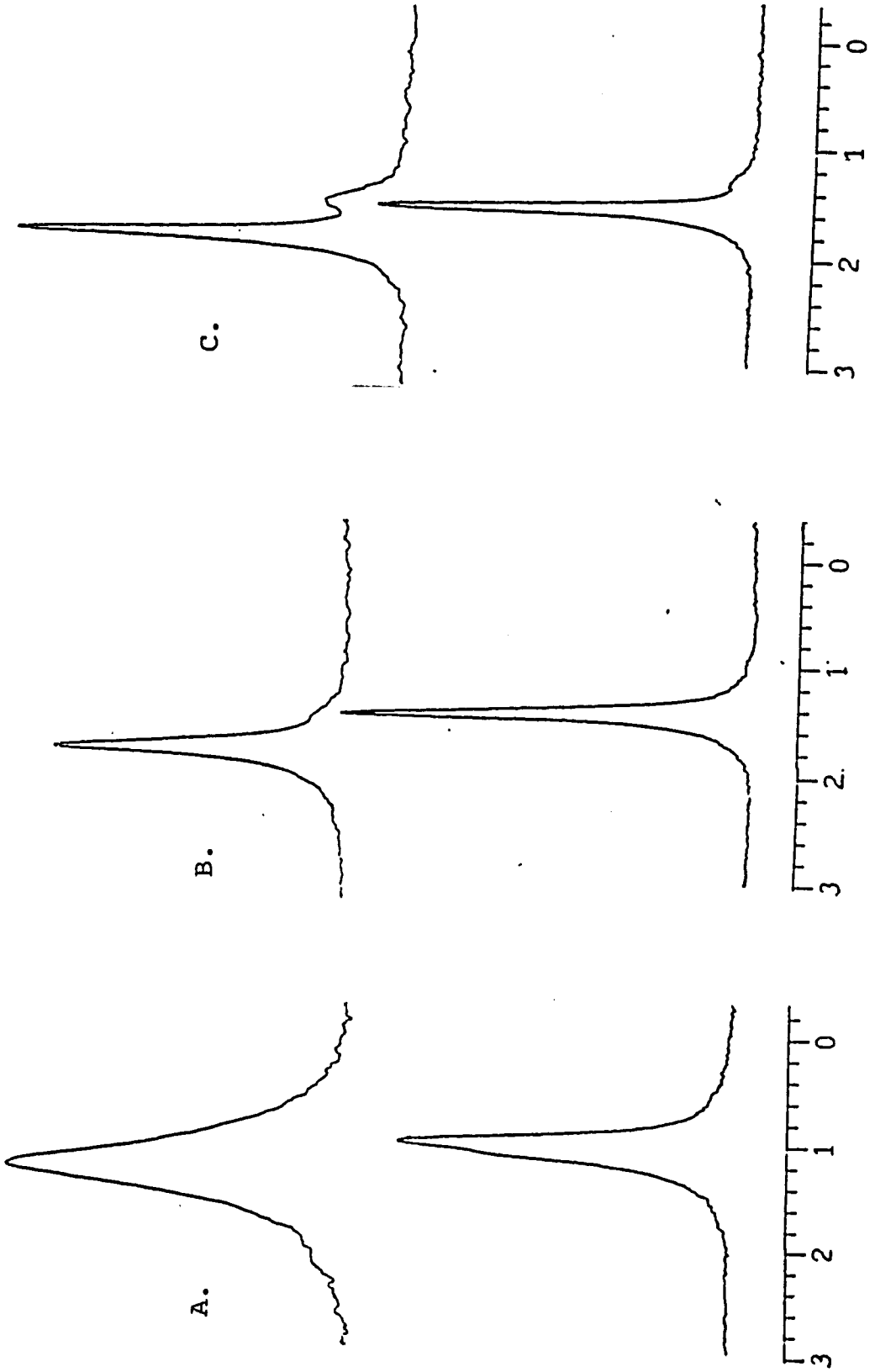
A.
B.
C.
0
1
2
3

dipalmitoylphosphatidic acid (DPPA) vesicles. Figure 27 shows the spectra acquired with soybean phosphatidylinositol (PI), dioleoylphosphatidylcholine (DOPC), and dioleoylphosphatidylethanolamine (DOPE) at 24°C and dipalmitoylphosphatidylethanolamine (DPPE) at 70°C. These four lipids are in the liquid crystalline state at the temperatures studied. Although the spectrum of DPPE is a "powder" type spectrum usually observed for lipid dispersions consisting of multilamellar aggregates (Figure 27 D), single isotropic peaks expected for sonicated unilamellar vesicles are observed in all other spectra (101). When alpha-factor is added to the vesicles, all spectra (except DPPE) show increased linewidth of the resonance which, however, remains an isotropic peak. In some spectra an extra component of unkown origin appears (discussed in Chapter V). Chemical shifts and linewidths are reported in Table X.

In order to determine any alterations in phosphate headgroup mobility upon interaction with alpha-factor, T_2 relaxation times for the phoshatidylcholine vesicles (DPPC, DSPC, and DOPC) were determined. T_2^* values were calculated from the linewidths and T_2 values were determined using a modified Hahn spin-echo sequence. The results in Table XI indicate a shortening of T_2 upon addition of alpha-factor to the vesicles.

Because it is possible that the interaction of alpha-factor with vesicle involves both the phosphate headgroup

FIGURE 27

^{31}P NMR spectra of PI, DOPC, DOPE, and DPPE vesicles with (top spectrum) and without (bottom spectrum) alpha-factor added.
A. soybean PI at 24°C
B. DOPC at 24°C
C. DOPE at 24°C
D. DPPE at 70°C
At these temperatures the pure lipids are in the liquid crystalline state.
In A,B, and C there is no chemical shift anisotropy observed; however, in D (DPPE) the spectra exhibit the anisotropy expectred for hexagonal$_{II}$ phase lipid (bottom) and for bilayer type lipid (top).

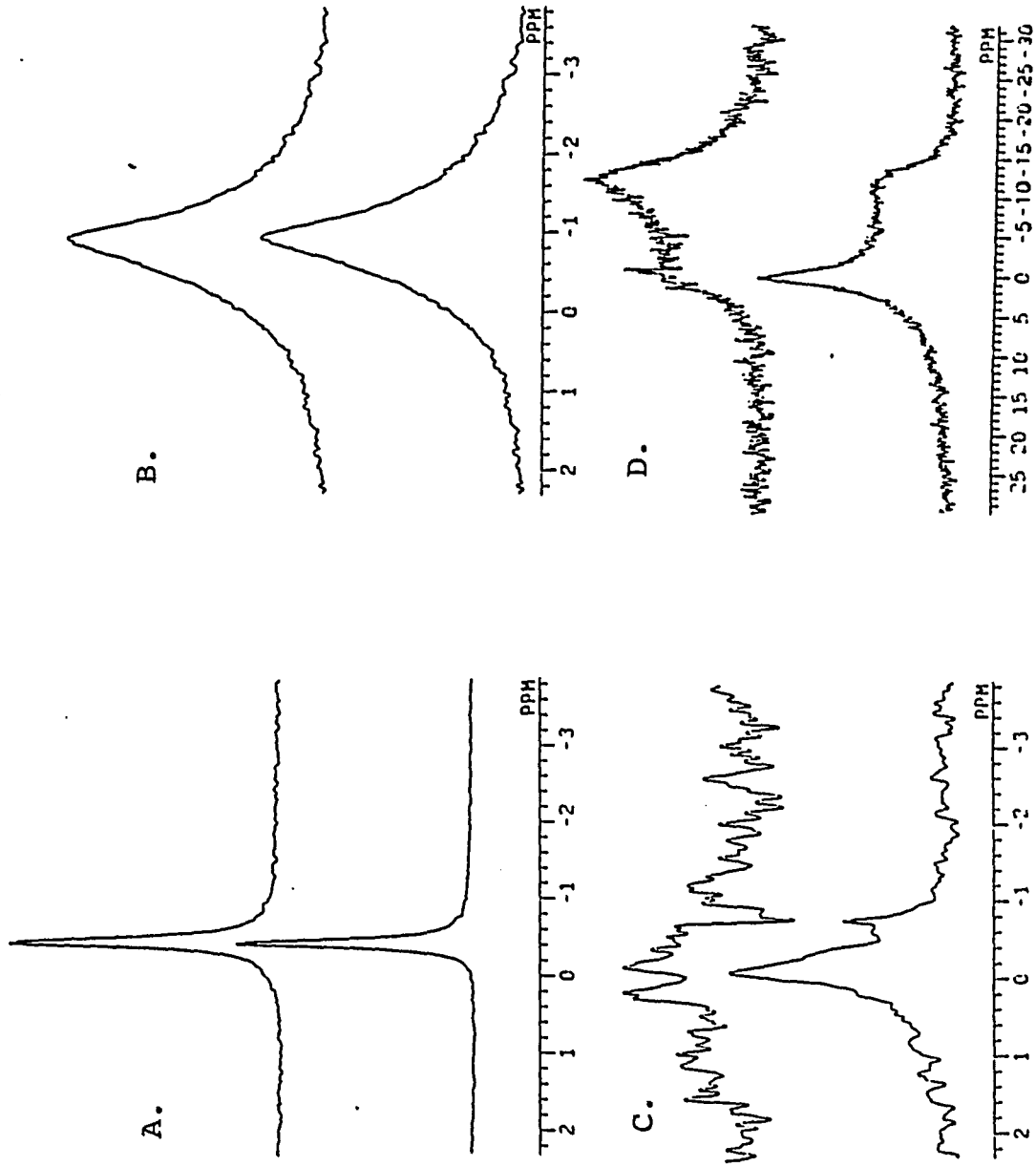
A.
B.
C.
D.
PPM
2 1 0 -1 -2 -3
25 20 15 10 5 0 -5 -10 -15 -20 -25 -30

TABLE X

^{31}P NMR Chemical Shifts and Linewidths

Sample	Temp. °C	δ(ppm) without peptide added	Linewidth (Hz) without peptide added	δ(ppm) with peptide added	Linewidth (Hz) with peptide added	Δδ(ppm)	% increase in Linewidth
DPPC	25	-0.31	175	-0.39	225	-0.08	29
	41	-0.24	85	-0.29	150	-0.04	88
	50	-0.17	65	-0.19	130	-0.02	100
DSPC	25	-0.39	175	-0.58	220	-0.19	26
	58	-0.09	65	-0.19	150	-0.10	131
	65	-0.07	50	-0.15	130	-0.08	160
DPPA	25	1.08	55	1.30	115	+0.22	109
	67	1.24	20	1.39	36	+0.15	80
	75	1.30	18	1.45	25	+0.15	19
DOPC	24	-0.87	120	-0.95	190	-0.07	58
soy PI	24	-0.44	20	-0.48	23	-0.04	15
DOPE	24	-0.13	85	*	*	*	*
DPPE	70	0.20	20 ppm	-12.46	20 ppm	-12.24	**

^{31}P chemical shifts are reported relative to an external 1% H_3PO_4 solution.

* The DOPE spectrum was broadened to baseline upon addition of alpha-factor, therefore these parameters could not be determined.

** The DPPE spectrum changed dramatically upon addition of alpha-factor (See Figure 35). The chemical shift reported in this table is that of the sharp component of the spectrum.

Reported linewidths are accurate to ± 5-10 Hz, chemical shifts are accurate to ± 0.03-0.06 ppm.

Where three temperatures are reported the first is lipid in the gel state, the second is near T_c, and the third is in the liquid crystalline state. When only one temperature is reported it is the liquid crystalline state.

TABLE XI ^{31}P NMR Spin-Spin Relaxation Data for pure lipid and alpha-factor - lipid samples.

Sample	Temp.°C	T_2^*(ms) without peptide	T_2(ms) without peptide	T_2^*(ms) with peptide	T_2(ms) with peptide
DPPC	25	1.8	1.6	1.4	0.9
	41	3.8	3.8	2.1	1.2
	50	5.0	3.8	2.5	2.0
DSPC	25	1.8	0.8	1.4	0.2
	58	5.0	2.4	2.1	1.3
	65	6.6	2.7	2.5	1.4
DOPC	24	2.7	2.1	1.7	1.5
soy PI	24	15.9	-	13.8	-
DPPA	25	6.0	-	3.0	-
	67	16.0	-	9.0	-
	75	18.0	-	13.0	-
DPPE	70	-	0.2	-	0.3

- = value not measured.
T_2^* values were determined from the linewidths reported in Table X and required approximately one hour of experimental time at each temperature. The T_2 values were determined by the spin-echo method and required at least 18 hours for each temperature. The T_2 values were determined using 8 tau values except in the case of DSPC where the S/N was so poor at 25°C (for both pure lipid and alpha-factor lipid samples) and upon addition of peptide that time permitted the use of only 5 tau values. T_2 experiments were repeated only for the DPPC samples and the error was ± 0.3 ms at 25°C.

and the fatty acyl chains, the effect of alpha-factor on the ^2H spectrum of specifically chain deuterated lipids was examined. Figure 28 shows the ^2H spectra of vesicles, prepared from DPPC deuterated along the entire hydrocarbon chain, at 25°, 41°, and 50°C . Figure 29 shows the 24°C spectra obtained from DOPC vesicles which were deuterated only at the oleoyl (9,10) positions of the hydrocarbon chain. The DPPC spectra show a broadening of the ^2H resonance at all temperatures (~55 Hz at 25°C, ~15 Hz at 41°C, and ~30 Hz at 50°C) upon addition of alpha-factor while there is no change in the DOPC resonance linewidth. At 25°C a small peak appears near 4.8 ppm due to residual ^2H in the deuterium depleted water. In the spectrum with alpha-factor (at 25°C) another small peak, of unknown origin, appears between 2 and 3 ppm. ^2H T_1 and T_2 values were determined for these vesicles in the absence and presence of alpha-factor. The data, presented in Table XII, show very little, if any, change in the DPPC T_1 and T_2 upon addition of alpha-factor and no changes in the DOPC relaxation times.

In order to further characterize the vesicle systems ^1H NMR spectra of the phospholipid vesicle preparations were acquired. Relatively sharp resonances were observed in all spectra, except those of DPPE, indicating that the sonicated lipids are present as unilamellar vesicles and not as multilamellar aggregates. At all temperatures a bimodal choline N methyl resonance indicative of two

FIGURE 28

^2H NMR spectra of deuterated (entire hydrocarbon chain) DPPC vesicles with (top spectrum) and without (bottom spectrum) alpha-factor added.
A. at 25°C
B. at 41°C
C. at 50°C
At 25°C pure DPPC is in the gel state, it undergoes a transition to the liquid crystalline state near 41°C (reported to be lower, 35.5°C, for perdeuterated DPPC), and is in the liquid crystalline state at 50°C.
No quadrupole splitting is observed.

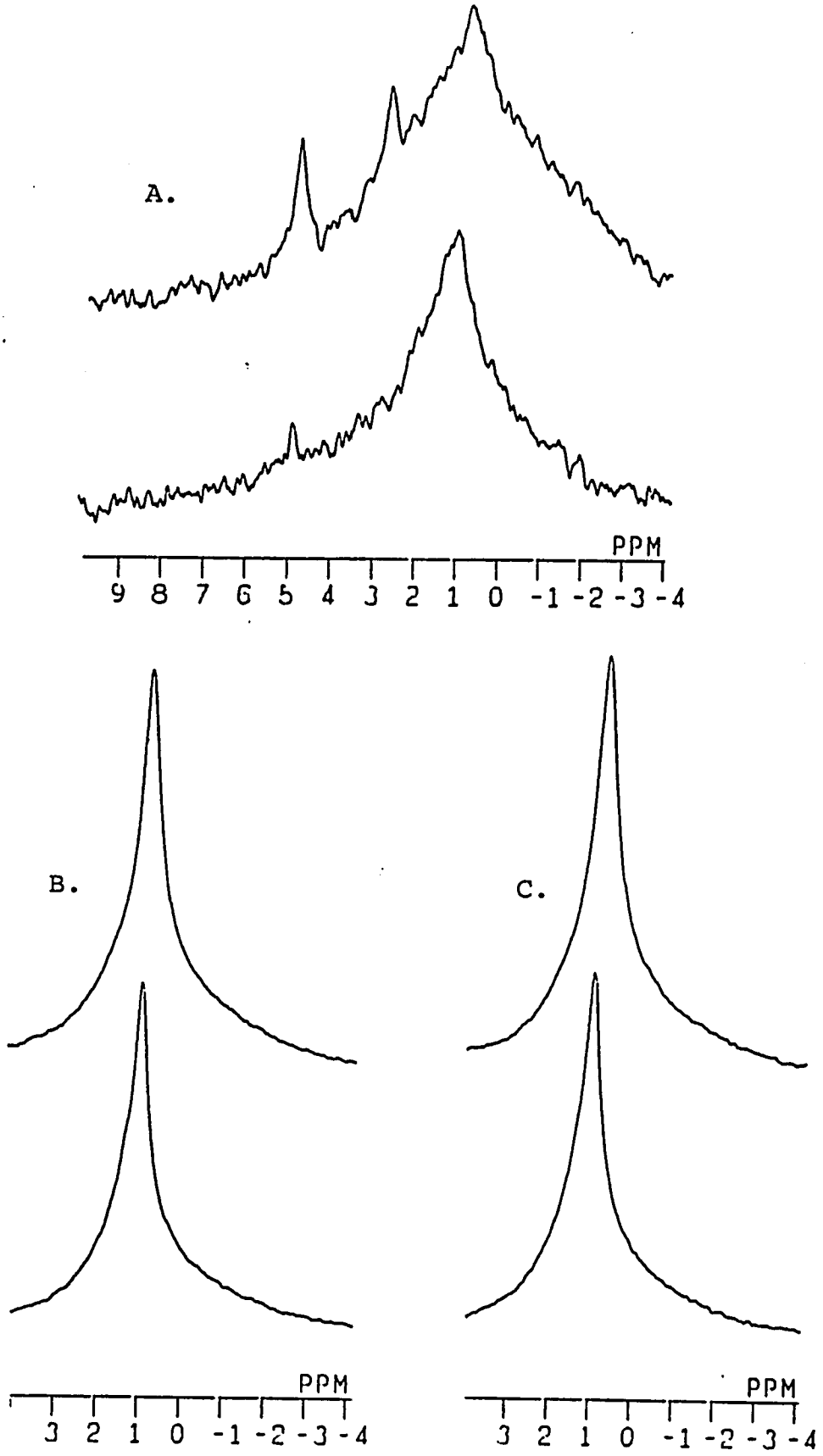
A.
PPM
9 8 7 6 5 4 3 2 1 0 -1 -2 -3 -4
B.
PPM
3 2 1 0 -1 -2 -3 -4
C.
PPM
3 2 1 0 -1 -2 -3 -4

FIGURE 29

^2H NMR spectra of deuterated (oleoyl position) DOPC vesicles with (top spectrum) and without (bottom spectrum) alpha-factor at 24°C (in the liquid crystalline lipid state). No quadrupole splitting is observed.

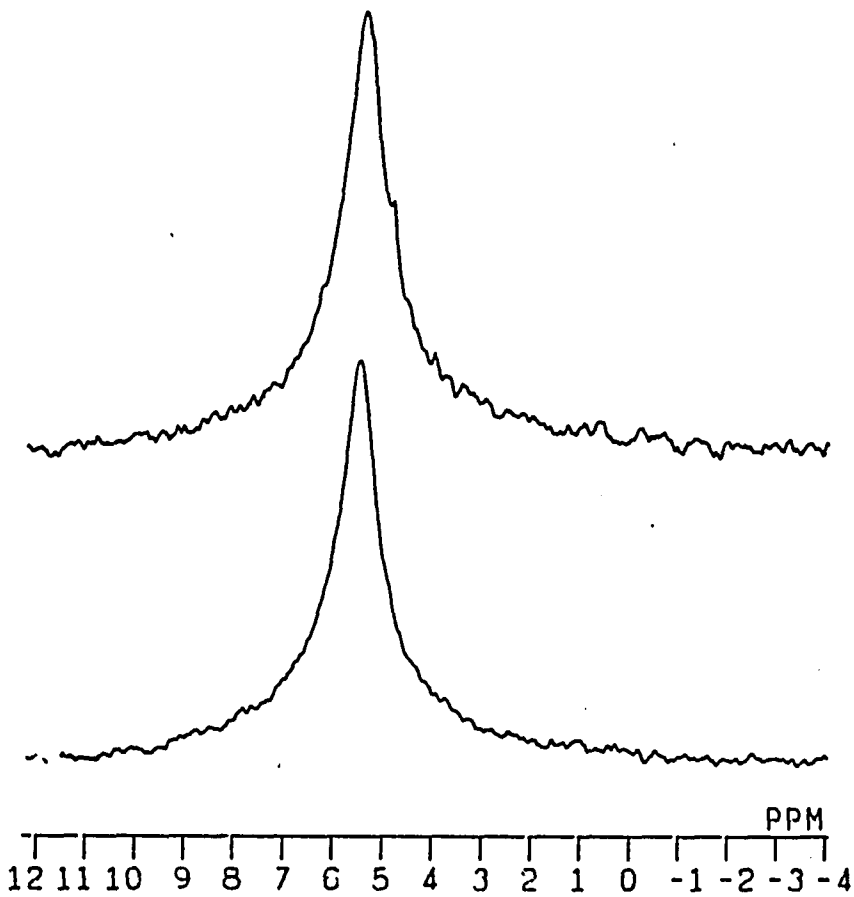
PPM
12 11 10 9 8 7 6 5 4 3 2 1 0 -1 -2 -3 -4

TABLE XII

^2H NMR Parameters

Sample	Temp. °C	δ(ppm)	Linewidth (Hz)	% increase in linewidth upon addition of peptide	T_2^* (ms)	T_2(ms)	T_1(ms)
DPPC	25	1.135	145		2.0	1.1	194
	41	1.019	60		5.3	5.0/6.4	378
	50	0.977	45		7.0	6.4/8.6	417
DPPC + α-factor	25	0.944	200	28	1.6	1.7/4.5	189
	41	0.860	75	25	4.3	3.9/8.8	382
	50	0.849	70	56	4.5	9.0/11.4	440
DOPC	25	5.496	85		3.8	3.9	16.6
DOPC + α-factor	25	5.401	85	0	3.8	3.9	16.6

Chemical Shifts are reported relative to natural abundance deuterium in water (which resonates at 4.78 ppm at 25 C, 4.60 ppm at 41 C, and 4.51 ppm at 50 C).

Where two values are listed for T_2, the first value is that determined by simply varying tau, the second value is that determined by acquiring successive echoes.

Linewidths are accurate to $\pm$ 5-10 Hz, chemical shifts are accurate to $\pm$ 0.08 ppm.

T_2 experiments were repeated for the DPPC sample only and the error was $\pm$ 0.6 msec.

Error for T_1s are $\pm$ 6 ms, for T_2^* $\pm$0.2 ms

populations (inner and outer leaflets of the bilayer) is observed in the spectra of all phosphatidylcholine samples (98, 99). This splitting is clearly observed in the 25° and 41°C spectra of DPPC shown in Figure 30.

The ^1H spectra of alpha-factor in the presence of DPPC vesicles at 25°, 35°, 41°, and 50°C are shown in Figure 31 (lipid:peptide ratio, 4:1). The alpha-factor resonances are broad at 25°C and sharpen as temperature increases. This is shown more clearly in the expansions of the downfield regions of the ^1H spectra (see Figure 32). Wakamatsu et al. report an increased broadening near T_c (~35°C for the perdeuterated DPPC, ~41°C for undeuterated DPPC) whereas we observe no such broadening (45). Figure 33 shows the 25°C alpha-factor spectrum with various concentrations of DPPC in D_2O. Peptide resonances are dramatically broadened even at lipid:peptide ratios of 1:1. ^1H spectra in the presence of DSPC were very similar to those in the presence of DPPC (acquired at temperatures above and below T_c, not shown).

Figure 34 shows expansions of the upfield and downfield region of the 25°C spectrum of PS vesicles with alpha-factor added. At lipid: peptide ratios of 2:1 the broadening is similar to that observed in the phosphatidylcholines at higher ratios (compare the Leu delta CH_3 resonances at ~0.8 ppm on this figure with those shown in the 8:1 spectrum in DPPC, Figure 32). Spectra in the presence of PI and the mixed lipid vesicles were

FIGURE 30

^{1}H NMR spectrum of pure DPPC vesicles.
At 41°C the bimodal choline $N(CH_3)_3$ resonance is observed.
At 25°C this resonance is broader but still has bimodal structure indicating the inner and outer leaflets of the vesicle bilayer.

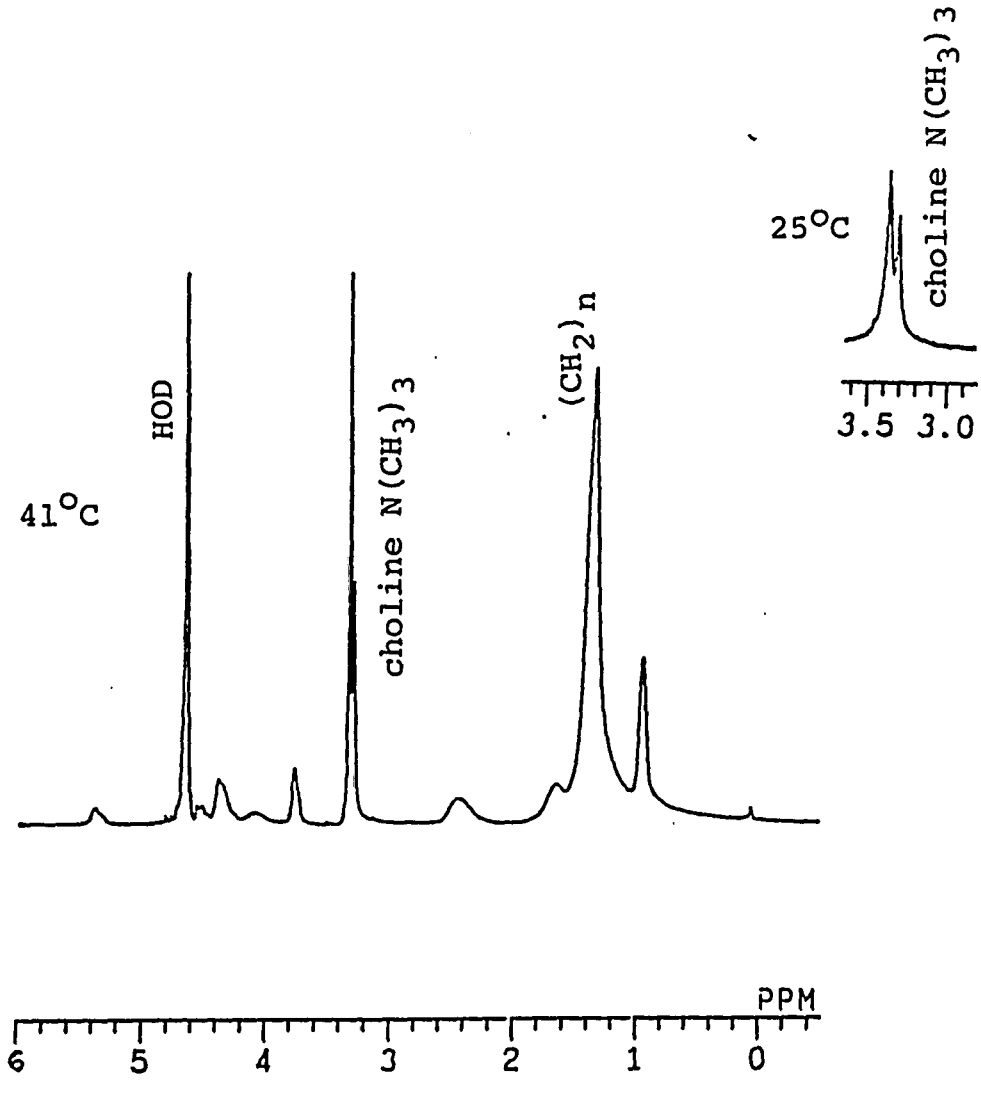
41°C
HOD
choline N(CH3)3
(CH2)n
PPM
6
5
4
3
2
1
0
25°C
choline N(CH3)3
3.5
3.0

FIGURE 31

^1H NMR spectra of alpha-factor in DPPC vesicles at various temperatures (in H_2O).
Lipid:peptide ratio is 4:1 in all spectra.
Peptide resonances are broad at 25°C and sharpen as temperature is increased.

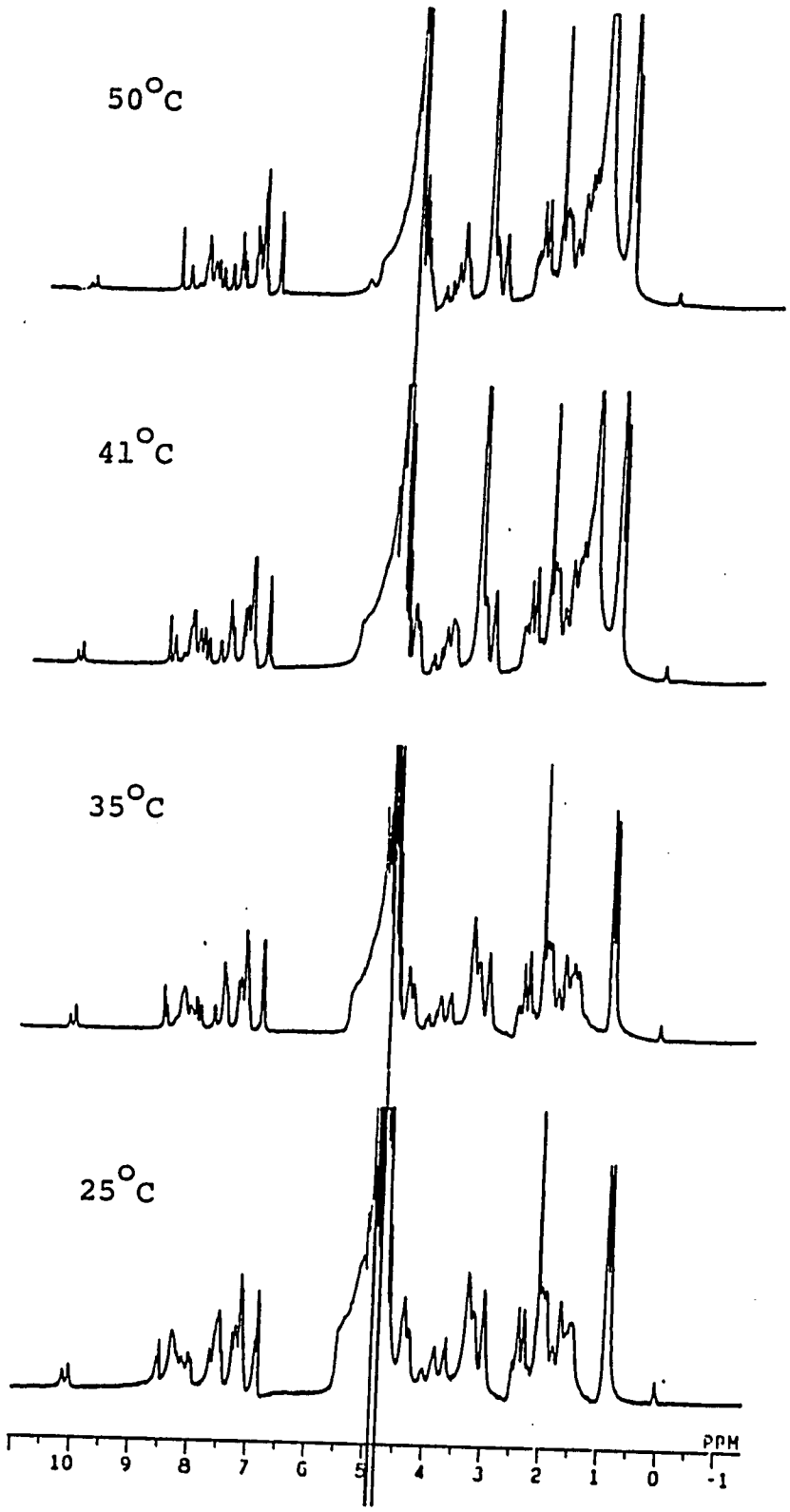
50°C
41°C
35°C
25°C
10
9
8
7
6
5
4
3
2
1
0
-1
PPM

FIGURE 32

Expansions of the ^{1}H NMR spectra of alpha-factor in DPPC vesicles at various temperatures. Resonances do not appear to broaden near the transition temperature (41^{o}C for pure DPPC) relative to the gel state spectrum (25^{o}C). Lipid:peptide ratio is 4:1.

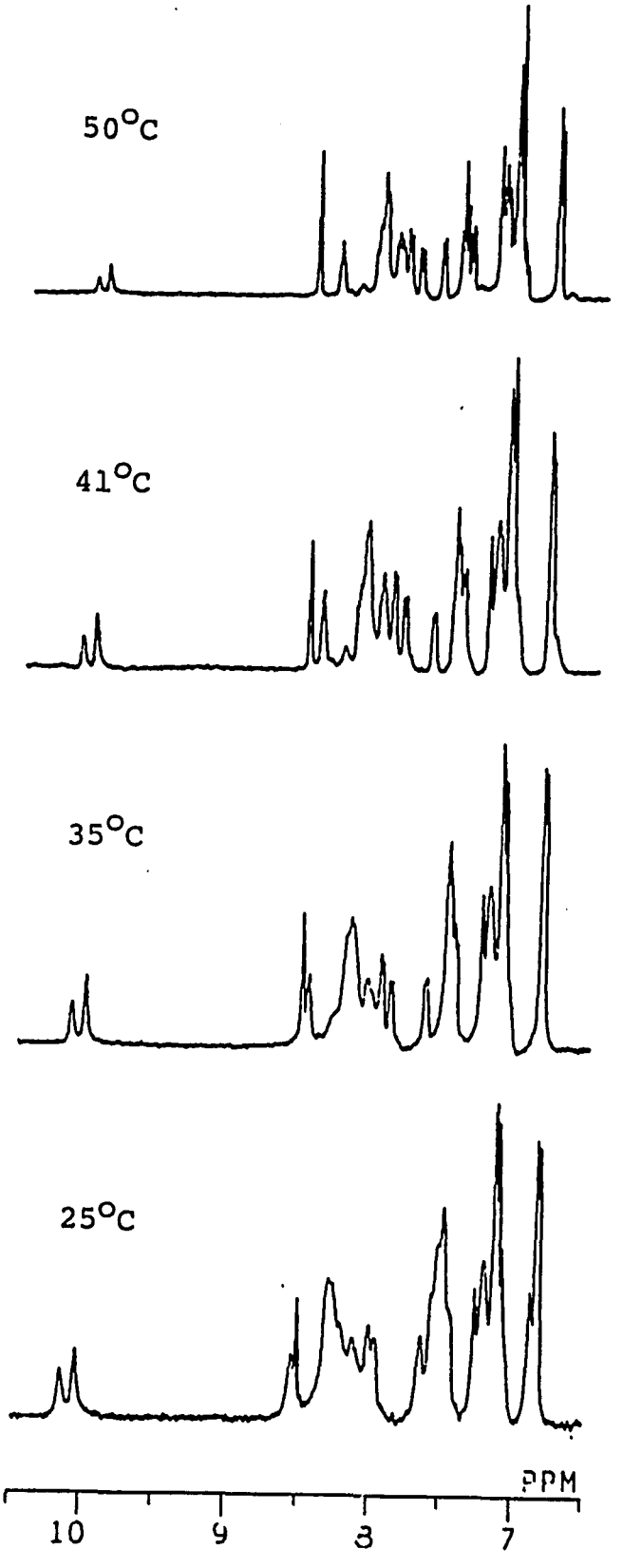
50°C
41°C
35°C
25°C
PPM
10
9
8
7

FIGURE 33

^1H NMR spectra of alpha-factor with various amounts of DPPC vesicles added (at 25°C) (in D_2O). Significant broadening of all peptide resonances is observed even at 1:1, lipid:peptide ratios. At 85:1, lipid:peptide, many alpha-factor resonances are no longer detectable.

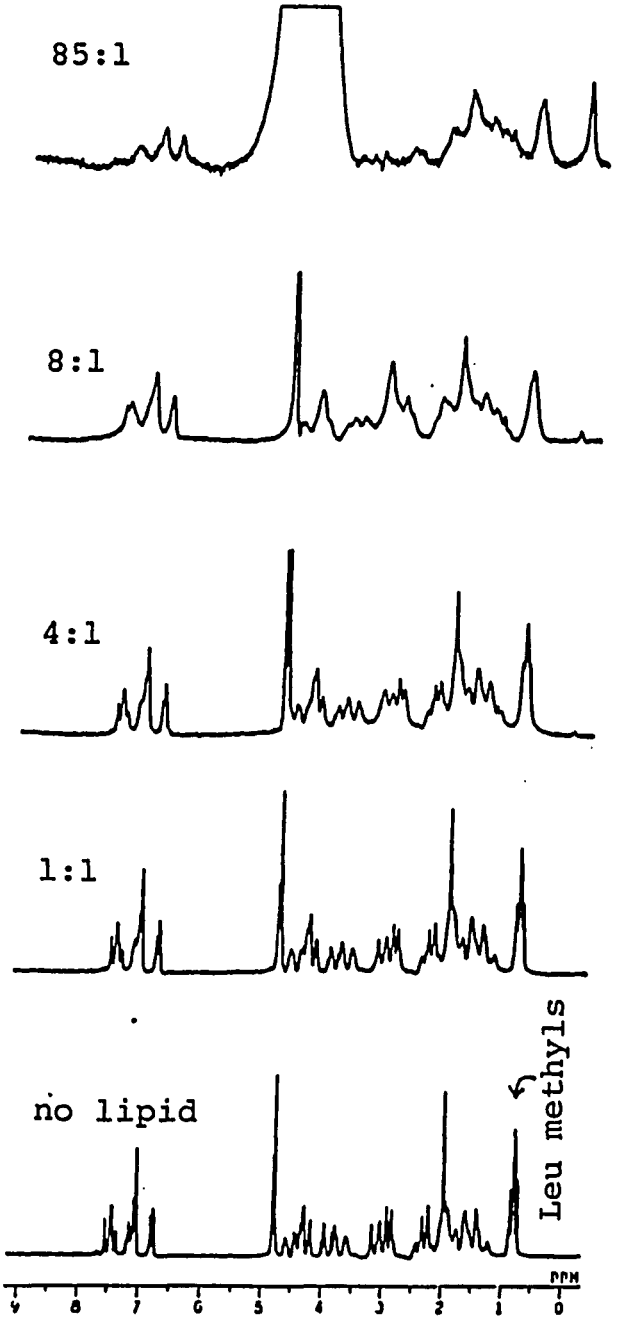
85:1
8:1
4:1
1:1
no lipid
Leu methyls
PPM
9
8
7
6
5
4
3
2
1
0

FIGURE 34

Expansions of the ^{1}H NMR spectrum of alpha-factor in bovine brain PS vesicles at 25°C (in D_2O). The broadening observed upon the addition of PS (lipid:peptide ratio of 2:1) is comparable to the broadening observed with higher lipid:peptide ratios of the other lipids (for example the 8:1 DPPC: alpha-factor spectrum in Figure 32). These vesicles are in the liquid crystalline state.

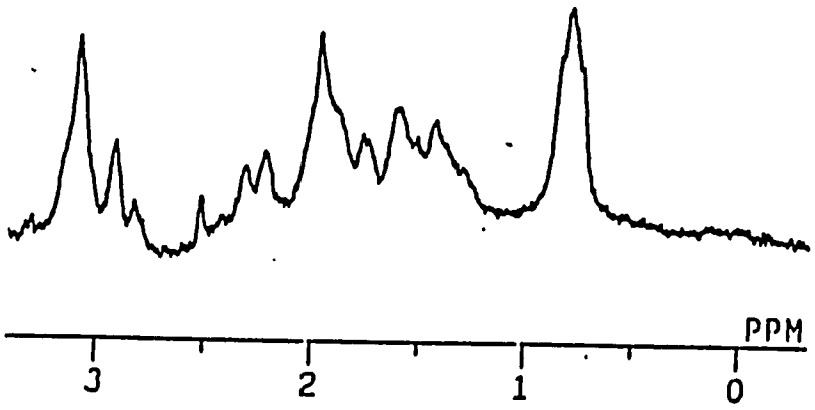
PPM
3
2
1
0

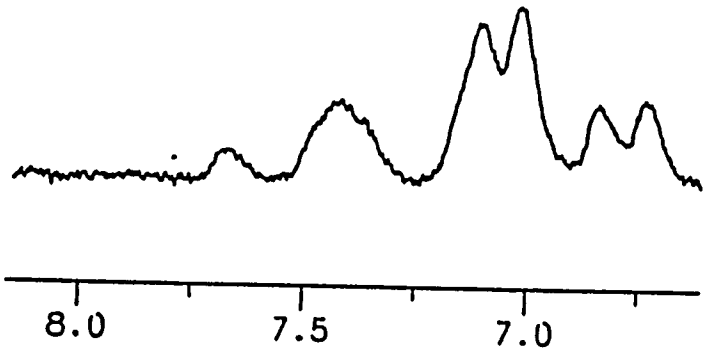
8.0
7.5
7.0

slightly less broadened than with PS vesicles (not shown). The extent of broadening by either DOPE (4:1, lipid : peptide, Figure 35) or DPPE (34:1, lipid : peptide, Figure 35) is much less than that observed with the other lipids. The DPPE spectrum with a lipid:peptide ratio of 34:1 is comparable to the spectrum in DPPC at a ratio of 4:1.

Separate resonances are not observed for the bound and free peptide; therefore, it can be concluded that the rate of exchange is fast on the NMR timescale. This allows the determination of binding constants as described in Chapter II. Binding studies were performed by adding successive known amounts of lipid (DPPC, DSPC, DPPE, mixed phospholipid vesicles, and PS) to a known amount of peptide. Because the concentration of free lipid was not known a modified version of the binding equation (given in Chapter II) was used:

$$K_{pl} = f_{pl} / (1-f_{pl}) (L - f_{pl} P_o)$$

K_{pl} is the affinity constant, L is the total concentration of lipid added, P_o is the initial peptide concentration, and f_{pl} is the mole fraction of peptide bound and is given by $(\delta_{obs} - \delta_f)/(\delta_{bd} - \delta_f)$ (102). δ_{obs}, δ_f, and δ_{bd} are the chemical shifts of a given resonance at the lipid concentration observed, free, and fully bound. The peptide was assumed to be fully bound when the resonance position no longer changed upon addition of more lipid.

As an example, the Tyr $^{13}C_{3,5}H$ resonance position, which does not overlap with any other peptide or lipid

FIGURE 35

^1H NMR spectra of alpha-factor in DOPE and in DPPE vesicles (in D_2O).
A. 4:1, DOPE: alpha-factor at 25°C
B. 34:1, DPPE: alpha-factor at 25°C

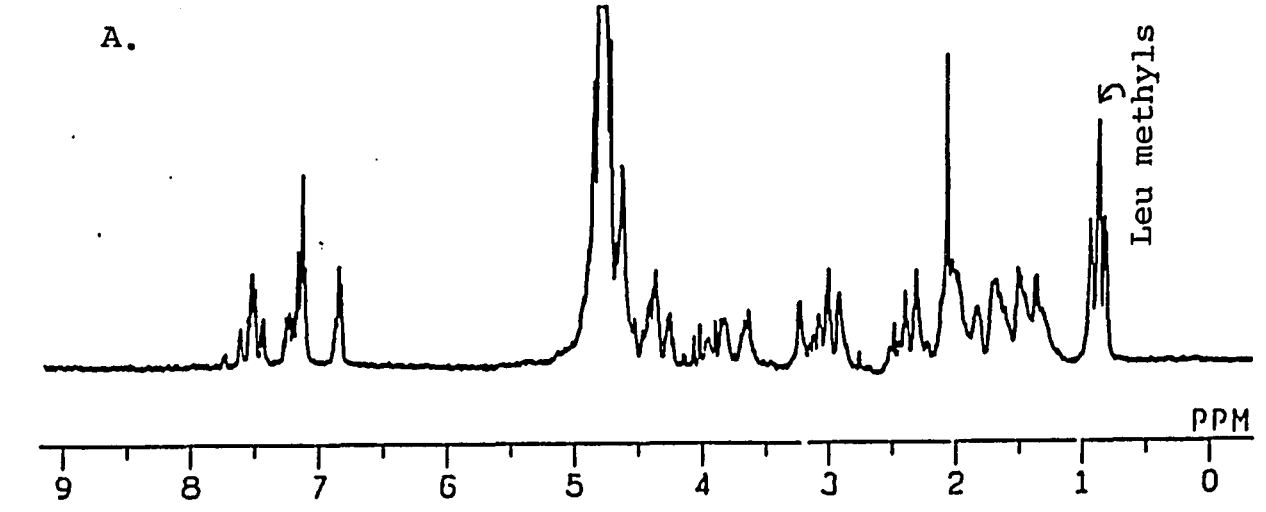
A.
δ
Leu methyls
PPM
9
8
7
6
5
4
3
2
1
0

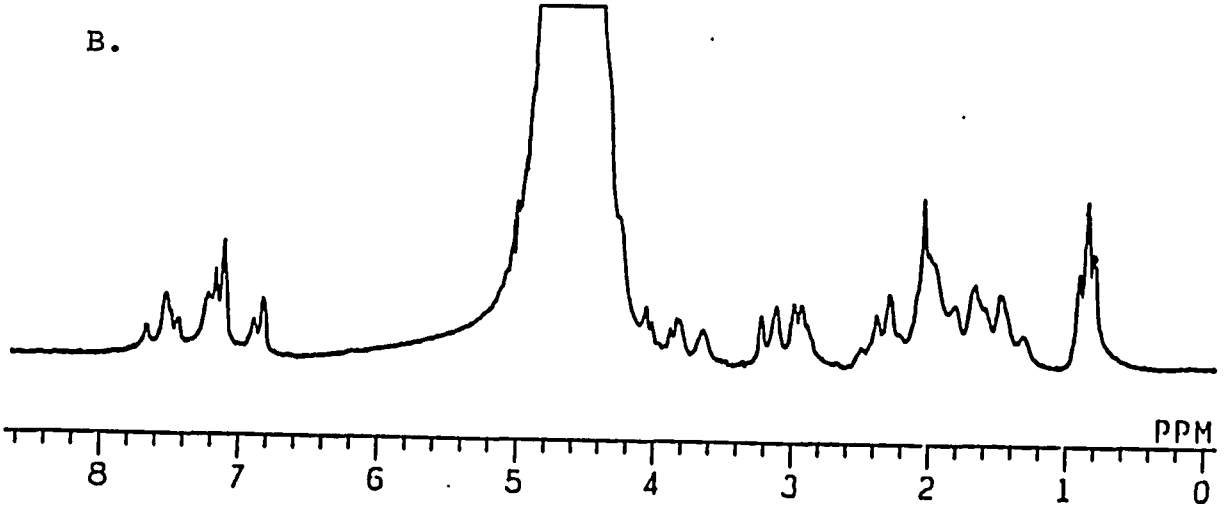
B.
PPM
8
7
6
5
4
3
2
1
0

resonance, was monitored while adding DOPC vesicles to the sample. The spectra of alpha-factor with different DOPC concentrations are shown in Figure 36 and the $Tyr^{13}C_{3,5}H$ resonance position (in Hz) is listed next to each spectrum (at 25°C). The peptide resonance position did not change from 24:1 through 97:1 (lipid :peptide ratios) and therefore the 24:1 position was taken as the fully bound resonance. A sample calculation of K_a is shown below:

$L = 29.55$ mM (at 8:1)

$P_o = 4$ mM

$\delta_{obs} = 2703.41$ Hz (at 8:1)

$\delta_f = 2695.34$ Hz

$\delta_{bd} = 2708.98$ Hz

$f_{pl} = 0.592$

$K_{pl} = 5.34 \times 10^1\ M^{-1}$

Resonances of several different amino acid residues ($Trp^{1,3}$, His^2, $Leu^{4,6}$, $Gln^{5,10}$, Met^{12}, and Tyr^{13}) were followed in these studies. K_a values for the different lipids are presented in Table XIII and are discussed in Chapter V.

To probe any conformation induced in alpha-factor by the lipid, 400 ms NOESY spectra of alpha-factor in the presence of various lipid vesicles (in D_2O) were acquired. In DPPC a large number of NOE crosspeaks are observed at both 25°C (Figure 37) and 41°C (not shown). NOESY spectra of alpha-factor in DPPC were acquired at pH ~7.0 and pH ~4.6. The same NOEs appear in both spectra (the spectrum

FIGURE 36

^{1}H NMR spectra of alpha-factor with various amounts of DOPC vesicles added (in D_2O). The position (in Hz) of the $Tyr^{13}C_{3,5}H$ is listed along with the lipid:peptide ratio of each spectrum and was used in the binding study.

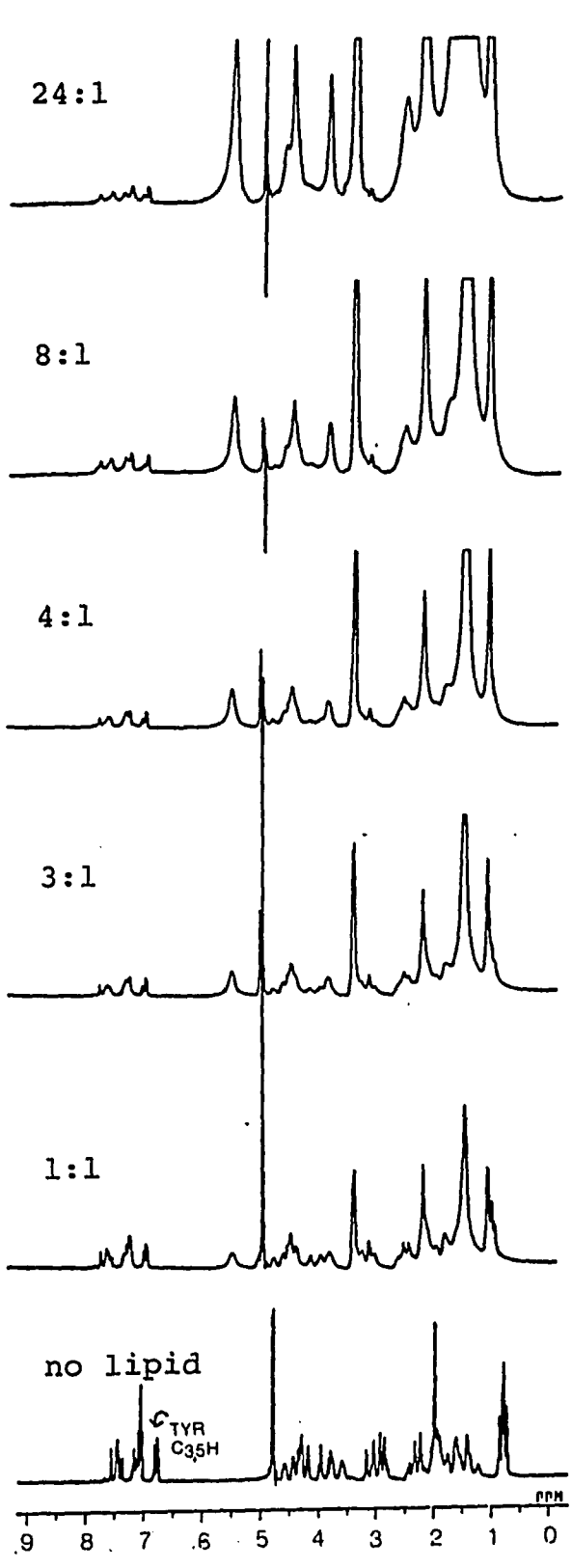
Tyr $^{13}C_{3,5}H$ position (Hz)
24:1
2708.98
8:1
2703.41
4:1
2702.48
3:1
2699.70
1:1
2697.84
no lipid
2695.34
C_{TYR} $C_{3,5}H$
ppm
9 8 7 6 5 4 3 2 1 0

TABLE XIII Affinity Constants determined from proton NMR binding studies

Sample	Resonance	K_a ($\times 10^1$ M^{-1})	Remarks
brain PS	Tyr^{13}C3,5H	23.0	
	$Trp^{1,3}$C2H/C5H	25.0	Overlap
	Trp^{3}beta CH_2	39.0	
	$Met^{12}SCH_3$	4.5	
DPPC	Tyr^{13}C3,5H	4.8	
	$Trp^{1,3}$C2H/C5H	4.6	Overlap
	$Leu^{4,6}$delta CH_3	4.8	Overlap
	Gln^{5}beta CH_2	7.7	Estimate
	Gln^{10}beta CH_2	7.7	Estimate
DOPC	Tyr^{13}C3,5H	5.3	
	$Trp^{1,3}$C2H/C5H	2.5	Overlap
	His^{2}C2H	1.8	
	His^{2}C4H	2.2	
DSPC	Tyr^{13}C3,5H	5.1	
	$Trp^{1,3}$C2H/C5H	4.4	Overlap
	His^{2}C2H	7.3	
	$Leu^{4,6}$delta CH_3	13.1	Overlap
DPPE	Tyr^{13}C3,5H	10.8	
	His^{2}C2H	1.7	
	$Leu^{4,6}$delta CH_2	0.8	Overlap
Mixed PL	Tyr^{13}C3,5H	5.8	
	$Trp^{1,3}$C2H/C5H	6.5	Overlap

All affinity constants were determined as described in the text. Errors determined by repeated determination are $\pm$ 0.2 x $10^1 M^{-1}$ (repeated for DPPC and DOPC).

FIGURE 37

400 ms, 25°C, 400 MHz NOESY spectrum of alpha-factor in DPPC vesicles (in D_2O at pH 4.6)

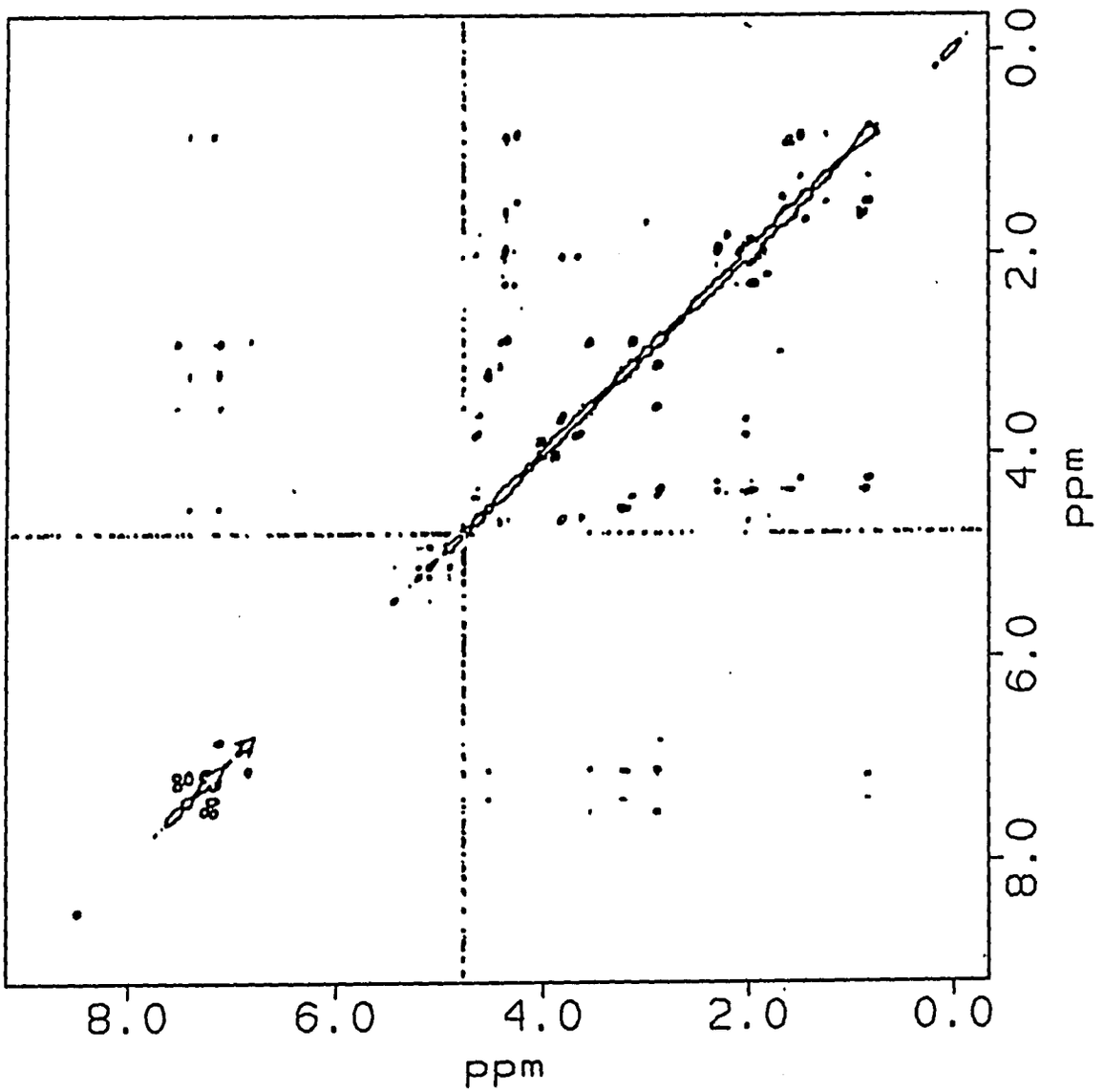
0.0
2.0
4.0
6.0
8.0
ppm
8.0
6.0
4.0
2.0
0.0
ppm

at pH ~4.6 is shown in Figure 37 and can be compared with Figure 19, the spectrum of alpha-factor in D_2O at pH ~4.6). No NOEs are observed in aqueous solution, therefore, NOEs observed in the presence of the lipid must be due to transfer of NOE, arising from the bound conformation, to free peptide resonances. Fewer NOEs were observed in the presence of DOPC, DOPE, or PS vesicles (all in the liquid crystalline state at 25°C) than in the presence of the gel state lipids (DPPC, DSPC, and DPPE). In the liquid crystalline state lipids the peptide may be more flexible than in the gel state lipids since the more fluid liquid crystalline state imposes fewer restrictions on peptide motion (discussed in more detail in Chapter V). Peptide side-chain - side-chain interactions observed in the spectra of alpha-factor in the presence of liquid crystalline state lipids (and near T_c) suggest a folding of the N-terminus which is similar to that observed in the gel state lipids (ie. crosspeaks observed in the spectra of alpha-factor in PS vesicles at 25°C and in the presence of DPPC vesicles at 41°C indicate close contact between Trp^1 and Trp^3, between His^2 and Trp^3, between Trp^3 and Leu^4, and between Leu^4 and Leu^6).

NOE studies in water were performed only on the DPPC samples and all NOEs observed in the presence of DPPC vesicles (in H_2O and D_2O at 25 °C) are reported in Table XIV. Those observed at 41°C in DPPC (in D_2O) are found in Table XV and those observed in DOPC, DOPE, or PS (in D_2O)

TABLE XIV

Crosspeaks observed in the 400 ms NOESY spectrum of alpha-factor in DPPC vesicles (in H_2O/D_2O, 9:1, at pH 4.6). Crosspeaks may be due to NOE, chemical exchange (as in the case for some of the amide - amide crosspeaks), or J interactions.

$Trp^{1}NH$ - $Gln^{5,10}$gamma NH_2
- Trp^{1}beta CH_2
- Leu^{4}delta CH_3
alpha CH - $Trp^{1}C2H$
- Trp^{1}beta CH_2
- $Trp^{3}C4H$
beta CH_2 - $Trp^{1}C2H$
C2H - Trp^{1}indole NH
C4H - Trp^{1}beta CH_2
- $Trp^{1}C5H$
- Trp^{3}alpha CH
- Leu^{4}delta CH_3
C5H - $Trp^{1}C6H$
C6H - $Trp^{1}C7H$
C7H - Trp^{1}indole NH
$His^{2}NH$ - His^{2}alpha CH
- His^{2}beta CH_2
- Trp^{1}beta CH_2
$Trp^{3}NH$ - $Trp^{1}NH$
- His^{2}alpha CH
- Trp^{3}beta CH_2
- Leu^{4}delta CH_3
- $Gln^{5,10}$gamma NH_2

Trp^{3}alpha CH - Trp^{3}beta CH_2
- $Trp^{3}C2H$
beta CH_2 - $Trp^{3}C2H$
C2H - Trp^{3}indole NH
C4H - $Trp^{3}C5H$
C5H - $Trp^{3}C6H$
C6H - $Trp^{3}C7H$
C7H - Trp^{3}indole NH
$Leu^{4}NH$ - $Trp^{1}NH$
- Leu^{4}gamma CH_2
- Leu^{4}delta CH_3
- Gln^{5}alpha
delta CH_3 - Leu^{4}gamma CH_2
- Leu^{4}alpha CH
- His^{2}beta CH_2
- Trp^{3}beta CH_2
- Gln^{5}alpha CH
- Gln^{5}gamma CH_2
- lipid $(CH_2)_n$
$Gln^{5}NH$ - $Trp^{1}NH$
- Trp^{3}beta CH_2
- Leu^{4}alpha CH
- $Gln^{5,10}$gamma NH_2

Gln^{5}gamma CH_2 - $His^{2}C2H$
- Gln^{5}beta CH_2
$Leu^{6}NH$ - Leu^{6}alpha CH
- Leu^{6}delta CH_3
- Gln^{5}beta CH_2
- Gln^{5}gamma CH_2
- Lys^{7}beta CH_2
delta CH_3 - Leu^{6}alpha CH
- Leu^{6}gamma CH_2
- Trp^{3}beta CH_2
- Gln^{5}gamma CH_2
- Lys^{7}epsilon CH_2
- lipid $(CH_2)_n$
$Lys^{7}NH$ - Trp^{3}alpha CH
- Trp^{3}beta CH_2
- $Leu^{4}NH$
- Leu^{4}alpha CH
- Lys^{7}alpha CH
- $Gln^{5,10}$gamma NH_2
- Pro^{8}beta CH_2
alpha CH - Lys^{7}beta CH_2
- Pro^{8}delta CH_2
gamma CH_2 - Lys^{7}delta CH_2

Lys^{7}delta CH_2 - Lys^{7}epsilon CH_2
Pro^{8}alpha CH - Pro^{8}bet CH_2
delta CH_2 - Pro^{8}delta CH_2
- Pro^{8}gamma CH_2
$Gly^{9}NH$ - Gly^{9}alpha CH
- Pro^{8}alpha CH
- Pro^{8}beta CH_2
- $Gln^{10}NH$
alpha CH - Gly^{9}alpha CH
$Gln^{10}NH$ - $Gln^{5,10}$gamma NH_2
- Pro^{8}alpha CH
- Pro^{11}beta CH_2
- Gly^{9}alpha CH
alpha CH - Gln^{10}beta CH_2
- Pro^{11} delta CH_2
Pro^{11}alpha CH - Pro^{11}beta CH_2
delta CH_2 - Pro^{11}delta CH_2
- Pro^{11}gamma CH_2
$Met^{12}NH$ - Met^{12}alpha CH
alpha CH - Met^{12}beta CH_2
beta CH_2 - Met^{12}gamma CH_2
$Tyr^{13}NH$ - $Trp^{1,3}$indole NH
- $Gln^{5,10}$gamma NH_2
- Lys^{7}epsilon NH_3^{+}
alpha CH - Tyr^{13}beta CH_2
beta CH_2 - $Tyr^{13}C3,5H$
C3,5H - $Tyr^{13}C2,6H$

TABLE XV

NOEs observed in the presence of DPPC at 41° C (400 msec, in D_2O).

Trp^1C2H - Trp^1beta CH_2	Leu^4alpha CH - Leu^4delta CH_3
Trp^1beta CH_2 - Trp^3C4H	Leu^4gamma CH_2 - Leu^4delta CH_3
Trp^1alpha CH - Trp^3C7H	$Leu^{4,6}$delta CH_3 - lipid $(CH_2)_n$
Trp^1alpha CH - Trp^1beta CH_2	Leu^6alpha CH - Leu^6beta CH_2
Trp^1C4H - Trp^1C5H	Leu^6alpha CH - Leu^6delta CH_3
Trp^1C5H - Trp^1C6H	Leu^6gamma CH_2 - Leu^6delta CH_3
Trp^1C6H -Trp^1C7H	$Pro^{8,11}$delta CH_2 - $Pro^{8,11}$delta CH_2
His^2alpha CH -Trp^3C7H	Gly^9alpha CH - Gly^9alpha CH
Trp^3alpha CH - Trp^3beta CH_2	Met^{12}beta CH_2 - Met^{12}gamma CH_2
Trp^3C4H - Trp^3C5H	Tyr^{13}alpha CH - Tyr^{13}beta CH_2
Trp^3C5H - Trp^3C6H	lipid $N(CH_3)_3$ - CH_2N
Trp^3C6H - Trp^3C7H	lipid $N(CH_3)_3$ - $(CH_2)_n$
Trp^3C2H - Trp^3beta CH_2	lipid $(CH_2)_n$ - CH_3 (end of acyl chain)

are reported in Table XVI.

The NOE crosspeaks between the exchangeable protons and alpha and side chain protons of alpha-factor in DPPC are shown in Figure 38. Figure 39 is a slice through the 2D spectrum showing all NOEs to the Gly^9 amide proton. The intense NOE between the Gly^9 amide and Pro^8 alpha protons, expected for a Type II beta turn is observed in both the contour plot and the 1D slice. Additionally, in lipid, several interactions suggesting stabilization of the beta-turn appear and are identified in Figures 38 and 39. There are also many side chain - side chain interactions involving the N-terminal portion of the peptide and several peptide - lipid NOEs.

The significance of experimental data with regard to conformation, conformational stability, and modes of peptide - lipid interactions are discussed in detail in Chapter V.

TABLE XVI

NOEs observed in the presence of DOPE, DOPC, or PS vesicles (400 msec, 25°C, in D_2O).

DOPE

Trp^3C4H - Trp^3C5H

$Leu^{4,6}$delta CH_3 - $Leu^{4,6}$delta CH_3

Gly^9alpha CH - Gly^9alpha-CH

DOPC (The upfield region is overwhelmed by lipid resonances, only the downfield region NOEs are listed.)

Trp^1C4H - Trp^1C5H

Trp^1C7H - Trp^3C4H

His^2C2H - His^2C4H

Trp^3C6H - Trp^3C7H

Trp^3C4H - Trp^3C5H

$Tyr^{13}C3,5H$ - $Tyr^{13}C2,6H$

PS

Trp^1C4H - Trp^1C5H

Trp^1C5H - Trp^1C6H

Trp^3C5H - Leu^4delta CH_3

Trp^3C6H - Trp^3C7H

Trp^3beta CH_2 - Trp^3beta CH_2

Trp^3alpha CH - Trp^3beta CH_2

Leu^4gamma CH_2 - Leu^4gamma CH_2

Leu^6gamma CH_2 - Leu^4gamma CH_2

Leu^6alpha CH - Leu^6beta CH_2

Lys^7gamma CH_2 - Lys^7gamma CH_2

Lys^7alpha CH - Pro^8delta CH_2

$Pro^{8,11}$delta CH_2 - $Pro^{8,11}$gamma CH_2

Gln^{10}alpha CH - Pro^{11}delta CH_2

Pro^{11}beta CH_2 - Pro^{11}gamma CH_2

Met^{12}beta CH_2 - Met^{12}gamma CH_2

Met^{12}gamma CH_2 - $Met^{12}SCH_3$

Tyr^{13}alpha CH - Tyr^{13}beta CH_2

$Tyr^{13}C3,5H$ - $Tyr^{13}C2,6H$

FIGURE 38

Expansion of NOESY spectrum of alpha-factor in DPPC vesicles (400 ms, pH 4.6, in H_2O/D_2O, 9/1, 25°C). The region presented shows all crosspeaks between the amide protons and alpha and side chain protons. The important connectivities identifying the Type II beta-turn are indicated by the solid lines.

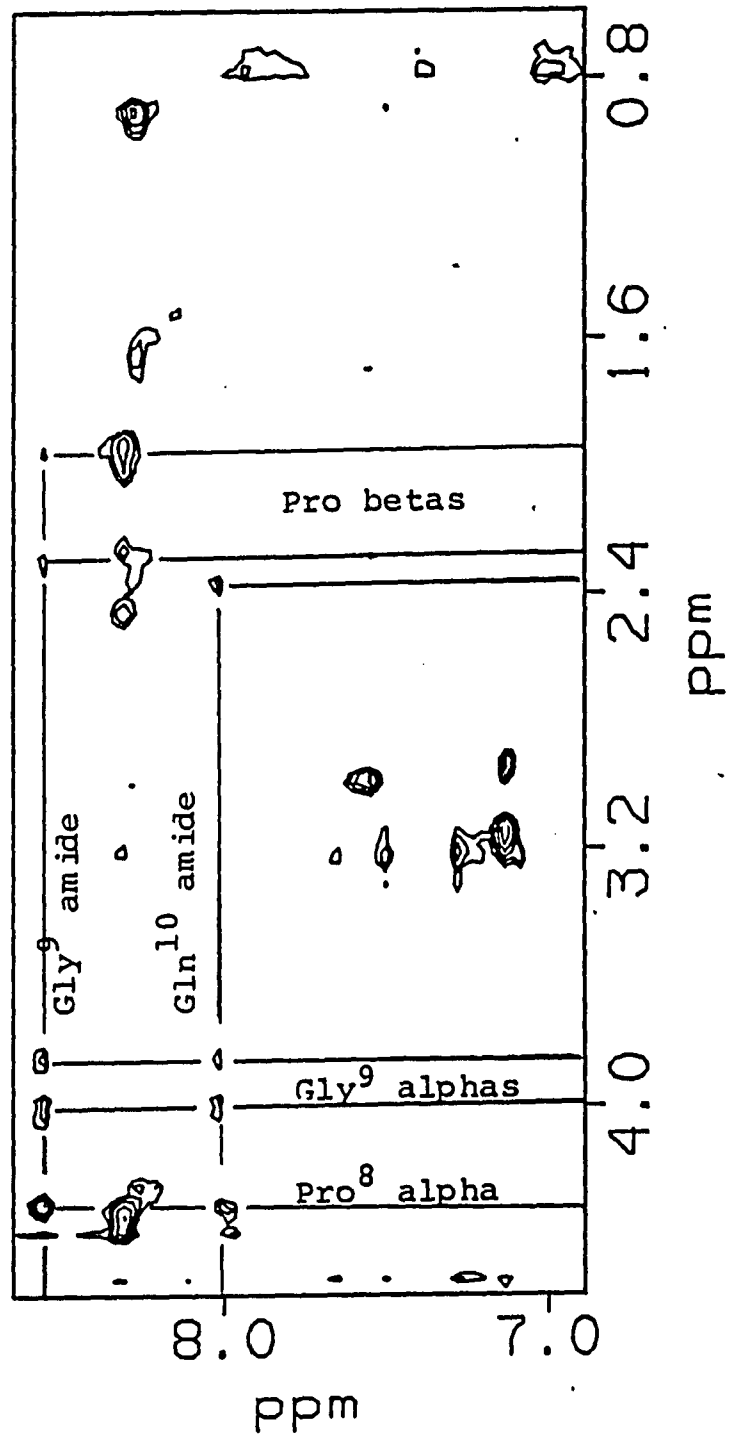
0.8
1.6
2.4
3.2
4.0
ppm
Pro betas
Gly9 amide
Gln10 amide
Gly9 alphas
Pro8 alpha
8.0
7.0
ppm

FIGURE 39

1D slice through the Gly^9 amide proton resonance of the NOESY spectrum of alpha-factor in DPPC (as in Figure 38). Important connectivities identifying the Type II beta-turn are indicated. In particular, note the NOE between the Gly^9 amide and Gln^{10} amide protons which is not shown in the contour plot expansion in Figure 38.

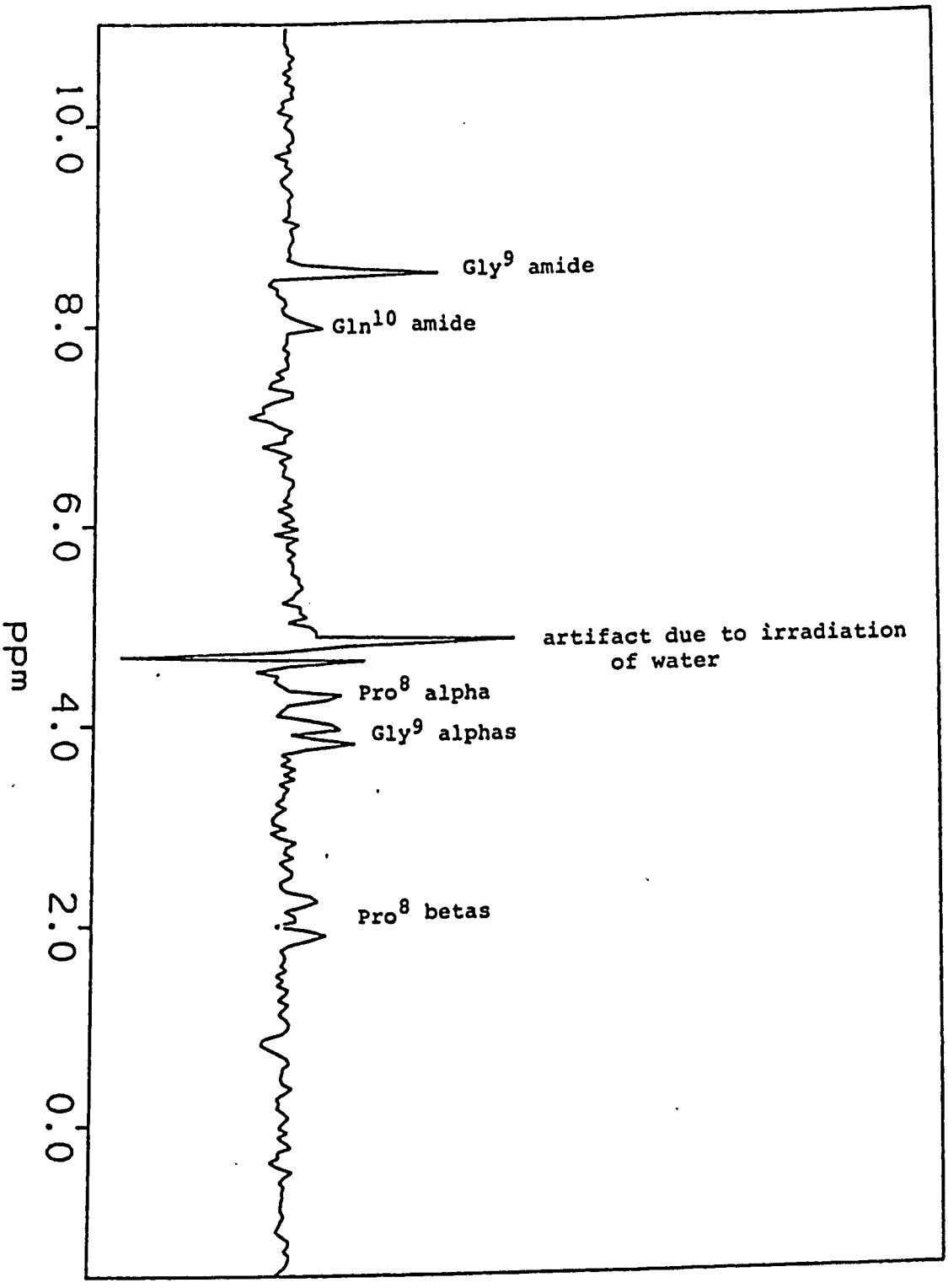
10.0
8.0
6.0
4.0
2.0
0.0
ppm
Gly9 amide
Gln10 amide
artifact due to irradiation of water
Pro8 alpha
Gly9 alphas
Pro8 betas

CHAPTER V

Discussion

Solution Studies

Proton chemical shifts of alpha-factor suggest the presence of conformations other than random coil. In DMSO the Leu^4, Leu^6 and Gln^5, Gln^{10} amide protons in each pair of duplicated residues have somewhat different chemical shifts (see Table II), implying that the residues may be located in or near conformationally distinct segments of the peptide (60). Some of these chemical shift differences are quite small and may simply be due to the sequence of the neighboring amino acid residues. Other chemical shift differences appear for the alpha protons of Pro^8, Pro^{11} and Gln^5, Gln^{10}. The two proline residue alpha proton resonances differ by 0.04- 0.07 ppm in all of the active peptides but these resonances are superimposed in the inactive peptides. The two glutamine residue alpha proton resonances are different for all of the peptides (Tables II-V), as are the glutamine amide proton resonances. As noted in Chapter IV the amide proton spectral patterns of active versus inactive peptides are quite different (Figure 14).

In aqueous solution, the glutamine amide proton and the proline alpha proton of the tridecapeptide alpha-factor exhibit trends similar to those found in DMSO. However, whereas the Leu^4 amide proton is always much further downfield than the Leu^6 amide proton in DMSO it is 0.09 ppm

upfield of the Leu^6 amide proton resonance in water. Hydrogen bonding of an amide proton to DMSO has been known to cause considerable downfield shifts of amide resonances (60), and external orientation of the Leu^4 amide proton, as indicated by the amide proton temperature coefficients (Table VI) would facilitate hydrogen bonding to DMSO molecules. With the exception of the two Leu amide proton assignments our proton assignments for the alpha-factor in aqueous solution agree with those reported by Higashijima et al. (44). The assignments reported herein have been confirmed by selective alpha-deuteration at these positions and are the reverse of those reported by Higashijima et al.

Several alpha proton resonances exhibit significant chemical shift differences in the two solvents. In water, the two glutamine alpha proton resonances are separated by 0.4 ppm, a much larger difference than that observed in DMSO (0.2 ppm) (Table II). The two leucine alpha proton resonances are also separated by a larger difference in water, 0.12 ppm (0.08 ppm in DMSO), though this difference is not as dramatic as that observed for the two glutamines. One other interesting observation is that in water the two glycine alpha protons are not equivalent while for the tridecapeptide and extended analogues in DMSO they are equivalent. For the des-Trp^1,Cha^3-dodecapeptide, which is less active than the tridecapeptide, these protons are not equivalent in DMSO. The observation of inequivalence of the two Gly^9 alpha protons in water contrasts the findings

of Koizuka et al. in an investigation of the CCK octapeptide (11). The two glycine alpha protons of the CCK octapeptide were found to be equivalent in water and not in DMSO. This was taken to indicate that the CCK octapeptide was more relaxed (unstructured) in aqueous solution than in DMSO. Applying the same arguments would suggest that the central to C-terminal portion of the tridecapeptide alpha-factor may actually be less relaxed in water than in DMSO although temperature coefficients suggest otherwise (vide infra).

The chemical shifts of the amide protons of the alpha-factor and the analogue peptides were compared with the corresponding random coil values suggested by Bundi and Wuthrich (95, 96). Differences between the observed chemical shifts and the random coil chemical shifts are plotted versus amino acid residue for each peptide in Figure 16. Examination of these plots reveals common trends for the active peptides in DMSO. To wit, the Leu^4 amide proton always has a large positive deviation (towards lower field) and the Gly^9 amide proton always has a small but measurable positive deviation from the random coil values. In the tridecapeptide in DMSO the Trp^3 amide proton also has a large positive deviation. In fact, in DMSO the residue 3 amide proton, of all peptides, is always the most downfield shifted of the amide protons, whereas this is not the case in water. These downfield shifts of the residue 3 (Trp or Cha) and Leu^4 amide protons in DMSO

cannot be attributed to ring current shifts caused by the two Trp aromatic rings since the shifts appear even in the des-Trp^{1},Cha^{3} analogues which lack both tryptophan residues.

Similar to the peptide with the natural Gly^{9} the active D-Leu^{9} dodecapeptide has a positive deviation of the residue 9 amide proton from the random coil value. This deviation is not as large as the deviation of the Leu^{4} amide proton. In the inactive L-Leu^{9} dodecapeptide the Leu^{4} amide proton still has a positive deviation from the random coil value. However, the L-Leu^{9} amide proton has a small negative deviation and is observed at the same chemical shift position as the Leu^{6} amide proton. This chemical shift is very close to the random coil value and suggests that in the inactive peptide the Leu^{6} and the L-Leu^{9} amide protons are situated in similar unrestricted environments. The behavior of the active D-Ala^{9} and inactive L-Ala^{9} analogues is similar to that described for the D-Leu and L-Leu analogues: the D-Ala^{9} amide proton is downfield shifted from the random coil value while the L-Ala^{9} amide proton is upfield shifted. The Gln^{10} amide proton of all pepetides, active and inactive, has a significant negative deviation (0.15 ppm) in DMSO. In water, all but the Gly^{9} amide protons of the tridecapeptide have no or negative deviations from the random coil values, including the Leu^{4} amide proton which has a large positive deviation in DMSO.

The temperature coefficients of the amide protons of the tridecapeptide alpha-factor in DMSO and in water and three of the analogue peptides in DMSO (Table VI) indicate that none of the amide protons in either solvent have temperature coefficients in the range expected for strongly hydrogen - bonded amide protons. Temperature coefficients under -2.0×10^{-3} ppm would indicate solvent - shielding and hydrogen bonding (60). Most of the temperature coefficients are above -4.0×10^{-3} ppm indicating external amide orientation. The Leu^4 amide proton, in particular, has a large temperature coefficient, -7.0×10^{-3} (in DMSO) and appears to be the most exposed amide proton in DMSO. The His^2, Leu^6, and Gln^{10} amide protons all have temperature coefficients in the intermediate range of -3.0×10^{-3} to -4.0×10^{-3} ppm. This range is difficult to interpret and is believed to indicate weak intramolecular hydrogen bonding (60). In the proposed beta-turn, the Gln^{10} amide proton should participate in an intramolecular hydrogen bond with the Lys^7 carbonyl. It should, therefore, exhibit little temperature dependence. It must be noted however, that the observation of a lowered temperature coefficient for the Gln^{10} amide proton does not correlate with activity and is therefore inconclusive. The Gln^{10} amide proton actually has a smaller temperature coefficient in the inactive L-Leu^9 dodecapeptide than in the active D-Leu^9 dodecapeptide analogue (see Table VI).

In water the temperature coefficients are much larger

than in DMSO. Because of its high polarity, water might destabilize intramolecular hydrogen bonds and cause some unfolding and exposure of amide protons in conformationally flexible peptides (60). Although all of the temperature coefficients in water are quite high, the value for the Gln^{10} amide proton is significantly lower than the temperature coefficients of most of the other amide protons, suggesting that this proton may be solvent - shielded or involved in weak intramolecular hydrogen bonding. The larger value for the Leu^{6} amide proton as compared with that of the Leu^{4} amide proton in water implies that in water the Leu^{6} amide proton is more exposed to solvent. The situation is reversed in DMSO and the chemical shift data support this conclusion. The values for the temperature coefficients in water (at pH 4.5) for the Gln^{5}, Leu^{6}, and Gly^{9} amide protons are somewhat higher than those reported by Higashijima et al. (at pH 6.5) (44).

As noted in Chapter IV the majority of the $^{3}J_{NH-\alpha CH}$ values determined for the tridecapeptide in DMSO and in water are between 6 and 8 Hz (Table VII), the range expected when there is rapid conformational averaging (59). These values along with the temperature coefficients and most of the chemical shift data suggest that the alpha-factor peptides are highly flexible molecules although there are hints of possible conformational preferences (chemical shift behavior of the duplicated residues and of the position 9 analogues and the lowered temperature

coefficient of residue 10).

One dimensional NMR parameters have been useful in determining alpha-helical or beta structures in highly ordered peptides, however, these parameters often do not yield enough detailed information to deduce structure in more flexible peptides. Two-dimensional NMR has proven to be very useful in determining the structural characteristics of proteins and nucleic acids in solution (27 - 34). The two-dimensional NOE experiment has proven to be particularly useful because it enables the determination of short internuclear separations by the identification of dipolar interactions. Several recent NMR studies of the solution conformations of peptides and small proteins have identified 2D NOE cross-peaks which are characteristic of specific secondary structures (27, 30 - 33). For example, strong interactions between amide protons of adjacent residues (residues i and i + 1, where the residue numbering begins at the amino terminal end of the peptide molecule) are characteristic of an alpha-helix, as are interactions between the alpha proton of residue i with the amide proton of residue i + 4 (33). A sequence of very strong interactions between adjacent alpha protons (residue i) and amide protons (residue i + 1) is indicative of extended chain structure (32). Tables XVII and XVIII list some of the important NOE interactions expected for beta-turns (Table XVII) and helical conformations (Table XVIII). Furthermore, the observation of dipolar

TABLE XVII

Several short distances expected for Beta Turns (reference 33).

Type I Turn (Å)	distance	Type II Turn (Å)
3.4	$d_{\alpha N}(2,3)$	2.2
3.2	$d_{\alpha N}(3,4)$	3.2
3.6	$d_{\alpha N}(2,4)$	3.3
2.4	$d_{NN}(3,4)$	2.4
2.9 - 4.1	$d_{\beta N}(2,3)$	3.6 - 4.4
2.8	$d_{N\alpha}(3,3)$	2.2

TABLE XVIII

Several short distances expected for alpha-helices and 3_{10} helices (reference 33).

Alpha-helix (Å)	distance	3_{10} helix (Å)
3.5	$d_{\alpha N}(i,i+1)$	3.4
4.4	$d_{\alpha N}(i,i+2)$	3.8
3.4	$d_{\alpha N}(i,i+3)$	3.3
4.2	$d_{\alpha N}(i,i+4)$	not observed
5.2	$d_{N\alpha}(i,i+1)$	5.1
2.8	$d_{NN}(i,i+1)$	2.6
4.2	$d_{NN}(i,i+2)$	4.1
2.5	$d_{NN}(i,i+3)$	3.1
4.5	$d_{N\beta}(i,i+1)$	4.3
4.9	$d_{N\beta}(i,i+2)$	5.0
2.5	$d_{\beta N}(i,i+1)$	2.9
5.1	$d_{\beta N}(i,i+2)$	4.8
2.2	$d_{N\alpha}$(intra-residue)	2.7
2.0	$d_{N\alpha}$(intra-residue)	2.0

connectivities between backbone protons from different amino acid residues, particularly those far apart in the primary structure of the molecule, gives information on tertiary structure (27).

The observation of dipolar connectivities in a 2D NOE spectrum depends on the cross-relaxation rates between interacting proton spins (see Chapter II). One consequence of this is that the mixing time in a given experiment defines the limits of observable internuclear separations (longer mixing times allow the detection of longer separations, up to ~4.5 Å) Furthermore, as discussed in Chapter II, the crosspeak intensity is a function of the correlation times of the motions modulating the internuclear interactions. Whereas the distance dependence of NOEs has been frequently exploited in conformational studies of macromolecular systems such as proteins, until recently the correlation time dependence of 2D NOE spectra has been ignored (27, 30 - 33). However, the dependence of NOE cross-peak intensity on the correlation time cannot be neglected in the analysis of small molecule spectra (17, 34, 103, 104). This is illustrated below for the alpha-factor peptides.

The NOESY spectra of the tridecapeptide alpha-factor in DMSO and in D_2O were acquired at several mixing times (100, 250, 400, and 600 ms) While most of the observed NOEs in DMSO are between protons which are spin-spin coupled and therefore in close proximity, there are several

inter-residue NOEs indicative of conformation (see Figure 17 and Table I). NOEs observed between the Lys^7 alpha proton and the Pro^8 delta protons and between the Gln^{10} alpha proton and the Pro^{11} delta protons indicate that these X-Pro peptide bonds are trans. In the trans bond the distance between the H_i alpha and the H_{i+1} delta is 2.0 - 3.9 Å whereas this distance is 4.3 - 5.0 Å in the cis bond (33). An intense crosspeak is also observed connecting the Gly^9 amide proton and the Pro^8 alpha proton (see the insert of Figure 17). Such a strong interaction is expected in a Type II beta-turn where the distance between these two protons has been calculated to be as short as 2.2 Å (105). This interatomic distance in a Type I beta-turn is considerably longer (3.4 Å) and, for such a structure, the Pro^8 alpha proton - Gly^9 amide proton NOE would not give rise to the very intense crosspeak which is observed even in the shortest mixing time experiment (100 ms).

The crosspeak between the residue 9 amide proton and the Pro^8 alpha proton appears in the spectra of all active peptides but is absent in spectra of the inactive peptides (Figures 17 and 18 and Table I). The observation of this crosspeak supports our proposal of a Type II beta-turn based on earlier CD and activity studies on analogue peptides (41, 42). As discussed in Chapter I, both CD spectral patterns and biological activity are sensitive to the stereochemistry of the amino acid at position 9. The des-Trp^1,Cha^3,D-Ala^9- and D-Leu^9-dodecapeptides are active

pheromones whereas substitution with L-Ala^9 or L-Leu^9 at position 9 results in pheromones which are at least two orders of magnitude less active. (A Type II beta turn readily tolerates D-amino acids but L-amino acids are found only infrequently at the i+2 position (58).)

In stark contrast to the spectra in DMSO (Figure 17), the NOESY spectra of the alpha-factor peptide in aqueous solution, regardless of mixing time, are almost void of crosspeaks (see Figure 19 for an example). In H_2O there are no crosspeaks involving the exchangeable protons and in both the H_2O and D_2O spectra no crosspeaks of structural significance are observed. Strikingly, very few of the crosspeaks arising from intra-residue interactions between non-exchangeable protons are present, in fact, the only crosspeaks in the spectra in D_2O or H_2O are those between the two Gly^9 alpha protons, between the two Pro delta protons, and between ring protons of the same Trp residue.

The differences found between the NOESY spectra of the tridecapeptide in DMSO and in water may be explained by a difference in conformational flexibility in the two solvents (DMSO being a more viscous solvent) (106). Because of the correlation time dependence of the dipolar interactions, a short internuclear separation will not manifest an NOE if that interaction is short-lived (34, 35). To observe a crosspeak in the NOESY spectrum, the correlation time of the corresponding dipolar interaction must be at least on the order of 0.5 nsec (104). The NOE

vanishes when $\omega_o \tau_c \sim 1$ (see Chapter II) and in a two-dimensional spectrum very low intensity negative crosspeaks appear if $\omega_o \tau_c < 1$ (74). The effective correlation time may be due to overall molecular tumbling, to internal motions, or to a combination thereof. The ROESY experiment (described in Chapter II) detects dipolar interactions modulated by higher frequency motions than those detectable using conventional NOEs (35, 75). Consequently, in the ROESY spectrum, positive crosspeaks of significant intensity will appear even when conventional NOEs are absent.

In contrast to the dearth of information present in the NOESY spectra of alpha-factor in D_2O and H_2O, both the intra-residue interactions and several conformationally significant crosspeaks have "re-appeared" in the aqueous ROESY spectra of the tridecapeptide pheromone. (Figure 20 shows the spectrum in D_2O, Insert III shows an expansion of the amide proton - alpha proton region of the spectrum obtained in H_2O:D_2O, 9:1.) The crosspeaks between the Pro delta protons and the Lys^7 or Gln^{10} alpha protons, present in the NOESY spectra in DMSO, are observed in the D_2O ROESY spectra of the alpha-factor. (Compare Insert II (NOESY, DMSO) and the box in the center of Figure 20.) These peaks, however, are absent in the NOESY spectra in D_2O (shown in Insert I of Figure 20). Most significantly, a very strong Pro^8 alpha proton - Gly^9 amide proton crosspeak, suggesting the Type II beta-turn, is present in

the ROESY spectrum of the alpha-factor in H_2O (shown in Insert III of Figure 20).

Figure 21 shows a comparison of the upfield regions of the NOESY spectrum and the ROESY spectrum of alpha-factor in DMSO. Many of the same crosspeaks appear in both spectra. Those crosspeaks that appear in the NOESY spectrum and not in the ROESY spectrum may be due to the differing mixing times employed in the two experiments. The NOESY experiment utilizes a 400 ms mixing time while the ROESY experiment mixing time is only 200 ms. Because the ROESY experiment employs a spinlocking field during the mixing time the experiment was not performed with longer mixing times which might damage the spectrometer probe. The longer mixing time of the NOESY experiment should allow the detection of dipolar interactions between protons which are farther apart in space. Another factor which may lead to fewer crosspeaks in the ROESY spectrum is that Hartmann-Hahn contributions to crosspeaks (excited during the spinlock, as described in Chapter II) between scalar coupled protons are negative in intensity in the ROESY experiment and may lead to cancellation of NOE crosspeaks between protons which are scalar coupled as well as in close proximity (several of the crosspeaks appearing in the NOESY spectrum but not in the ROESY spectrum are between scalar coupled nuclei). Figure 22, showing the same comparison as in Figure 21 for the alpha-factor in D_2O, clearly demonstrates the advantage of ROESY in cases where

the conventional NOEs are undetectable.

The ROESY experiment allows the separation of NOE (positive) and chemical exchange (negative) crosspeaks (Chapter II and Figure 13) and the negative contours of the ROESY spectrum of alpha-factor in D_2O are shown in Figure 23. The only negative crosspeaks in the D_2O spectrum are those between the two Gly^9 alpha protons, between the Pro beta, gamma, and delta proton pairs, between the two Leu beta protons, and between the Trp ring protons. These crosspeaks may be due to Hartmann-Hahn transfer (they are all between scalar coupled nuclei) or chemical exchange (for example, puckering of the Pro rings or rotation about the Leu beta carbon). Although ROESY experiments are acquired such that Hartmann-Hahn transfer is minimal (~2-3 KHz spinlocking field strength and optimized carrier placement), interactions between scalar coupled nuclei are still possible and have been observed with significant intensity for geminal proton pairs (107). A comparison of Figure 23 (negative ROESY contours) and Figure 19 (NOESY spectrum) shows that the only crosspeaks present in the NOESY spectra are actually due to chemical exchange and scalar coupling interactions and not NOE.

Table I lists the NOEs and rotating frame NOEs observed for the different peptides. As discussed above all active peptides exhibit an NOE between the Pro^8 alpha proton and the Gly^9 or $\underline{D}\text{-}X^9$ amide proton which is highly suggestive of a Type II beta-turn. This NOE is present for

the alpha-factor in both solvents studied. The longer range NOEs expected for beta-turns (Pro^8 alpha proton - Gln^{10} amide proton, Gly^9 amide proton - Gln^{10} amide proton, and Gly^9 alpha proton - Gln^{10} amide proton, see Table XVII) are observed in the 250 - 600 ms NOESY spectra in DMSO, but are not observed in the 200 ms ROESY spectra in either solvent (see Table I). The absence of these particular crosspeaks in the ROESY spectra may be due to the different mixing times as discussed above. The data suggest that the preferred conformation is the same in both solvents, although the lifetime might be different.

In addition to the Pro^8 alpha proton - Gly^9 amide proton interaction, another NOE that correlates with activity is that between the Gly^9 alpha proton and the Gln^{10} amide proton. The distance between these protons is expected to be 3.2 Å in beta-turns and the NOE is observed in the 250 ms NOESY spectra of all active peptides. Beta-turns are also expected to give rise to an NOE between the amide proton resonances of residues i+2 and i+3 of the turn. This NOE appears with very weak intensity only in the spectra of the tridecapeptide in DMSO. An NOE is also expected between the alpha proton of residue i+1 and the amide proton of residue i+3 of a Type II beta turn (this distance, 3.3 Å in a Type II turn, is longer in a Type I turn, 3.6 Å). This NOE is also observed only in tridecapeptide spectra in DMSO and has weak intensity. Because of instrument limitations, longer mixing time ROESY

experiments could not be performed to determine the presence of these longer range NOEs in the aqueous solution spectra of the tridecapeptide. However, we believe that the beta-turn is present in the tridecapeptide in both solvents, particularly in light of our results in the lipid studies (vide infra). The other peptides, active or inactive, do not exhibit these NOEs. These observations are not inconsistent with the importance of the Type II beta-turn for biological activity of the pheromone: the tridecapeptide has the highest activity and it would be expected to exhibit the most stable turn.

In all peptides, both active and inactive, an NOE is observed connecting residues 3 and 4 (see Table I). The amide protons of these residues also exhibit interesting chemical shift behavior in DMSO (significant downfield shifts). This behavior does not correlate with biological activity and the structural significance is not known as there are no other observed NOEs supporting a specific conformation at this position. The structural significances of the other NOEs listed in Table I are also not known since there are no sequences of NOEs which might identify specific secondary structures (see Table XVIII).

The one- and two-dimensional ^{1}H NMR data presented above support the presence of a Type II beta-turn spanning residues 7 -10. No other specific structural features can be unambiguously identified. This beta-turn, which has been correlated with activity, appears to be more stable in

organic solvent, DMSO, than in aqueous solution.

Lipid Studies

Vesicle Characterization

The vesicle sizes determined by QLS (Table VIII) indicate a diameter range from ~400-~1200 Å, which is comparable to the range of sizes obtained by other laboratories using similar preparation procedures (83, 99). As noted in Chapter IV the vesicles prepared from unsaturated lipids are smaller with more dispersity of size than those formed from the saturated lipids. A polydispersity index (V) of greater than 30% indicates a broad size distribution (108). This value is highest for brain PS, DPPA, and DOPC and therefore the diameters listed represent the average of large distributions.

^{31}P NMR of phospholipids has been shown to be very sensitive to the fluidity of the phospholipid (gel versus liquid crystalline state), headgroup conformation, and the lipid phase (multilamellar bilayer dispersions, isotropic (micelles, inverted micelles and sonicated bilayer vesicles), or hexagonal$_{II}$ dispersions) (97). The shape of the ^{31}P NMR spectrum has been used as a diagnostic tool to categorize the phase of lipid systems (Figure 40 shows the ^{31}P spectra expected for bilayer and hexagonal$_{II}$ dispersions), although the shape is also dependent on the headgroup orientation and therefore should be used cautiously and in conjunction with other studies (electron microscopy, light scattering) (109, 110). Thayer and

FIGURE 40

^{31}P NMR spectra of bilayer and hexagonal$_{II}$ phase lipids

The powder patterns expected for bilayer phase and hexagonal$_{II}$ phase lipids are shown along with the type of molecular packing in each phase.

(Taken from reference 112)

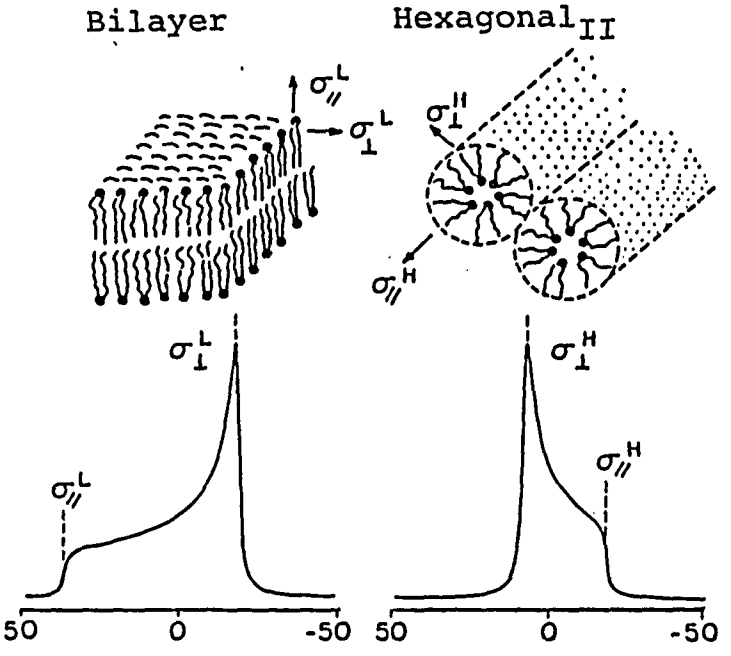
Bilayer
Hexagonal II
σ//L
σ⊥L
σ⊥H
σ//H
σ⊥L
σ//L
σ⊥H
σ//H
50
0
-50
50
0
-50

Kohler (111) have calculated the ^{31}P spectrum of a bilayer system with various headgroup orientations and have been able to mimic "isotropic" and "hexagonal$_{II}$" type spectra by simple reorientation of the headgroup while maintaining the bilayer structure.

As illustrated in Figures 24-26 and 27 (a-c), one narrow symmetric ^{31}P resonance is observed at all temperatures studied. Linewidths range from 20 Hz (PI) to 175 Hz (DPPC). ^{31}P linewidths are related to vesicle size and the rate of lateral diffusion of the individual phospholipid molecules on the vesicle surface (98). The linewidths observed are in the range expected for vesicles of 500-1000 Å in diameter (112); sizes also indicated by QLS parameters. The one exception is the DPPE vesicle preparation (Figure 27 d). This spectrum is a "powder" type spectrum of the shape and breadth expected for a "hexagonal$_{II}$" phase lipid ("phase", in this case, refers to the polymorphism of the lipid - bilayer, micellar, etc., and not the state of the hydrocarbon chains - gel, liquid crystalline) (109). This is discussed in more detail below.

As with most of the ^{31}P spectra, the ^{2}H spectra consist of a single Lorentzian line (Figures 28 and 29). A single symmetric line is always observed for deuterated fatty acids intercalated in sonicated single bilayer egg PC vesicles whereas quadrupolar powder patterns are observed for large bilayers and multilamellar aggregates (113). This evidence also suggests that we have prepared small

unilamellar vesicles.

The ^{1}H NMR spectra of DPPC vesicles at 25° and 41°C, presented in Figure 30, show bimodal choline N methyl resonances, indicative of unilamellar vesicles (98 - 100, 114). These bimodal resonances represent the outer and inner leaflets of the bilayer vesicle. A smaller upfield resonance is expected for the inner leaflet because the curvature in a vesicle leads to a smaller population in the inner monolayer than in the outer monolayer. Had micelle formation occurred, the smaller resulting sizes would be indicated by QLS and the N methyl resonance would consist of only one population, as would also be true for inverted micelles (100). If the bimodal spectra arose from two size populations, we would expect a sharper resonance for the smaller vesicles and a broader one for the larger vesicles, whereas both N methyl resonances we observe are sharp. The polydispersity determined by QLS for DSPC vesicles is quite low and the dispersity for DPPC vesicles is within the range expected for a small size dispersion. Unilamellar vesicle formation was confirmed by adding an NMR shift reagent, praesidium chloride, to the sonicated DPPC vesicles. This reagent shifts the resonance position of nuclei in the outer leaflet of the bilayer relative to those in the inner leaflet (98). The ^{1}H and ^{31}P NMR spectra (not shown) of the DPPC vesicles with praesidium chloride added show two different resonances representing the inner and outer leaflets of the bilayer.

Interaction of Alpha-Factor with Lipid

^{31}P and ^{2}H NMR Studies: Effect of alpha-factor on lipid

Examination of the ^{31}P NMR spectra in Figures 24-27 shows that addition of alpha-factor leads to a broadening of the resonance for all but DPPE. The line broadening effect is most pronounced in the DOPE spectrum which is broadened beyond detectability when alpha-factor is added (Figure 27 c). The greatest % increase in linewidth is observed for DSPC near T_c and in the liquid crystalline state. In the neutral lipids DPPC and DSPC, which were studied in both the liquid crystalline and gel state, there is increased broadening in the liquid crystalline state compared to that observed in the gel state lipid while for the negatively charged DPPA broadening is much greater in the gel state than in the liquid crystalline state. The effect on the gel state spectrum of soybean PI (also negatively charged) is quite small (3 Hz) and is within the expected experimental error.

Increased broadening of spectra at temperatures when the pure lipid is in the liquid crystalline state suggests that alpha-factor may act in a manner such that it increases the packing and rigidity of the phospholipids in the bilayer vesicles, making the phospholipid more gel-like at temperatures when it is normally more fluid (115). The increased broadening observed at higher temperatures may be due to sample heterogeneity induced by interaction with alpha-factor (116-120). The linewidth of pure DSPC

vesicles prepared in the liquid crystalline state increases from 175 Hz to 220 Hz (at 25°C) upon addition of alpha-factor. However, when DSPC was prepared by sonication in the gel state (temperature never reaching T_c), the linewidth was 220 Hz and did not change upon addition of alpha-factor. This, along with the greater % increase in linewidth observed in the liquid crystalline spectra, suggests a preferential interaction with liquid crystalline state lipid.

In vesicle systems sample heterogeneity may be the result of a range of differing headgroup orientations or may be caused by the presence of "boundary" lipids (those lipids adjacent to peptide) along with more fluid lipids (those adjacent to other lipid molecules) (97, 111, 116-121). Of these possibilities only headgroup dispersion can be involved in the heterogeneity of the pure lipid sample, while "boundary" and fluid domains may be present in the peptide - lipid samples. Several studies have shown that some peptides bind preferentially to non-bilayer phases (ie. small patches of hexagonal$_{II}$ phase lipids, deformations caused by changes in lateral compressibilty near T_c) present in the bilayer (97, 119, 121 - 124). In biological membranes these non-bilayer "defect" structures can form as the various phospholipid components undergo transitions from the gel to liquid crystalline state (T_c being different for phospholipids with different headgroups and hydrocarbon chain lengths) (120). In pure lipid

dispersions all phospholipid molecules undergo this transition at the same temperature, however defects can form near T_c as the lateral compressibility of the lipids change. This change in compressibility is accompanied by increased fluctuations in the cross-sectional area of the hydrocarbon chains and results in increased permeabilty and transport near T_c (121). Because defect structures are more prevalent near T_c, as the bilayer becomes more easily deformable, peptides binding to these structures can stabilize the more rigid gel state (119, 123). One further consideration is that the pure lipid system itself, which may be subject to considerable strain due to the extreme curvature present in unilamellar vesicles, might exist in a metastable state (119) and interaction of the peptide with this system might have a stabilizing effect.

The lipid ^{31}P T_2 and T_2^* values decrease upon addition of peptide (Table XI). Similar decreases in the ^{31}P T_2 of phospholipids in membranes containing protein as compared with those of protein- lacking membranes have been observed by Yeagle et al. (116). It is unlikely that the decreased T_2^* values observed for vesicles with alpha-factor added, are due simply to vesicle aggregation since sample turbidity did not increase as alpha-factor was added and the spectra for linewidth studies were acquired within 2 hours. The T_2 values measured by the spin echo method for the pure lipid samples and samples with alpha-factor added are shorter than those determined from the linewidth. T_2

is always equal to or longer than T_2^* because the spin echo experiment removes contributions to the linewidth resulting from sample inhomogeneity. Differences between the T_2^* and T_2 values are most likely due to physical changes of the sample during the time required for the T_2 measurements (>18 hours for each experiment). As these lipids (pure or with peptide) age, aggregation is observed; aggregation would lead to longer correlation times and shorter T_2 values.

In some spectra (DPPC at all three temperatures, DSPC at 25°C, and DPPA at both 67°C and 75°C) a second ^{31}P peak appears upon addition of alpha-factor. In DPPC it is a very small, downfield shifted (~1 ppm) peak. In DSPC the new peak is larger than the one observed in DPPC and is downfield shifted by a greater amount (~2.25 ppm). At 75°C the spectrum of DPPA with alpha-factor has a distinct small, broad peak shifted upfield of the main peak by ~0.3 ppm. The significance of these peaks is not clear. Deslauriers et al. have observed the appearance of a small isotropic peak in the ^{31}P spectrum of egg PE - methemoglobin samples which had been heated to 50°C, whereas no such peak was observed in pure egg PE samples (125). Methemoglobin has been shown to increase the lipid transition temperature and appears to stabilize bilayer phases. The origin of the small isotropic component in the egg PE - methemoglobin samples is attributed to the formation of small bilayer vesicles from lipids present in

the bilayer dispersions as hexagonal$_{II}$ defect structures. These structures do not appear as separate peaks in the ^{31}P spectrum of the pure lipid (125). It is possible that alpha-factor interacts with lipid vesicles in a manner similar to that suggested for methemoglobin and that the small additional peaks may represent the different size populations indicated by the increased polydispersity observed in the QLS measurements upon addition of peptide.

The ^{31}P resonances of all neutral lipids studied are shifted upfield (0.4 - 0.19 ppm) upon addition of alpha-factor. Upfield shifts of the ^{31}P lipid resonance upon addition of drug molecules (epinephrine, norepinephrine, spinephrine) have been observed previously by Srivastava et al. (126), Kuroda and Fujiwara (127), and Fung et al. (128). It has been postulated that the upfield shift of the resonance upon addition of drug indicates strong electrostatic interaction and/ or binding to the polar phosphate headgroup (128). Those shifts reported by Fujiwara and Kuroda are similar to the shifts we observe upon addition of alpha-factor to lipid vesicles although those reported by Fung et al. are larger (2.8 ppm). These three studies were performed on lipids in the liquid crystalline state. Our studies, at several temperatures, show greater shifts in the gel state. These larger shifts may be indicative of stronger electrostatic interactions (surface adsorption of the peptide) at lower temperatures. The origin of the downfield shifts of the ^{31}P resonance of

the negatively charged DPPA is unknown.

The one phospholipid system which differs dramatically from the others is DPPE. This phospholipid was sonicated much longer (several hours) than any other sample before it became translucent. Upon cooling to room temperature it became opaque and resonication did not result in translucence. Because of the opacity the sample was not centrifuged as were the other samples. (A previous attempt at making DPPE samples using centrifugation gave no ^{31}P spectrum suggesting removal of most of the lipid.) The ^{31}P NMR spectrum observed at 70°C (in the liquid crystalline state, no ^{31}P NMR signal was observed at lower temperature) is a "powder" type spectrum (see Figure 27 d) of the shape usually observed in the solid state spectrum of a hexagonal$_{II}$ phase lipid (97). Of course, as discussed above, this spectral shape could simply be the result of an unusual headgroup orientation (111). However, Hornby and Cullis have observed this spectral shape for egg PE in the liquid crystalline state (129). In the gel state egg PE exists in the bilayer phase (bilayer type ^{31}P spectra are observed) and a transition to hexagonal$_{II}$ phase occurs as the temperature is increased above T_c (129). In our studies addition of alpha-factor to liquid crystalline state DPPE results in a dramatic change in the ^{31}P spectral shape. The spectrum with alpha-factor is more like that expected for a bilayer although the edge to edge breadth is smaller than it would be in a true powder spectrum of a

bilayer phase lipid (97). This observation provides further indication that alpha-factor interacts with lipid in a manner such that the gel state and bilayer phase are stabilized. Hexagonal$_{II}$ phase lipids have been found at protein binding sites on biological membranes and may be important for biological activity (130). It is possible that hexagonal$_{II}$ lipids are important for alpha-factor activity and binding to the yeast plasma membrane.

T_2 experiments performed on the DPPE samples yielded T_2 values for only the sharp component in the spectra (shown in Figure 27 d) and are inconclusive since the increase from 0.21 ms to 0.33 ms cannot be compared to the trends observed in the spectra of the other lipids consisting of a single isotropic resonance. QLS measurements could not be obtained for this sample and therefore no correlation of the ^{31}P NMR parameters with vesicle size can be made.

Overall the ^{31}P spectra indicate an interaction of the alpha-factor with the lipid headgroup, an increase in vesicle size upon addition of alpha-factor, and/or a phase/state change. There are also indications that the peptide preferentially interacts with liquid crystalline state lipids in such a manner as to make them more rigid. This interaction may hinder the cooperative transition of gel state lipid molecules to the liquid crystalline state thereby leading to a more stable gel state.

The ^{2}H spectra of chain deuterated DPPC in Figure 28

show broadening and upfield shifts upon addition of alpha-factor. The shifts are greatest for the gel phase spectrum while the % increase in linewidth is greatest in the liquid crystalline state. Both chemical shift and % increase in line width trends are similar to that observed in the ^{31}P spectra. The spectra (with and without alpha-factor) at 41° and 50°C show one symmetric resonance. At 25°C a new smaller sharp resonance appears at ~ 2 ppm downfield of the main peak (the peak near 4.8 ppm is due to residual deuterium in the deuterium depleted water). The significance of the new peak is unknown but, as described above for the ^{31}P data, it may be due to differing populations. Figure 30 shows the ^{2}H spectra of DOPC deuterated at the oleoyl position. Addition of alpha-factor to DOPC does not result in any linewidth or chemical shift change.

Deuterium relaxation rates of phospholipid chains in vesicles are sensitive to the position of the label, vesicle size, temperature, and to the presence of solutes such as cholesterol (113). While T_1 measurements give insight into rapid local motions, T_2 is sensitive to slower vesicle tumbling rates, lateral diffusion, and order (113, 131, 132). If the rotational correlation time is less than $1/\omega_0$ (rapid motion) then $T_1 \sim T_2$ for systems of low order (113). For ordered systems, like vesicles, T_1 is usually greater than T_2.

Stockton et al. have compared ^{2}H T_1 relaxation times

for lipid molecules in chloroform (isotropic solution), in bilayers, and in sonicated lipids, and they have calculated theoretical T_1s for vesicles (113). They have found that the T_1 of lipid dispersions is only slightly affected by sonication (formation of vesicles) and increases with temperature suggesting rapid motion (extreme narrowing) (113, 131, 132). In these studies by Stockton et al. T_2 was found to be much smaller than T_1 for both dispersions and sonicated lipids, indicating partial ordering even in small bilayer vesicles.

The results of our ^2H relaxation studies are shown in Table XII. In all cases the relaxation times increase with temperature and T_2 is much smaller than T_1 indicating partial ordering of the vesicle bilayer. The difference between T_1 and T_2 is much larger in DPPC than in DOPC. Addition of alpha-factor to the DOPC sample leads to a small upfield shift of the resonance (0.095 ppm) but has no effect on the linewidth (T_2^*), T_1, or T_2. This suggests that alpha-factor is not penetrating far enough into the bilayer to interact directly with the label and is not causing any reorientation or change in order at that position. An alternate interpretation is that while interaction of the peptide with lipid leads to increased vesicle size, increased vesicle correlation time, and decreased T_2, an additional internal interaction leads to decreased hydrocarbon chain correlation times (due to mobile pockets) and therefore an increased T_2. These two

effects may cancel leading to the negative findings. The origin of the upfield shift of the ^2H resonance is unknown but may be due to some change in the environment of the ^2H which is not reflected in the linewidth.

Addition of alpha-factor to the chain deuterated DPPC also leads to a small upfield shift (~0.13 - ~0.19 ppm) of the ^2H resonances as well as significant broadening of the resonance at the three temperatures studied (25°, 41°, and 50°C). Upon addition of alpha-factor to this lipid there is little change in the T_1 or T_2 relaxation times measured at 25°C and 41°C and there are small increases in those measured at 50°C. These results suggest no change in hydrocarbon chain mobility or order at the lower temperatures. The increased relaxation times at 50°C may indicate some increase in hydrocarbon chain mobility (T_1) and decrease in chain order (T_2). Whereas most of the T_2 and T_2^* values agree, within experimental error, there is a difference between T_2 and T_2^* for the DPPC sample with alpha-factor added at 50°C. It must be emphasized that T_2 and T_2^* are not necessarily equivalent. The determination of T_2 from the linewidth is based on the assumption that extreme narrowing applies and that there are no chemical shift contributions to the linewidth from different pools in slow exchange with respect to the Larmor frequency. It is probable that the samples with alpha-factor added are more heterogeneous and the heterogeneity may be more pronounced at higher temperatures. In particular, lateral

diffusion would contribute to the line broadening at higher temepratures but is negligible in gel state lipids (124).

Rice et al. have shown that while the phosphate headgroup is immobilized and ordered by protein (^{31}P NMR), hydrocarbon chains are either unaffected or slightly disordered by the interaction (^{2}H NMR) (117). Further, in a study of the melittin - DMPC interaction, Jahnig et al. have observed decreases in the order determined by ^{2}H NMR while Raman spectroscopy and fluorescence anisotropy results indicate increases in order (133). These differences were interpreted to indicate slow order (fluctuations of preferred axes of orientation as lipids undergo lateral diffusion) and fast order (local fluctuations of lipid chain orientation). Decreases in slow order upon addition of peptide or protein to vesicles have been attributed to interaction of the relatively "smooth" hydrocarbon chain surfaces with "rough" peptide surfaces (peptide "roughness" is due to the varying amino acid side-chains) (117). This interaction appears to affect lateral diffusion as the preferred directional axes of the individual phospholipid molecules are changed by interaction with the peptide (133). Our results suggest that alpha-factor may affect the lateral diffusion rate of the liquid crystalline state lipid molecules.

It is difficult to identify specific interactions of alpha-factor with the deuterated DPPC vesicles because the lipid is labeled at all positions along the hydrocarbon

chain. Although it is possible that the peptide has greater effects at certain locations,the relaxation time observed may an averaged value representing contributions from deuterons with different correlation times and different relaxation behavior. Studies with a single ^{2}H label at varying positions along the lipid hydrocarbon chain can show quite different relaxation behavior for different positions (124).

QLS measurements reported in Tables VIII and IX show that as alpha-factor is added to saturated lipid systems both vesicle size and polydispersity increase. As seen in the titration study (Table IX), even at very low peptide concentrations (ie. 16:0.2, DPPC:peptide) vesicle size and polydispersity are increased. Fresh DPPC samples with alpha-factor were consistently found to have diameters of 5000 - 6000 Å (V~ 40%); however, after several days the size increased dramatically from ~5000 to ~30,000 Å and samples became quite turbid indicating vesicle aggregation (even samples without peptide became turbid after ~1 week). The NMR studies were always performed on freshly prepared lipid - peptide samples and since powder patterns are not expected for vesicles with diameters of ~5000 Å undergoing rapid motion it is not surprising that the ^{31}P and ^{2}H resonances remained isotropic (101). QLS measurements of DOPC vesicles also indicate an increase in size upon addition of alpha-factor; however, the polydispersity is high in the absence or presence of alpha-factor.

The mixed phospholipid system is the one vesicle system which did not experience an increase in size upon addition of alpha-factor. While polydispersity did increase upon addition of alpha-factor, the vesicle size decreased. Only one preparation of soybean PI vesicles was made and QLS measurements were not obtained before vesicle aggregation became apparent (sample turbidity). Meaningful diameters could not be determined from QLS measurements of the DPPE samples as diameters of 18,000 - 28,000 Å (with a polydispersity of 70%) were obtained from successive QLS measurements on the same sample preparation. These two lipids make up a large percentage of the total phospholipid (35% PI and 28% PE) of the mixed vesicles and both exhibit ^{31}P NMR behavior which is different from the other lipids (there is no change in the ^{31}P NMR spectrum of PI upon addition of alpha-factor and DPPE seems to be present in non-bilayer forms). QLS measurements for single constituent vesicles (DPPC, DSPC, DPPA, DOPE, and DPPE) show increases in size consistent with the broadening observed in the ^{31}P spectra (Figures 24-26,27 a-c).

Phosphorus and deuterium NMR studies and QLS studies all indicate an interaction of alpha-factor which results in increased vesicle size. The interaction appears to be strongest at the phosphate headgroup (electrostatic interaction) as evidenced by ^{31}P NMR data which indicate changes in headgroup orientation, lipid state, and/ or lipid phase. Although an interaction of alpha-factor with

the fatty acyl chains (hydrophobic interaction) may be suggested by the increased DPPC ^{2}H linewidths, the specifics of the interaction are not clear. The absence of broadening in the DOPC ^{2}H NMR spectrum suggests that alpha-factor may not penetrate deeply enough into the vesicle bilayer to interact with the oleoyl deuterons.

^{1}H NMR Studies: Effect of lipid on alpha-factor

Addition of lipid to alpha-factor leads to a broadening and upfield shifting of most peptide ^{1}H resonances. Broadening of resonances and disappearance of multiplet structure is observed even at DPPC:peptide ratios of 1:1 (Figure 31). Most linewidths are doubled at this lipid:peptide ratio (from ~8 Hz to ~16 Hz). As more lipid is added linewidths continue to increase such that at 3:1 the linewidths are ~24 Hz and at 8:1 they are ~32 - 40 Hz. Only one peak is observed for each peptide resonance indicating fast exchange between free and bound peptide. At a given lipid:peptide ratio, increase in temperature results in the sharpening of the peptide resonances. Similar behavior is observed upon addition of the other lipids to alpha-factor.

The observation of sharpened peptide resonances upon increase in temperature is different from the observations reported by Wakamatsu et al. in their study of alpha-factor - lipid interaction (48). In that study peptide was added to perdeuterated DPPC vesicles and the resonances,

which were broad at 25°C, broadened further near the transition temperature (35.5°C for perdeuterated DPPC) and then sharpened in the liquid crystalline state. This was interpreted as indicating slow to intermediate exchange below the transition temperature and fast exchange above. In that report it is not stated whether the peptide was added to the vesicles at temperatures above T_c or at the specific temperatures studied and therefore our results are not necessarily in contradiction. In an earlier study by Wakamatsu et al. significant broadening was observed upon addition of alpha-factor to lipid vesicles in the liquid crystalline state, however the broadening upon addition to lipids in the gel state was negligible (44). In the one experiment in which we added alpha-factor directly to gel state lipid (DSPC), we observed a similar "non-effect" in the ^{31}P NMR spectrum.

Examination of Table XIII shows that the apparent affinity of alpha-factor for PS vesicles is an order of magnitude greater than that observed for the other lipids. PS differs from the other lipids used in the binding studies in that its headgroup carries a net negative charge while the other lipid headgroups are neutral. This strong binding of alpha-factor to PS is consistent with the extensive broadening of peptide resonances observed even at low peptide to PS ratios. The K_a values determined for alpha-factor interaction with vesicles prepared from PS and the phosphatidylcholines (DPPC, DSPC, and DOPC) are similar

to those reported for enkephalin - lipid binding. Deber and Benham have observed a greater affinity of enkephalin for PS than for PC and have attributed this enhanced binding to an electrostatic interaction of enkephalin with the charged PS headgroup in addition to the hydrophobic interaction with the membrane (102).

Affinity constants were calculated from data obtained with peptide resonances at different positions along the peptide chain. In some cases lipid resonances (or other peptide resonances) overlap with the peptide resonances under study and therefore the K_a values should be regarded qualitatively (cases of overlap are indicated in Table XIII). In all lipid systems the $Tyr^{13}C_{3,5}H$ peptide resonance is clearly distinguishable and may be used to compare the binding of the C-terminus of alpha-factor to the different lipids. The values for DPPE are not true affinity constants because a fully bound resonance position was not determined (spectra were obtained only up to a lipid:peptide ratio of 34:1). Alpha-factor appeared to be fully bound to the other neutral lipids at lipid:peptide ratios of ~24:1. Figures 41-44 present plots of representative peptide resonances versus mole ratio of lipid:peptide for alpha-factor in DPPE and in DOPC and clearly shows that alpha-factor is not fully bound at 34:1, DPPE:peptide. In addition, the behavior indicated in the plots is quite different for DPPE and DOPC. While there is a rapid change in the peptide resonance position upon

FIGURE 41

Plot of the Tyr$^{13}C_{3,5}H$ resonance position (Hz) versus the DPPE : alpha-factor ratio.
The peptide is not fully bound at 34:1.

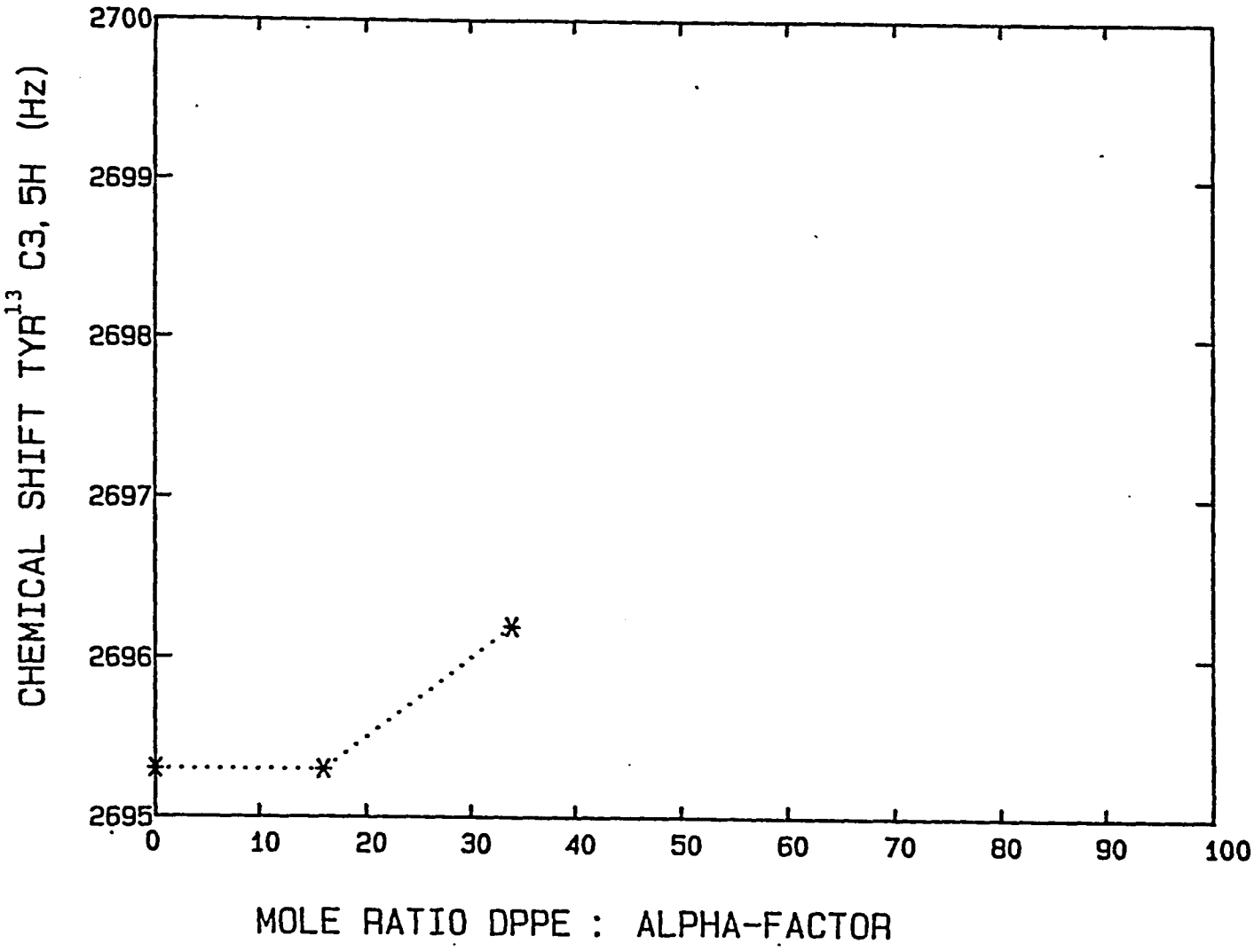
CHEMICAL SHIFT TYR^{13} C3, 5H (Hz)
2700
2699
2698
2697
2696
2695
0
10
20
30
40
50
60
70
80
90
100
MOLE RATIO DPPE : ALPHA-FACTOR

FIGURE 42

Plot of the $Leu^{4,6}$ delta CH_3 resonance position (Hz) versus DPPE:alpha-factor ratio.
The peptide is not fully bound at 34:1.

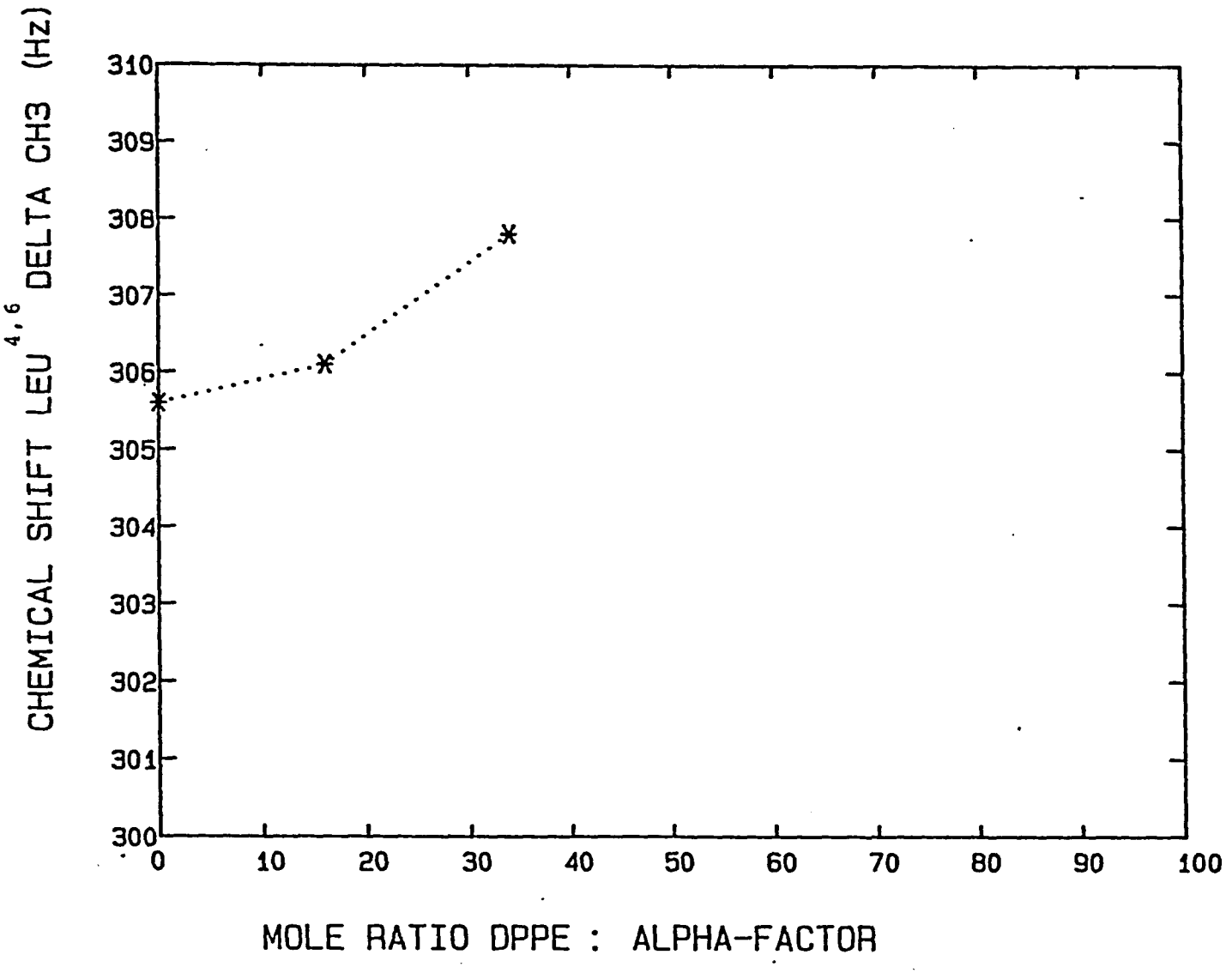
CHEMICAL SHIFT LEU 4,6 DELTA CH3 (Hz)
310
309
308
307
306
305
304
303
302
301
300
0
10
20
30
40
50
60
70
80
90
100
MOLE RATIO DPPE : ALPHA-FACTOR

FIGURE 43

Plot of the $Tyr^{13}C_{3,5}H$ resonance position (Hz) versus DOPC:alpha-factor ratio.
In DOPC the peptide appears to be fully bound at a ratio of 24:1 since the resonance position does not change upon increase of the DOPC concentration.

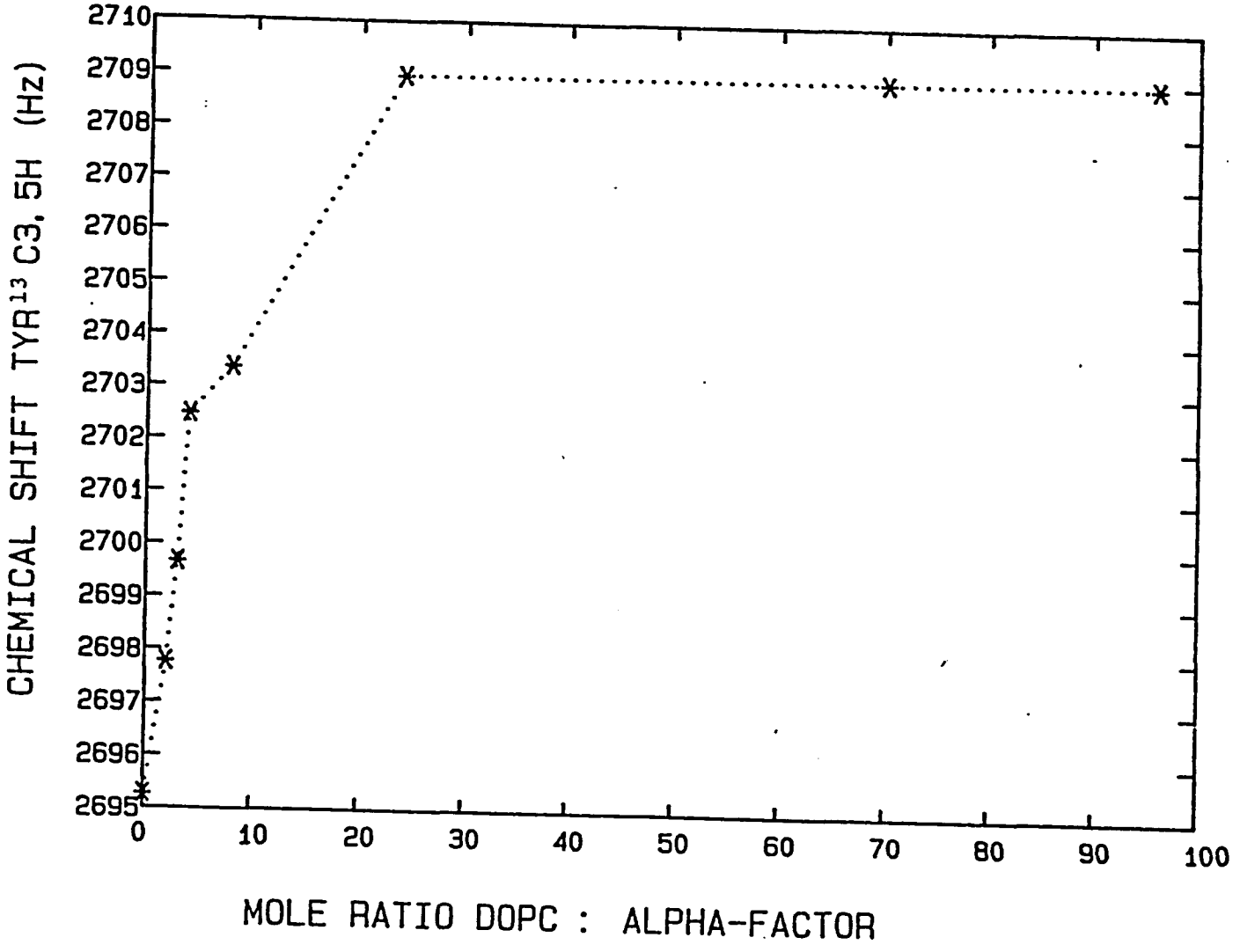
CHEMICAL SHIFT TYR^{13} C3, 5H (Hz)
2710
2709
2708
2707
2706
2705
2704
2703
2702
2701
2700
2699
2698
2697
2696
2695
0
10
20
30
40
50
60
70
80
90
100
MOLE RATIO DOPC : ALPHA-FACTOR

FIGURE 44

Plot of the His^{2}C2H resonance position (Hz) versus DOPC:alpha-factor ratio.
This resonance does not appear to be fully bound until a lipid:peptide ratio of approximately 70:1 is reached. The His^{2} binding constants were smaller than those determined for the Tyr^{13} and $Trp^{1,3}$ residues.

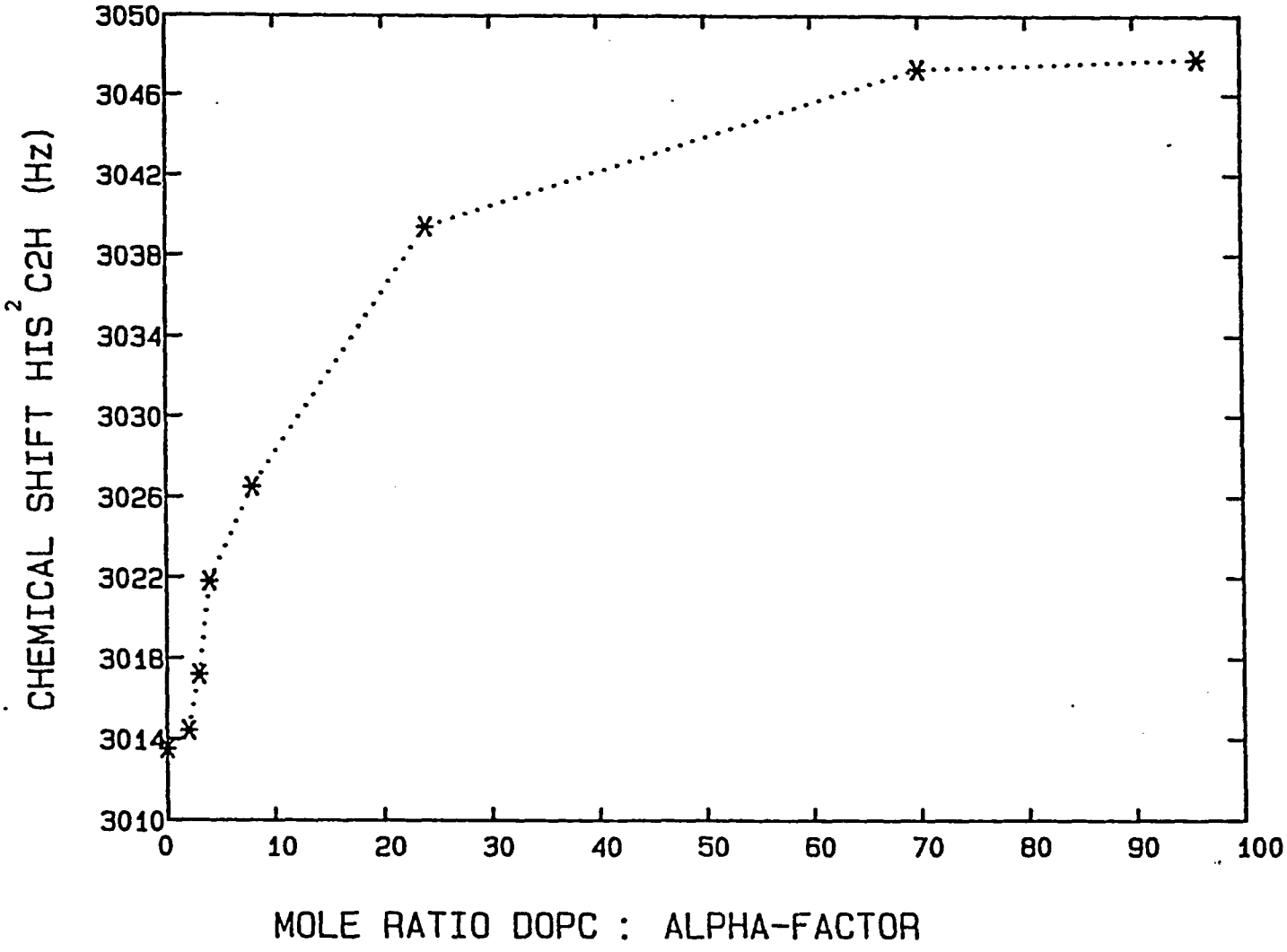
CHEMICAL SHIFT HIS 2 C2H (Hz)
3050
3046
3042
3038
3034
3030
3026
3022
3018
3014
3010
0
10
20
30
40
50
60
70
80
90
100
MOLE RATIO DOPC : ALPHA-FACTOR

addition of small amounts of DOPC (and the other lipids studied), there is no change in the resonance position in DPPE until greater lipid:peptide ratios are reached (~16:1). The K_a values determined for neutral lipids using the $Tyr^{13}C_{3,5}H$ resonance are very similar: 4.8×10^1 M^{-1} for DPPC, 5.1×10^1 M^{-1} for DSPC, and 5.3×10^1 M^{-1} for DOPC. Because the mixed lipid system contains a small amount (7.5%) of PS enhanced binding (K_a : $5.8 \times 10^1 M^{-1}$) is not unexpected.

In DPPC the K_as determined using the Tyr^{13} $C_{3,5}H$, $Trp^{1,3}$ C2H/C5H, and $Leu^{4,6}$ delta CH_3 resonances are very similar. With DOPC the His^2C2H and His^2 C4H could be followed and the K_as for these were about one half of that determined for the Tyr^{13} $C_{3,5}H$. The $Trp^{1,3}$ C2H/C5H K_a in DOPC was also about one half the K_a of the Tyr^{13} $C_{3,5}H$ but because there is overlap with the Tyr^{13} $C_{4,6}H$ the K_a may not accurately reflect the behavior of the $Trp^{1,3}$ rings. This was true of the $Trp^{1,3}$ C2H/C5H resonance in all of the binding studies. In DSPC the K_a values for the His^2 C2H and the $Leu^{4,6}$ delta CH_3 are higher than those determined for the Tyr^{13} and $Trp^{1,3}$ resonances; because of overlap with the $Trp^{1,3}$ rings and lipid resonances there is uncertainty in the "observed" and "bound" chemical shifts for these protons. K_a values for the Gln^5 and Gln^{10} beta protons (in DPPC) were estimated using the 4:1 (lipid:peptide) spectrum as the fully bound spectrum. These estimated values are slightly higher than the K_a values

determined from other resonances, however the behavior of these two resonances is identical. Wakamatsu et al. observe stronger binding of the Gln^5 than Gln^{10} (48). In PS both the Trp^3 beta CH_2 and Met^{12} SCH_3 were monitored in addition to the Tyr^{13} and $Trp^{1,3}$ ring protons. The K_a values for the Trp^3 beta CH_2, $Trp^{1,3}$ ring protons, and the Tyr^{13} $C_{3,5}H$ were similar while the Met^{12} SCH_3 K_a was an order of magnitude smaller.

It is possible that once bound, the N-terminus of the peptide, with the hydrophobic Trp and Leu residues, is inserted into the vesicle bilayer and the C-terminal is partially immobilized on the lipid surface. In such a structure differential binding might not be observed. This binding behavior is consistent with the very small differences we observe in K_a values for different regions of the peptide. The low K_a for Met^{12} SCH_3 may result from a conformation in which the Met^{12} side chain is oriented away from the vesicle bilayer surface. These results are discussed in light of the 2D NOE results (vide infra).

Wakamatsu et al. have proposed a membrane - bound conformation for alpha-factor that includes a possible 3_{10} helix at the N-terminus (residues 1-5), which inserts into the bilayer, and an extended structure for residues 6-9 (45). It has been proposed that the C-terminal residues, 10-13, extend out into the aqueous environment and that binding of these residues is weaker than binding of residues 1-9 (45). The K_a values we have determined for

the Tyr^{13} ring protons and for the $Trp^{1,3}$ and $Leu^{4,6}$ side chains are very similar. Furthermore, the K_a values we estimated for the Gln^5 and Gln^{10} side chains are the same. In a more recent study Wakamatsu et al. propose that the Trp and Leu side chains are oriented toward the hydrophobic portion of the bilayer while the terminal NH_3^+, His^2 ring, and Gln^5 side chain are oriented toward the hydrophilic portion (48). The lower K_a we observe for the His^2 ring protons seems to support this arrangement of the sidechains. In the same study Wakamatsu et al. have observed enhanced binding of alpha-factor to mixed vesicles prepared with 1:1 ratios of DPPC and dilauroylphosphatidyl-serine which is in agreement with the enhanced binding we observe in PS vesicles and mixed phospholipid vesicles containing a small amount of PS (48).

Whereas Wakamatsu et al. propose an extended structure for residues 6-9 and no preferred structure for residues 10-13 (based on TRNOEs performed in $\underline{D_2O}$) the results of our 2D NOE studies of alpha-factor in DPPC vesicles (in $\underline{H_2O}$, shown in Figures 39 and 40 and compiled in Table XIV) clearly demonstrate that the Type II beta-turn observed in solution is present and is much more stable in lipid. In addition to the Pro^8 alpha proton - Gly^9 amide proton NOE observed in aqueous solution we observe NOEs between the Pro^8 alpha proton and the Gln^{10} amide proton, the Gly^9 amide proton and the Gln^{10} amide proton, the Gly^9 alpha protons and the Gln^{10} amide proton, the Pro^8 beta protons

and the Gly^9 amide proton, and the Gly^9 amide proton and the Gly^9 alpha protons. The distances expected for these contacts in Type I and Type II beta-turns are presented in Table XVII. The NOEs between the Pro^8 alpha proton and the Gly^9 amide proton and the Gly^9 amide proton and the Gly^9 alpha protons are the most intense and for Type II turns these are the shortest contacts expected (2.2 Å). The Gly^9 amide proton - Gln^{10} amide proton, Pro^8 alpha proton - Gln^{10} amide proton, and Gly^9 alpha proton - Gln^{10} amide proton NOEs were previously observed only in DMSO with very weak to weak intensity. The NOE between the Gly^9 amide proton and Gly^9 alpha protons was also previously observed in DMSO (intra-residue NOEs are not presented in Table I); however, the NOE between the Pro^8 beta protons and the Gly^9 amide proton was not observed in any solution spectra (DMSO or water). These results are consistent with our earlier activity studies and indicate the importance of the beta-turn for biological activity.

Several NOEs are observed involving residues 11, 12, and 13, however, most are between scalar coupled nuclei (Met^{12} amide proton - alpha proton, alpha proton - beta protons, beta protons - gamma protons, Pro^{11} alpha proton - beta protons, and Tyr^{13} $C_{3,5}H$ - $C_{2,6}H$), between chemically exchanging protons (Tyr^{13} amide proton - $Trp^{1,3}$ indole amino proton, - $Gln^{5,10}$ gamma amide protons, - Lys^7 epsilon amine protons), or are intra-residue contacts (Tyr^{13} $C_{3,5}H$ - beta protons). The only other NOEs observed involving

these residues are those between the Gln^{10} alpha proton and Pro^{11} delta protons (diagnostic of a trans X-Pro peptide bond) and between the Gln^{10} amide proton and the Pro^{11} beta protons. This latter NH_i - $beta_{i+1}$ NOE cannot be correlated with any specific structural feature (the NH_i - $beta_{i+1}$ distance in alpha helices, 3_{10} helices, turns , and beta sheet is too long to be detected by the NOESY experiment (33)). Other than this apparent folding of the Pro^{11} side chain toward the Gln^{10} amide proton the C-terminus does not appear to assume any specific ordered structure. It is possible that the peptide inserts into the membrane such that the N-terminal portion (residues 1-6) penetrates into the bilayer. The beta-turn spanning residues 7-10 would then allow the peptide chain to change orientation and lie along the vesicle surface. In this conformation the Tyr^{13} side chain could be adsorbed to the bilayer surface while the Met^{12} side chain might be oriented toward the aqueous solution. This arrangement of the C-terminal side chains would explain the decreased affinity of the Met^{12} SCH_3 and the apparent similar affinities of the Tyr^{13} and N-terminal Trp and Leu side chains (see Table XIII).

The N-terminus of the peptide appears to be compactly folded in partial agreement with the findings of Wakamatsu et al. (45, 48). Many inter-residue contacts are observed in the NOESY spectra (Figure 38, Tables XIV - XVI) that suggest a compact folding of this region of the peptide.

In particular, NOEs between the Trp^1 and Trp^3 aromatic rings, between both Leu^4 and Leu^6 side chains and the $Trp^{1,3}$ rings, and between the His^2 and Gln^5 side chains are observed. These NOEs imply a folded conformation which has an amphiphilic nature: allowing close contact between the hydrophobic $Trp^{1,3}$ and $Leu^{4,6}$ side chains and hydrophilic contact between the His^2 and Gln^5 side chains. NOEs are also observed between both Leu side chains and the lipid hydrocarbon chain (the $(CH_2)_n$ resonance); however, no other peptide - lipid NOEs are observed. The NOEs described above are consistent with the N-terminal structure for membrane - bound alpha-factor proposed by Wakamatsuet al. However, we additionally observe NOEs between the Leu^4 delta CH_3 and the His^2 and Gln^5 side chains. These NOEs suggest that the peptide may assume and interconvert between more than one long-lived bound conformation. Figure 45 shows the structure proposed by Wakamatsu et al. from the proximity relations they determined form TRNOEs (presented in Table XIX) (48). Figure 46 shows a qualitative model of the lipid - bound alpha-factor based on the NOEs we have observed in DPPC (in H_2O/D_2O). This model includes an alpha-helical structure involving residues 1-6 and a Type II beta-turn involving residues 7-10. The model was built assuming bond angles reported for these specific conformations (33) and can account for most of the alpha-factor NOEs observed in the presence of DPPC vesicles.

FIGURE 45

Model for the membrane - bound alpha-factor conformation as proposed by Wakamatsu et al. This model, proposed by Wakamatsu et al. (45, 48), is based on the proximity relations determined by TRNOEs in D_2O.

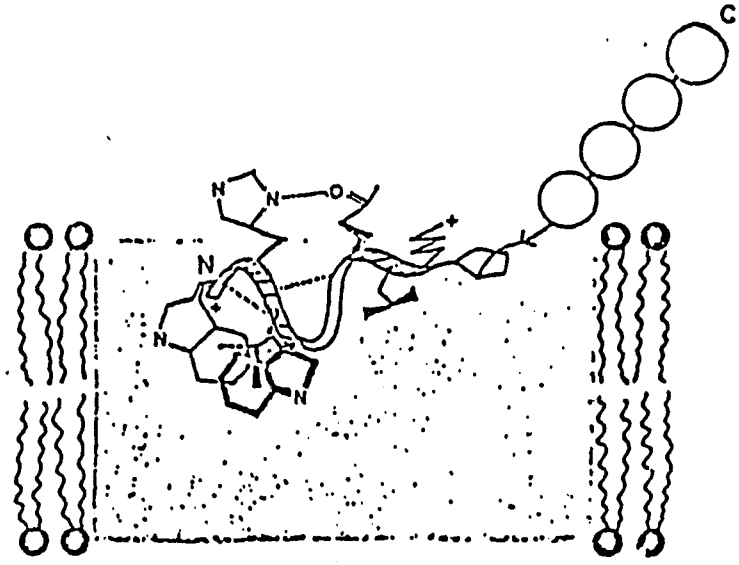
C
N
N
O
N
N
N
+

TABLE XIX
Proximity Relations Determined from TRNOEs (Wakamatsu et al., reference 45)

(distances < 5 Å)

Trp^1 ring - Leu^4 delta CH_3

Trp^1 beta CH_2 - Leu^4 delta CH_3

His^2 beta CH_2 - Gln^5 gamma CH_2

Trp^3 ring - Leu^4 delta CH_3

Trp^3 beta CH_2 - Leu^4 delta CH_3

Leu^4 alpha CH - Leu^4 delta CH_3

Leu^6 delta CH_3 - Gln^5 gamma CH_2

Leu^6 delta CH_3 - Lys^7 epsilon CH_2

Lys^7 alpha CH - Pro^8 delta CH_2

FIGURE 46

Computer generated model of the conformation of alpha-factor in the presence of DPPC vesicles. The model is based on an alpha-helical conformation at the N-terminus involving residues 1-6 and a Type II beta-turn involving residues 7-10. The model was constructed using the torsion angles expected for the given conformations (ref. 33). The figure shows the stereo pairs of a side view of the molecule and illustrates the change in peptide chain direction at the beta turn. The small figure (I) shows a view looking down the long axis of the alpha-helical structure.
The model was displayed on an Evans and Sutherland PS390 Graphics System using the DOCK program.

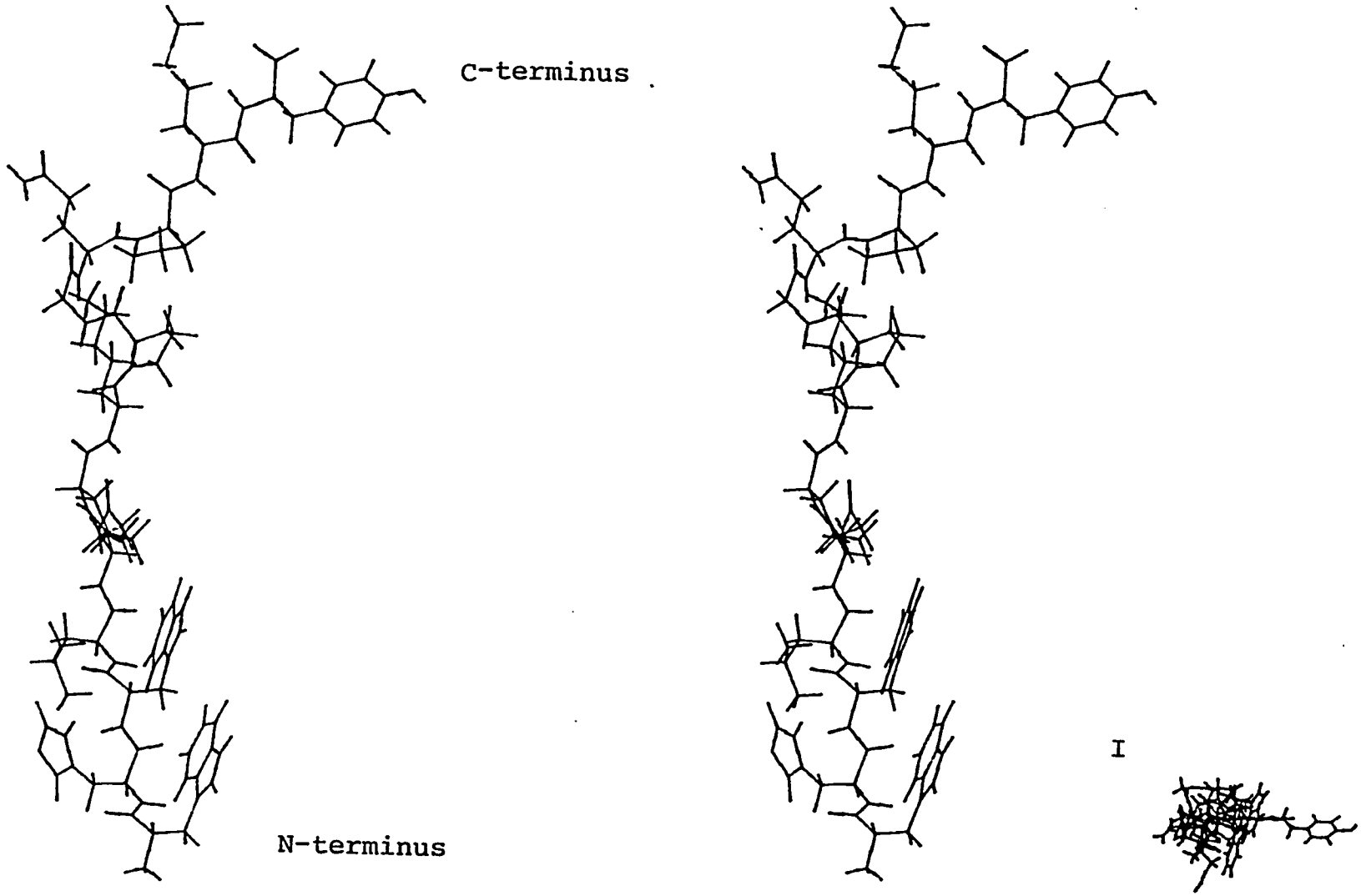
C-terminus
N-terminus
I

In addition to side chain - side chain interactions Table XIV shows that several amide proton - amide proton, amide proton - alpha proton, and amide proton - beta proton interactions are observed for the N-terminus. As indicated in Table XVIII, which lists the distances expected for these contacts in alpha and 3_{10} helices, several NOEs appear between protons which we would expect to be farther apart than the ~4.5 Å the NOESY experiment detects. These include the $d_{\beta N}(i,i+2)$ contacts between Trp^3 and Gln^5 (5.1, 4.8 Å in alpha and 3_{10} helices), the $d_{N\beta}(i,i+1)$ contacts between Leu^6 and Lys^7 and Lys^7 and Pro^8 (4.5, 4.3 Å), and the $d_{\alpha N}(i,i+4)$ contact between Trp^3 and Lys^7 (4.2 Å in alpha-helices). This last NOE, $d_{N}(i,i+4)$, is used to differentiate alpha-helices from 3_{10} helices. In a 3_{10} helix this distance is too long to be detected by the NOESY experiment regardless of the mixing time chosen. The CD spectral patterns of alpha-factor in lipid are not those expected for alpha helical peptides (unpublished data, communicated by Prof. Fred Naider), but it is possible that a compact structure is induced by the lipid which does not conform to an alpha-helical, 3_{10} helical, or beta-turn arrangement. Our NOE studies suggest that both Leu^6 and Lys^7 participate in this compact structure whereas Wakamatsu et al. propose that these two residues are involved in an extended structure (48).

NOESY spectra of alpha-factor in DSPC and DPPE (in D_2O, spectra not shown) were similar to those in DPPC

(Figure 38 shows the spectrum in D_2O) and indicate interaction between the $Trp^{1,3}$ and $Leu^{4,6}$ side chains and between the $Leu^{4,6}$ side chains and the lipid chains. Because the exchangeable protons are not observed in D_2O those NOEs indicative of the beta-turn do not appear. Table XV lists the NOEs observed in DPPC at 41°C (in D_2O). The NOEs present at this temperature (the transition temperature of pure DPPC) are similar to those observed at 25°C (in D_2) but have reduced intensity. This suggests that the conformation of the peptide is similar at both temperatures, however at the higher temperature motion may be more rapid (shorter correlation times) leading to less NOE intensity. Epand et al. have observed increased interaction between peptide and lipid in the liquid crystalline state, however this is accompanied by an increased rate of dissociation of the peptide from the peptide - lipid complex (119, 122). When the temperature was reduced such that the lipid was in the gel state the rate of dissociation of the peptide from the complex was found to be very slow. Thus, although the lipid - bound conformation of alpha-factor may be the same in both the liquid crystalline and gel state, increased dissociation at temperatures above T_c could contribute to increased peptide flexibility and decreased NOE intensity. At 41°C several expected lipid - lipid NOEs appear and are also found in Table XV.

In DOPC, the upfield region of the spectrum is

overwhelmed by lipid resonances, which are in the liquid crystalline state at 25°C, and therefore very few NOEs between peptide resonances were detectable (spectrum not shown, see Table XVI). In DOPE, which is also liquid crystalline at 25°C, very few NOEs appear (not shown) and the spectrum is very similar to that obtained for the alpha-factor in D_2O. This suggests that either the correlation time in DOPE vesicles is similar to that in solution or that the peptide is binding very weakly or not at all to this lipid. The NOEs observed in PS vesicles (found in Table XVI) were of very weak intensity. Peptide binding to this lipid is stronger than to the other lipids, further suggesting that the correlation time in the liquid crystalline lipids is such that NOEs are very small.

The results of the 2D NOE studies indicate that lipid (in particular DPPC) induces a compact N-terminal conformation and stabilization of the beta-turn spanning residues 7-10. Some differences are observed for the lifetime of this structure in the various lipids; however, side chain - side chain interactions of the peptide suggest similar folding in most lipids studied. Conclusions based on the experimental results are found in Chapter VI.

CHAPTER VI

Conclusions

The results of our 2D NOE studies demonstrate the presence of a Type II beta-turn spanning residues 7-10 of active alpha-factor peptides both in solution and in the presence of lipid. This turn, which has been correlated with activity, is stabilized in lipid suggesting that it may be necessary for proper orientation of the peptide at the membrane - bound receptor. Binding and 2D NOE studies in lipid suggest that a compact N-terminal structure with an amphiphilic arrangement of hydrophobic and hydrophilic side-chains is induced by interaction of the peptide with lipid.

Our conclusions are in partial agreement with those of Wakamatsu et al. (45,48) with the major discrepancy being the identification of the beta-turn. We have correlated the presence of this turn with the biological activity of alpha-factor and analogue peptides (41, 42). Our NMR identification of this structure is based on NOEs involving exchangeable protons observed in spectra of alpha-factor and of alpha-factor and lipid vesicles in H_2O/D_2O (9:1). Because the TRNOE studies of Wakamatsu et al. were performed in D_2O only, these important NOEs could not be observed. Without the results of NOE experiments in H_2O, only an "incomplete" structure for the alpha-factor can be proposed. Our results clearly demonstrate the importance of performing experiments in both D_2O and H_2O.

Another discrepancy between the Wakamatsu structure and ours is that we also observe interactions indicative of the participation of Leu^6 in the helical structure whereas Wakamatsu et al. suggest that this residue is involved in an extended structure. Furthermore, our results in H_2O/D_2O (9:1) identify many amide proton - side chain proton NOEs which are more reliable in identifying secondary structure than side chain - side chain connectivities alone. This again emphasizes the necessity of performing experiments in H_2O/D_2O (9:1) as well as in D_2O.

Our QLS studies and ^2H and ^{31}P NMR results indicate that alpha-factor causes an increase in vesicle size, imparts rigidity into the fluid lipid states, with which it preferentially interacts, and "stabilizes" gel state and bilayer phase lipids. The alpha-factor appears to induce changes in lipid structure which facilitate vesicle fusion, as opposed to simple aggregation (where several vesicles merely "stick" together). It is possible that alpha-factor acts in a similar manner on the membrane of a-cells to induce some of the changes in the yeast plasma membrane structure involved in fusion of the two haploid cells (α and a) during mating. Our NMR studies on the lipid - peptide interaction indicate that both electrostatic and hydrophobic interactions are important for binding of alpha-factor to the lipid vesicles. The results of the alpha-factor - lipid binding studies should prove useful in separating the effects of "non-specific" (hydrophobic and

electrostatic binding of peptide to membrane) and "specific" (actual binding to receptor) binding of peptide to actual yeast cell membrane preparations containing the alpha-factor receptor.

REFERENCES

1. Gierasch, L. M., Rockwell, A. L., Thompson, K. F., and Briggs, M. S. (1985) Biopolymers 24 117.

2. Gierasch, L. M., Karle, I. L., Rockwell, A. L., and Yenal, K. (1985) J. Am. Chem. Soc. 107 3321.

3. Bach, A. C. II and Gierasch, L. M. (1985) J. Am. Chem. Soc. 107 3349.

4. Davis, D. G., Gisin, B. F., and Tosteson, D. C. (1976) Biochemistry 15 768.

5. Rao, B. N. N., Kumar, A., Balaram, H., Ravi, A., and Balaram, P. (1983) J. Am. Chem. Soc. 105 7423.

6. Baniak, E. L., Rivier, J. E., Struthers, S. R., Hagler, A. T., and Gierasch, L. M. (1987) Biochemistry 26 2642.

7. Hollosi, M., Kover, K. E., Holly, S., and Fasman, G. D. (1987) Biopolymers 26 1527.

8. Hollosi, M., Kover, K. E., Holly, S., and Fasman, G. D. (1987) Biopolymers 26 1555.

9. Pastore, A., Temussi, P. A., Salvadori, S., Tomatis, R., and Mascagni, P. (1985) Biophys. J. 48 195.

10. Chassaing, G., Convert, O., and Lavielle, S. (1986) Eur. J. Biochem. 154 77.

11. Koizuka, I. Watari, H., Yanaihara, N., Nishina, Y., Shiga, K., and Nagayama, K. (1984) Biomed. Res. 5 Suppl. 161.

12. Loomis, R. E., Lee, P.- C., Tseng, C. -C. (1987) Biochim. Biophy. Acta 911 168.

13. Szollosy, A., Otter, A., Stewart, J. M., and Kotovych G. (1986) J. Biomol. Struc. Dyn. 4 501.

14. Mammi, S., Goodman, M., Peggion, E., Foffani, M. T., Moroder, L., and Wuensch, E. (1986) Int. J. Pep. Pro. Res. 27 145.

15. Geysen, H. M., Tainer, J. A., Rodda, S. J., Mason, T. J., Alexander, H., Getzoff, E. D., and Lerner, R. A. (1987) Science 235 1184.

16. Baldwin, R. L. (1986) Trends Biochem. Sci. 11 6.

17. Jelicks, L. A., Shenbagamurthi, P., Becker, J. M., Naider, F. R., and Broido, M. S. (1988) Biopolymers 27 431.

18. Benham, B. A. and Deber, C. M. (1984) J. Biol. Chem. 259 14935.

19. Wakamatsu, K., Higashijima, T., Fujino, M., Nakajima, T., and Miyazawa, T. (1983) FEBS Lett. 162 123.

20. Higashijima, T., Fujimura, K., Masui, Y., Sakakibara, S., and Miyazawa, T. (1983) FEBS Lett. 159 229.

21. Higashijima, T., Wakamatsu, K., Takemitsu, M., Fujino, M., Nakajima, T., and Miyazawa, T. (1983) FEBS Lett. 152 227.

22. Wu, C. -S. C., Leu, N. M., Loh, H. H., Yang, J. T., and Li, C. H. (1979) Proc. Natl. Acad. Sci. USA 76 3656.

23. Wu, C. -S. C., Hachimori, A., and Yang, J. T. (1982) Biochemistry 21 4557.

24. Wuthrich, K., Bosch, C., and Brown, L. R. (1980) Biochem. Biophys. Res. Commun. 95 1504.

25. Braun, W., Wider, G., Lee, K. H., and Wuthrich, K. (1983) J. Mol. Biol. 169 921.

26. Sankaran, M. B. and Easwaran, K. R. K. (1984) J. Bioscience 6 635.

27. Wuthrich, K., Billeter, M., and Braun, W. (1984) J. Mol. Biol. 180 715.

28. van de Ven, F. J. M., de Bruin, J. H., and Hilbers, C. W. (1984) FEBS Lett. 169 107.

29. Broido, M. S., James, T. L., Zon, G., and Keepers, J.W. (1985) Eur. J. Biochem. 150 117.

30. Leach, S. J., Nemethy, G., and Scheraga, H. A. (1977) Biochem. Biophys. Res. Commun. 75 207.

31. Zuiderweg, E. R. P., Kaptein, R., and Wuthrich, K. (1983) Proc. Natl. Acad. Sci. USA 80 5837.

32. Bystrov, V. F. (1984) Sov. Sci. Rev. D. Physicochem.

Biol.5 207.

33. Wuthrich, K. (1984) Biomed. Res. 5 Suppl. 151.

34. Castiglione- Morelli, M. A., Motta, A., Picone, D., Tancredi, T., Temussi, P. A., and Trivellone, E. (1987) Book of Abstracts Fifth Conv. Biomol. Stereodyn. 329.

35. Bax, A. and Davis, D. G. (1985) J. Magn. Reson. 63 207

36. Crandall, M., Egel, R., and Mackay, V. L. (1977) Adv. in Microbiol. Physiol. 15 307.

37. Shenbagamurthi, P., Baffi, R., Khan, S. A., Lipke, P., Pousman, C., Becker, J. M., and Naider, F. (1983) Biochemistry 22 1298.

38. Masui, Y., Chino, N., Sakakibara, S., Tanaka, T., Murakami, T., and Kito, H. (1977) Biochem. Biophys. Res. Commun. 78 534.

39. Baffi, R. A., Becker, J. M., Lipke, P. N., and Naider, F. (1985) Biochemistry 24 3332.

40. Shenbagamurthi, P., Steinfeld, A. S., Khan, S. A., Becker, J. M., and Naider, F. (1983) Biopolymers 22 815.

41. Naider, F. R., Shenbagamurthi, P., Broido, M. S., Hughes, L. A., Raths, S., and Becker, J. M. (1985) in "Peptides: Structure and Function," Deber, C. M., Hruby, V. J., and Kopple, K. D., Eds., Pierce Chemical Company, USA, 687.

42. Shenbagamurthi, P., Kundu, B., Raths, S., Becker, J. M., and Naider, F. (1985) Biochemistry 24 7070.

43. Higashijima, T., Miyazawa, T., Masui, Y., Chino, N., Sakakibara, S., and Kito, H. (1979) in "Peptide Chemistry," Yonahara, H., Ed., Protein Res. Found., Osaka, 155.

44. Higashijima, T., Masui, Y., Chino, N., Sakakibara, S., Kito, H., and Miyazawa, T. (1984) Eur. J. Biochem. 140 163.

45. Wakamatsu, K., Okada, A., Suzuki, M., Higashijima, T., Masui, Y., Sakakibara, S., and Miyazawa, T. (1986) Eur. J. Biochem. 154 607.

46. Masui, Y., Tanaka, T., Chino, N., Kita, H., and

Sakakibara, S. (1979) Biochem. Biophys. Res. Commun. 86 982.

47. Khan, S. A., Merkel, G. J., Becker, J. M., and Naider, F. (1981) Int. J. Pept. Prot. Res. 17 219.

48. Wakamatsu, K., Okada, A., Miyazawa, T., Masui, Y., Sakakibara, S., and Higashijima, T. (1987) Eur. J. Biochem. 163 331.

49. Thorner, J. (1980) in "Molecular Genetics of Development: An Introduction to Recent Research on Experimental Systems," Leighton, T. J. and Loomis, W. A., Jr., Eds.; Academic Press, New York, 119.

50. Thomas, G., Gordon, J., and Rogg, H. (1978) J. Biol. Chem. 253 1101.

51. Rose, A. H. (1969) in "The Yeasts" Volume 1, Rose, A. H. and Harrison, J. S., Eds; Academic Press, New York, Introduction.

52. de Robichon-Szulmajster, H. and Surdin-Kerjan, Y. (1969) in "The Yeasts" Volume 2, Rose, A. H. and Harrison, J. S., Eds. (1969) Academic Press, New York, Nucleic Acid and Protein Synthesis in Yeast: Regulation of Synthesis and Activity.

53. Strassman, M. and Weinhouse, S. (1953) J. Am. Chem. Soc 751 680.

54. Betz, R., Crabbe, J. W., Meyer, H. E., Wittig, R., and Duntze, W. (1987) J. Biol. Chem. 262 546.

55. Becker, J. M., Marcus, S., Kundu, B., Shenbagamurthi, P., and Naider, F. (1987) Mol. Cell. Biology 7 4122.

56. Chou, P. Y. and Fasman, G. D. (1978) Adv. in Enzymol. 47 45.

57. Gierasch, L. M., Deber, C. M., Madison, V., Nui, C., and Blout, E. P. (1981) Biochemistry 20 4730.

58. Ventkatchalam, C. M. (1968) Biopolymers 6 1425.

59. Balaram, P. (1985) Proc. Indian Acad. Sci. (Chem. Sci.) 95 21.

60. Kessler, H. (1982) Angew. Chem. Int. Ed. Engl. 21 512.

61. Farrar, T. C. and Becker, E. D. (1971) in "Pulse and

Fourier Transform NMR. Introduction to Theory and Methods", Academic Press, New York.

62. Shaw, D. (1984) in "Fourier Transform NMR Spectroscopy", Elsevier Science Publishing Company, Amsterdam.

63. Fukushima, E. and Roeder, S. B. (1981) in Experimental Pulse NMR. A Nuts and Bolts Approach", Addison Wesley Publishing Company, Massachussets.

64. Brown, T. R. and Ugurbil, K. (1984) in "Structural and Resonance Techniques in Biological Research", Bell Telephone Laboratories, New Jersey.

65. Brevard, C. and Granger, P. (1981) in "Handbook of High Resolution Multinuclear NMR", John Wiley and Sons, New York.

66. Becker, E. D. (1969) in "High Resolution NMR. Theory and Chemical Applications", Academic Press, New York.

67. Bax, A. (1982) in "Two Dimensional Nuclear Magnetic Resonance in Liquids", Delft University Press, Holland.

68. Muller, S. and Ernst, R. R. (1979) Mol. Phys. 38 963.

69. Slichter, C. P. (1980) in "Principles of Magnetic Resonance", Springer Verlag, New York.

70. Hartmann, S. R. and Hahn, E. L. (1962) Physical Review 128 2042.

71. Davis, D. G. and Bax, A. (1985) J. Am. Chem. Soc. 107 2820.

72. Noggle, J. H. and Schirmer, R. E. (1971) in "The Nuclear Overhauser Effect: Chemical Applications", Academic Press, New York.

73. Sanders, J. K. M. and Hunter, B. K. (1987) in "Modern NMR Spectroscopy. A Guide for Chemists", Oxford University Press, New York.

74. Macura, S. and Ernst, R. R. (1980) Molecular Physics 41 95.

75. Bothner- By, A. A., Stephens, R. L., and Lee, J. (1984) J. Am. Chem. Soc. 106 811.

76. Davis, D. G. and Bax, A. (1985) J. Magn. Reson. 64 533.

77. Clore, G. M. and Gronenborn, A. M. (1982) J. Magn. Reson. 48 402.

78. Connors, K. A. (1987) in "Binding Constants. Measurement of Molecular Complex Stability," John Wiley and Sons, New York, Chapter 5.

79. Jardetzky, O. and Roberts, G. C. K. (1981) in "NMR in Molecular Biology", Academic Press, New York.

80. Martin, M. L. and Delpeuch, J.-J. (1980) in "Practical NMR Spectroscopy", Heyden and Sons, Ltd., London.

81. Ernst, R. R., Bodenhausen, G., and Wokaun, A. (1987) in "Principles of Nuclear Magnetic Resonance in One and Two Dimensions", Oxford University Press, New York.

82. Turner, D. L. (1985) Prog. NMR Spect. 17 281.

83. Prendergast, F. G., Lu, J., Wei, G. J., and Bloomfield, V. A. (1982) Biochemistry 21 6963.

84. Mazer, N. A., Benedek, G. B., and Carey, M. C. (1976) J. Phys. Chem. 80 1075.

85. Burns, R. A., Donovan, J. M., and Roberts, M. F. (1983) Biochemistry 22 964.

86. Henry, S. A. (1982) in "Molecular Biology of the Yeast Saccharomyces: Metabolism and Gene Expression" Cold Spring Harbor Laboratory, 101.

87. Tallon, M. A., Shenbagamurthi, P., Marcus, S., Becker, J. M., and Naider, F. (1987) Biochemistry 26 7767.

88. Barany, G. and Merrifield, R. B. (1980) in " The Peptides, Analysis, Synthesis, Biology", Volume 2 Gross, E. and Meienhofer, J. Eds., 1.

89. Tam, J. P., Kent, S. B. H., Wong, T. W., and Merrifield, R. B. (1979) Int. J. Meth. Syn. Org. Chem. 12 955.

90. Kaiser, E., Colescott, R. L., Bossinger, C. D., and Cook, P. I. (1970) Anal. Biochem. 34 595.

91. Barrow, D. A. and Lentz, B. R. (1980) Biochim. Biophys. Acta 597 92.

92. States, D. J., Haberkorn, R. A., and Ruben, D. J. (1982) J. Magn. Reson. 48 286.

93. Macura, S., Wuthrich, K., and Ernst, R. R. (1982) J. Magn. Reson. 47 351.

94. Julius, D., Blair, L., Brake, A., Sprague, G., and Thorner, J. (1983) Cell 32 839.

95. Bundi, A. and Wuthrich, K. (1979) Biopolymers 18 285.

96. Wuthrich, K. (1976) in "NMR in Biological Research: Peptides and Proteins," North Holland, Amsterdam.

97. Cullis, P. R. and de Kruijff, B. (1979) Biochim. Biophys. Acta. 559 399.

98. Gabriel, N. E. and Roberts, M. F. (1986) Biochemistry 25 2812.

99. Sheetz, M. P. and Chan, S. I. (1972) Biochemistry 11 4573.

100. Schuh, J. R., Banjerjee, U., Muller, L., and Chan, S. I. (1982) Biochim. Biophys. Acta. 687 219.

101. Tilcock, C. P. S., Cullis, P. R., and Gruner, S. M. (1986) Chem. Phys. Lipids 40 47.

102. Deber, C. M. and Benham, B. A. (1985) Biopolymers 24 105.

103. Stark, R. E., Storrs, R. W., Levine, S. E., Yee, S., and Broido, M. S. (1986) Biochim. Biophys. Acta 860 399.

104. Glickson, J. D., Gordon, S. L., Pitner, J. P., Agresti, D. G., and Walter, R. (1976) Biochemistry 15 5721.

105. Khaled. M. A. and Urry, D. (1976) Biochem. Biophys. Res. Commun. 70 485.

106. Marion, D. (1985) FEBS Lett. 192 99.

107. Kessler, H., Griesinger, C., Kerresbaum, R., Wagner, K., and Ernst, R. R. (1987) J. Am. Chem. Soc. 109 607.

108. Stark, R. E., Gosselin, G., Donovan, J. M., Carey, M. C., and Roberts, M. F. (1985) Biochemistry 24 5599.

109. Cullis, P. R. and Hope, M. J. (1978) Nature 271 672.

110. Dufourc, E. J., Smith, I. C. P., and Dufourcq, J. (1986) Biochemistry 25 6448.

111. Thayer, A. M. and Kohler, S. J. (1981) Biochemistry 20 6831.

112. Smith, I. C. P. and Ekiel, I. H. (1984) in "Phosphorus-31 NMR. Principles and Application," Gorenstein, D. G., Ed., Academic Press, New York, Chapter 15.

113. Stockton, G. W., Polnaszek, C. F., Tulloch, A. P., Hasan, F., and Smith, I. C. P. (1976) Biochemistry 15 954.

114. Bergelson, L. D. and Barsukov, L. I. (1977) Science 197 224.

115. Ostro, M. J. (1983) in "Liposomes", Marcel Dekker Inc., New York.

116. Yeagle, P. L., Selinsky, B. S., and Albert, A. D. (1984) Biophys. J. 45 1085.

117. Rice, D. M., Meadows, M. D., Scheinman, A. O., Goni, F. M., Gomez-Fernandez, J. C., Moscarello, M. A., Chapman, D., and Oldfield, E. (1979) Biochemistry 18 5893.

118. Skarjune, R. and Oldfield, E. (1979) Biochemistry 18 5903.

119. Epand, R. M. and Surewicz, W. K. (1984) Can. J. Biochem., Cell. Biol. 62 1167.

120. Ruppel, D. and Kapitin, H.-G. (1982) Biochim. Biophys. Acta 6921.

121. Marcelja, S. and Wolfe, J. (1979) Biochim. Biophys. Acta 557 24.

122. Epand, R. M., Epand, R. F., Orlowski, R. C., Schlueter, R. J., Boni, L. T., and Hui, S. W. (1983) Biochemistry 22 5074.

123. Papahadjapoulous, D., Moscarello, M., Eylar, E. H., and Isac, T. (1975) Biochim. Biophys. Acta 401 317.

124. Davis, J. H. (1986) Chem. Phys. Lipids 40 223.

125. Deslauriers, R., Butler, K. W., and Smith, I. C. P.

(1986) Bull. Magn. Res. 8 106.

126. Srivastava. S., Phadke, R. S., and Govil, G. (1984) Indian J. Chemistry 23 1148.

127. Kuroda, Y. and Fujiwara, Y. (1987) Biochim. Biophys. Acta. 903 395.

128. Fung, L. W.-M., Pratt, E. A., and Ho, C. (1979) Biochemistry 18 317.

129. Hornby, A. P. and Cullis, P. R. (1981) Biochim. Biophys. Acta 647 285 (1981).

130. Scheule, R. K. (1987) Biochim. Biophys. Acta 899 185.

131. Stockton, G. W., Polnaszek, C. F., Leitch, L. C., Tulloch, A. P., and Smith, I. C. P. (1974) Biochem. Biophys. Res. Commun. 60 844.

132. Stark, R. E., Manstein, J. L., Curatolo, W., and Sears, B. (1983) Biochemistry 22 2486.

133. Jahnig, F., Vogel, H., and Best, L. (1982) Biochemistry 21 6790.